Molecular analysis of aggressive colorectal cancer

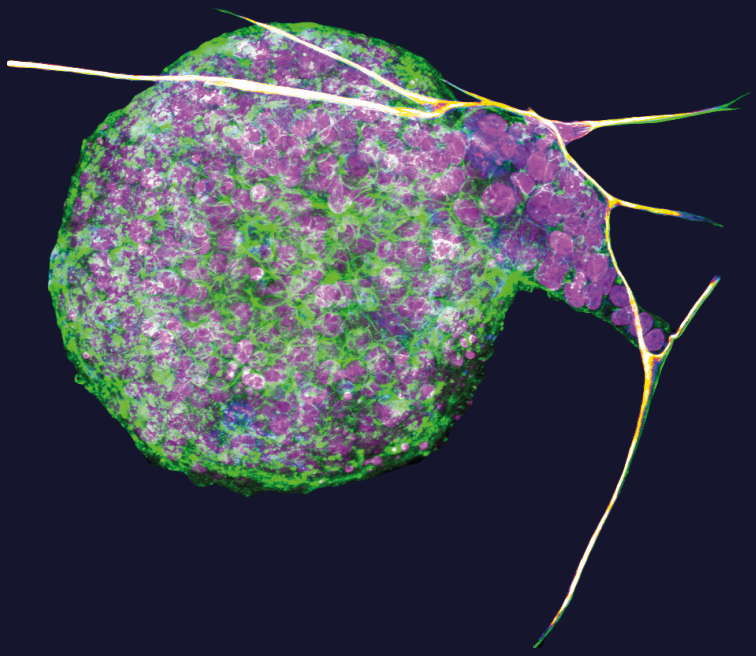

Thomas T. Vellinga

Molecular analysis of aggressive colorectal cancer

Thomas Tiede Vellinga

Molecular analysis of aggressive colorectal cancer
PhD thesis, Utrecht University, The Netherlands

The work described in this thesis was financially supported by the Dutch Cancer Society/ Koningin Wilhelmina Fonds (KWF; grant number UU2011-5226)

Publication of this thesis was financially supported by Cancer Center UMC Utrecht, Chipsoft.

Cover	Image was kindly provided by Cornelia Veelken
Lay-out	proefschriftmaken
Printed by	proefschriftmaken
ISBN	9789463802796

Molecular analysis of aggressive colorectal cancer

Moleculaire analyse van agressieve darmkanker
(met een samenvatting in het Nederlands)

Proefschrift

ter verkrijging van de graad van doctor aan de Universiteit Utrecht
op gezag van de rector magnificus, prof. dr. H.R.B.M. Kummeling
ingevolge het besluit van het college voor promoties
in het openbaar te verdedigen
op donderdag 18 april 2019 des middags te 2.30 uur

door

Thomas Tiede Vellinga
Geboren op 2 februari 1985
te Delft

Promotoren:
Prof. dr. I.H.M. Borel Rinkes
Prof. dr. O.W. Kranenburg

Copromotor:
Dr. J. Hagendoorn

Content

CHAPTER 1

General introduction

Over 1.8 million new colorectal cancer (CRC) cases and 881,000 deaths are estimated to occur in 2018.[1] The incidence continues to rise to an estimated 2.2 million new cases annually by 2030.[2] Death due to CRC is mainly the result of distant metastases, which occur in 50% of cases. The main sites of metastases are the liver and lungs (70%). [3] Despite improvements in surgical procedures, systemic therapy and local radiation techniques, the prognosis of patients with metastatic CRC remains poor with a five-year survival of only 15%.[4] To date surgery is the only curative option, but only 25% of patients are eligible surgical candidates at disease presentation.[5,6] Treatment options for the remaining 75% of patients are limited to systemic therapy or local ablation/radiotherapy. For these patients the current adjuvant systemic therapy prolong life expectancy approximately 2 years.[7] First line chemotherapy for CRC in the Netherlands consists of regiments with either capecitabine (tablet of prodrug 5-fluorouracil (5-FU)) and oxaliplatin (CAPOX) or 5-FU, leucovorin and oxaliplatin (FOLFOX). Interestingly, since the introduction of the FOLFOX regimen in 2004/05[8,9] and despite the development of multiple targeted therapies, including against vascular endothelial growth factor receptor (VEGF) and epidermal growth factor receptor (EGFR), the FOLFOX regimen has remained unchanged over the past 14 years.[10] Current guidelines recommend the use of adjuvant systemic therapy in patients with high-risk stage II and stage III CRC. The CAPOX/FOLFOX regimens reduce the risk of distant recurrence after surgery from 50% to 35% in these patients. Thus, only 15% of patients benefit from current adjuvant treatment regiments.[11] This stresses the importance of developing new, more effective therapeutic strategies and methods for patient selection.

One of the major challenges in the treatment of CRC is the difficulty to predict accurate disease response to adjuvant therapy; it is currently impossible to predict which patients benefit most from which exact adjuvant therapy. Staging is a useful tool to stratify patients and assign specific therapies. Traditionally, CRC is staged solely on the basis of histopathological characteristics of the resected specimen. This Tumor, Nodes, Metastasis (TNM) classification system therefore has its limitations and fails to predict response to systemic therapy.[12] In search for factors that predict therapeutic outcome, multiple molecular factors were identified. For example patients with high frequency microsatellite instable (MSI) tumors show significantly less benefit from 5-fluorouracil (5-FU) in the adjuvant setting.[13,14] In addition, mutant Kirsten Rat Sarcoma (KRAS) CRC are resistant to antibodies targeting the epidermal growth factor receptor (EGFR).[13,15] These findings boosted the interest in tumor classification based on molecular features and led to the development of gene expression-based classification systems of CRC. Multiple of such systems were published with variable numbers of different subtypes.[16–21] To create consensus among the different classification systems, facilitate clinical utility and advance drug development an international consortium was formed. The CRC Subtyping Consortium (CRCSC) coalesced six independent classification systems into four consensus

molecular subtypes (CMS) with their respective distinct characteristics: CMS1 (14%), hypermutated, microsatellite instable and with strong immune activation; CMS2 (37%), epithelial, chromosomally unstable with marked WNT and MYC signaling activation; CMS3 (13%), epithelial, activating mutations in KRAS and evident metabolic dysregulation; CMS4 (23%), mesenchymal, high transforming growth factor β (TGF-β) activation, extracellular matrix remodeling and angiogenesis. Survival analysis revealed patients with tumors classified as subtype CMS1-3 tumors have a similar prognosis, while patients with tumors classified as CMS4 have a significant worse prognosis.[22] Therefore, this subtype is commonly referred to as the poor prognosis or aggressive subtype in CRC.

The gene expression analyses used to develop the CMS classifier were performed on resection specimens of whole tumors. Thus, the RNA originated from both stromal and tumor cells. This raises the question which highly expressed genes belong to which cell type. Therefore, certain molecular features could be attributed to tumor cells, while others may be present in the stroma. Indeed, two reports show the genes used to classify the poor prognosis subtype of CRC (CMS4) are predominantly expressed by stromal cells.[23,24] These classifier genes are mainly mesenchymal. The mesenchymal phenotype of CMS4 CRC could therefore be due to high levels of (mesenchymal) stromal fibroblasts, and/or to epithelial-to-mesenchymal transition (EMT) in (neoplastic) tumor cells. EMT is a developmental process characterized by loss of epithelial characteristics (such as tight and adherens junctions and apico-basal polarity) and gain of mesenchymal properties (such as increased motility) and contributes to metastasis. Many studies have shown that EMT plays an essential role in cancer progression and metastasis in many types of malignancies, including CRC. [25,26] In chapter 2, we studied both the stromal and neoplastic compartment of tumors to better understand the role of mesenchymal gene expression in CRC. The invasive behavior of cancer cells does not only depend on the biology and signaling within the cancer cells itself, but is to a large degree due to the cancer associated stroma and its extracellular matrix (ECM). The ECM mainly consists of collagen and proteoglycans. Aside from providing the necessary physical support, the ECM also plays an important signaling role in cancer progression. For example, growth factors present in the ECM activate signaling pathways in tumors involved in progression and invasion.[27] CRC patients with tumors containing high amounts of stroma have a worse prognosis.[28,29] Cancer associated fibroblasts (CAFs) produce many components of the ECM and are one of the most abundant cell types in the stroma of poor prognosis CRC tumors.[23,24] In chapter 3, we focused on the effect of different ECMs on invasive behavior of CRC organoids and designed a co-culture system with fibroblasts to study the tumor cell-fibroblast interaction.

Resistance to cancer chemotherapy is a common phenomenon and a major cause of cancer-related mortality. In CRC 40–50% of tumors survive the FOLFOX/CAPOX

regiments.[30] This highlights the importance of unravelling resistance mechanisms to optimize therapy. Multiple resistance mechanisms have been described and are generally divided into non-cellular and cellular resistance mechanisms. Non-cellular mechanisms are extracellular factors, such as limited vascular accessibility and high interstitial pressure in the tumor microenvironment. Cellular mechanisms concern drug targets, enzymes and transport systems inside the cancer cells.[31] For example the high expression levels of ABC transporters or enhanced active DNA repair mechanisms. In chapter 4, we studied the effect of chemotherapy on colorectal cancer liver metastasis (CRLM). We compared gene expression profiles of chemotherapy naïve versus chemotherapy treated liver metastases and found a significant upregulation of genes involved in cellular energy metabolism.

As early as the eighteenth century, the French surgeon Le Dran made the observation that breast cancer patients with metastases in the axillary lymph nodes had a worse prognosis than patients without axillary lymph node involvement.[32] Since then, lymphatic spread is considered as one of the most important prognostic factors in many cancer types, including CRC. Patients with primary colorectal cancer and no lymph node metastasis have 5-year survival rates of 87%, in contrast to 5-60% in patients with lymph node metastases.[33] Therefore, lymphadenectomy is part of the standard surgical procedure to remove primary CRC. Partial hepatectomy in case of colorectal liver metastasis (CRLM) does not include standard lymphadenectomy. Approximately 1/3 of patients undergoing partial hepatectomy for CRLM has synchronous hepatic lymph node metastases.[34–36] Furthermore, the presence of lymph node metastasis in the hepatoduodenal ligament is the worst prognostic factor after partial hepatectomy for CRLM.[37–39] However, routine lymphadenectomy did not improve survival after partial hepatectomy.[40–42] In chapter 5, we studied lymphatic gene expression in relation to the different molecular subtypes in CRC and CRLM. We show lymphatic gene expression is associated with worse prognosis in both primary and metastatic CRC. Lymphatic factors Vascular Endothelial Growth Factor C (VEGF-C) and Neuropilin (Nrp) could function as a tool to identify CRC patients at risk for lymphatic dissemination.

Systemic therapy for CRC has only a modest effect on long-term survival, and the individual response to therapy is hardly predictable. Molecular characterization of CRC led to the discovery of important oncogenes, such as KRAS, Rapid Accelerated Fibrosarcoma (RAF) and Phosphoinositide 3-kinase (PI3K) and tumor suppressor genes, such as Adenomatous Polyposis Coli (APC), Tumor Protein p53 (TP53) and Phosphatase and Tensin homolog (PTEN).[43–45] Mutations in the RAS genes are among the most common mutations in CRC and are present in approximately 50% of all CRC patients.[46] These mutations result in a permanently activated mitogen-activated protein kinase (MAPK) cascade that no longer relies on upstream signals from the EGFR or other receptor tyrosine kinases. Therefore, mutational status of KRAS is being used to exclude anti-EGFR therapy. Downstream of

KRAS are the 3 RAF kinases (ARAF, BRAF and CRAF/RAF1), which in turn also activate the MAPK pathway, which is a critical cell signaling pathway, involved in many cellular processes, including proliferation, differentiation, survival and apoptosis. The BRAF gene carries activating mutations in 10% of CRC and inhibition of BRAF in combination with EGFR- and/or MEK- inhibitors showed promising results in the clinic.[47,48] Despite the fact that both ARAF and RAF1 can replace BRAF in activating the MEK-ERK pathway, these two other RAF kinases have received little attention in CRC research, mostly due to the absence of activating mutations in these genes. Interestingly, micro-array data show that RAF1 is highly expressed in human CRC.[49–51] In chapter 6, we investigated the role of RAF1 in CRC. Knockdown or pharmalogical inhibition of RAF1 reduced tumor growth, impaired clonogenic capacity and partially restored normal colonic architecture.

References

1. Bray F, Ferlay J, Soerjomataram I, Siegel RL, Torre LA, Jemal A. Global cancer statistics 2018: GLOBOCAN estimates of incidence and mortality worldwide for 36 cancers in 185 countries. *CA Cancer J Clin*. 2018. doi:10.3322/caac.21492
2. Arnold M, Sierra MS, Laversanne M, Soerjomataram I, Jemal A, Bray F. Global patterns and trends in colorectal cancer incidence and mortality. *Gut*. 2017. doi:10.1136/gutjnl-2015-310912
3. Riihimaki M, Hemminki A, Sundquist J, Hemminki K. Patterns of metastasis in colon and rectal cancer. *Sci Rep*. 2016. doi:10.1038/srep29765
4. Hackl C, Neumann P, Gerken M, Loss M, Klinkhammer-Schalke M, Schlitt HJ. Treatment of colorectal liver metastases in Germany: A ten-year population-based analysis of 5772 cases of primary colorectal adenocarcinoma. *BMC Cancer*. 2014. doi:10.1186/1471-2407-14-810
5. Ye LC, Liu TS, Ren L, et al. Randomized controlled trial of cetuximab plus chemotherapy for patients with KRAS wild-type unresectable colorectal liver-limited metastases. *J Clin Oncol*. 2013. doi:10.1200/JCO.2012.44.8308
6. Lam VWT, Spiro C, Laurence JM, et al. A systematic review of clinical response and survival outcomes of downsizing systemic chemotherapy and rescue liver surgery in patients with initially unresectable colorectal liver metastases. *Ann Surg Oncol*. 2012. doi:10.1245/s10434-011-2061-0
7. Koopman M, Antonini NF, Douma J, et al. Sequential versus combination chemotherapy with capecitabine, irinotecan, and oxaliplatin in advanced colorectal cancer (CAIRO): a phase III randomised controlled trial. *Lancet*. 2007. doi:10.1016/S0140-6736(07)61086-1
8. Goldberg RM, Sargent DJ, Morton RF, et al. A randomized controlled trial of fluorouracil plus leucovorin, irinotecan, and oxaliplatin combinations in patients with previously untreated metastatic colorectal cancer. *J Clin Oncol*. 2004. doi:10.1200/JCO.2004.09.046
9. Colucci G, Gebbia V, Paoletti G, et al. Phase III randomized trial of FOLFIRI versus FOLFOX4 in the treatment of advanced colorectal cancer: A Multicenter Study of the Gruppo Oncologico Dell'Italia Meridionale. *J Clin Oncol*. 2005. doi:10.1200/JCO.2005.07.113
10. André T, Boni C, Mounedji-Boudiaf L, et al. Oxaliplatin, Fluorouracil, and Leucovorin as Adjuvant Treatment for Colon Cancer. *N Engl J Med*. 2004;350(23):2343-2351. doi:10.1056/NEJMoa032709
11. Böckelman C, Engelmann BE, Kaprio T, Hansen TF, Glimelius B. Risk of recurrence in patients with colon cancer stage II and III: A systematic review and meta-analysis of recent literature. *Acta Oncol (Madr)*. 2015. doi:10.3109/0284186X.2014.975839
12. Edge SB, Fritz AG, Byrd DA, Greene FL, Trotty A, Compton CC. *AJCC Cancer Staging Manuel, 7th Edition*.; 2010. doi:10.1007/978-1-4757-3656-4
13. Ribic CM, Sargent DJ, Moore MJ, et al. Tumor Microsatellite-Instability Status as a Predictor of Benefit from Fluorouracil-Based Adjuvant Chemotherapy for Colon Cancer. *N Engl J Med*. 2003. doi:10.1056/NEJMoa022289
14. Jo WS, Carethers JM. Chemotherapeutic implications in microsatellite unstable colorectal cancer. *Cancer Biomarkers*. 2006. doi:10.3233/CBM-2006-21-206

15. De Roock W, Claes B, Bernasconi D, et al. Effects of KRAS, BRAF, NRAS, and PIK3CA mutations on the efficacy of cetuximab plus chemotherapy in chemotherapy-refractory metastatic colorectal cancer: A retrospective consortium analysis. *Lancet Oncol*. 2010. doi:10.1016/S1470-2045(10)70130-3
16. Sadanandam A, Lyssiotis CA, Homicsko K, et al. A colorectal cancer classification system that associates cellular phenotype and responses to therapy. *Nat Med*. 2013. doi:10.1038/nm.3175
17. Muzny DM, Bainbridge MN, Chang K, et al. Comprehensive molecular characterization of human colon and rectal cancer. *Nature*. 2012. doi:10.1038/nature11252
18. Roepman P, Schlicker A, Tabernero J, et al. Colorectal cancer intrinsic subtypes predict chemotherapy benefit, deficient mismatch repair and epithelial-to-mesenchymal transition. *Int J Cancer*. 2013. doi:10.1002/ijc.28387
19. Perez Villamil B, Romera Lopez A, Hernandez Prieto S, et al. Colon cancer molecular subtypes identified by expression profiling and associated to stroma, mucinous type and different clinical behavior. *BMC Cancer*. 2012. doi:10.1186/1471-2407-12-260
20. De Sousa E Melo F, Wang X, Jansen M, et al. Poor-prognosis colon cancer is defined by a molecularly distinct subtype and develops from serrated precursor lesions. *Nat Med*. 2013. doi:10.1038/nm.3174
21. Budinska E, Popovici V, Tejpar S, et al. Gene expression patterns unveil a new level of molecular heterogeneity in colorectal cancer. *J Pathol*. 2013. doi:10.1002/path.4212
22. Guinney J, Dienstmann R, Wang X, et al. The consensus molecular subtypes of colorectal cancer. *Nat Med*. 2015;21(11):1350-1356. doi:10.1038/nm.3967
23. Isella C, Terrasi A, Bellomo SE, et al. Stromal contribution to the colorectal cancer transcriptome. *Nat Genet*. 2015. doi:10.1038/ng.3224
24. Calon A, Lonardo E, Berenguer-Llergo A, et al. Stromal gene expression defines poor-prognosis subtypes in colorectal cancer. *Nat Genet*. 2015. doi:10.1038/ng.3225
25. Spaderna S, Schmalhofer O, Hlubek F, et al. A Transient, EMT-Linked Loss of Basement Membranes Indicates Metastasis and Poor Survival in Colorectal Cancer. *Gastroenterology*. 2006. doi:10.1053/j.gastro.2006.06.016
26. Singh A, Settleman J. EMT, cancer stem cells and drug resistance: An emerging axis of evil in the war on cancer. *Oncogene*. 2010. doi:10.1038/onc.2010.215
27. Miles FL, Sikes RA. Insidious Changes in Stromal Matrix Fuel Cancer Progression. *Mol Cancer Res*. 2014. doi:10.1158/1541-7786.MCR-13-0535
28. Hansen TF, Kjær-Frifeldt S, Lindebjerg J, et al. Tumor–stroma ratio predicts recurrence in patients with colon cancer treated with neoadjuvant chemotherapy. *Acta Oncol (Madr)*. 2018. doi:10.1080/0284186X.2017.1385841
29. Mesker WE, Junggeburt JMC, Szuhai K, et al. The carcinoma-stromal ratio of colon carcinoma is an independent factor for survival compared to lymph node status and tumor stage. *Cell Oncol*. 2007. doi:10.1155/2007/175276

30. Krishna R, Mayer LD. Multidrug resistance (MDR) in cancerMechanisms, reversal using modulators of MDR and the role of MDR modulators in influencing the pharmacokinetics of anticancer drugs. *Eur J Pharm Sci*. 2000. doi:10.1016/S0928-0987(00)00114-7
31. Holohan C, Van Schaeybroeck S, Longley DB, Johnston PG. Cancer drug resistance: An evolving paradigm. *Nat Rev Cancer*. 2013. doi:10.1038/nrc3599
32. LeDran H, Gataker T, Chelsden W HC and DR. *Traite Des Operations de Chirurgie*.; 1752.
33. Rosenberg R, Friederichs J, Schuster T, et al. Prognosis of patients with colorectal cancer Is associated with lymph node ratio a single-center analysis of 3026 patients over a 25-year time period. *Ann Surg*. 2008. doi:10.1097/SLA.0b013e318190eddc
34. Beckurts KTE, Hölscher AH, Thorban S, Bollschweiler E, Siewert JR. Significance of lymph node involvement at the hepatic hilum in the resection of colorectal liver metastases. *Br J Surg*. 1997. doi:10.1002/bjs.1800840811
35. Bennett JJ, Schmidt CR, Klimstra DS, et al. Perihepatic lymph node micrometastases impact outcome after partial hepatectomy for colorectal metastases. In: *Annals of Surgical Oncology*. ; 2008. doi:10.1245/s10434-007-9802-0
36. Oussoultzoglou E, Romain B, Panaro F, et al. Long-term survival after liver resection for colorectal liver metastases in patients with hepatic pedicle lymph nodes involvement in the era of new chemotherapy regimens. *Ann Surg*. 2009. doi:10.1097/SLA.0b013e3181a334d9
37. Jaeck D, Nakano H, Bachellier P, et al. Significance of hepatic pedicle lymph node involvement in patients with colorectal liver metastases: A prospective study. *Ann Surg Oncol*. 2002. doi:10.1245/aso.2002.9.5.430
38. Elias D, Sideris L, Pocard M, et al. Results of R0 resection for colorectal liver metastases associated with extrahepatic disease. *Ann Surg Oncol*. 2004. doi:10.1245/ASO.2004.03.085
39. Elias D, Ouellet JF, Bellon N, Pignon JP, Pocard M, Lasser P. Extrahepatic disease does not contraindicate hepatectomy for colorectal liver metastases. *Br J Surg*. 2003. doi:10.1002/bjs.4071
40. Hodgson R, Sethi H, Ling AH, Lodge P. Combined hepatectomy and hepatic pedicle lymphadenectomy in colorectal liver metastases is justified. *HPB*. 2017. doi:10.1016/j.hpb.2017.01.025
41. Grobmyer SR, Wang L, Gonen M, et al. Perihepatic lymph node assessment in patients undergoing partial hepatectomy for malignancy. *Ann Surg*. 2006. doi:10.1097/01.sla.0000217606.59625.9d
42. Pindak D, Pavlendova J, Tomas M, Dolnik J, Duchon R, Pechan J. Selective versus routine lymphadenectomy in the treatment of liver metastasis from colorectal cancer: a retrospective cohort study. *BMC Surg*. 2017. doi:10.1186/s12893-017-0233-y
43. Vogelstein B, Papadopoulos N, Velculescu VE, Zhou S, Diaz LA, Kinzler KW. Cancer genome landscapes. *Science (80-)*. 2013. doi:10.1126/science.1235122
44. Vogelstein B, Fearon ER, Hamilton SR, et al. Genetic Alterations during Colorectal-Tumor Development. *N Engl J Med*. 1988. doi:10.1056/NEJM198809013190901
45. Fearon ER, Vogelstein B. A genetic model for colorectal tumorigenesis. *Cell*. 1990. doi:10.1016/j.freeradbiomed.2005.06.014

46. Sorich MJ, Wiese MD, Rowland A, Kichenadasse G, McKinnon RA, Karapetis CS. Extended RAS mutations and anti-EGFR monoclonal antibody survival benefit in metastatic colorectal cancer: A meta-analysis of randomized, controlled trials. *Ann Oncol*. 2015. doi:10.1093/annonc/mdu378
47. Van Geel RMJM, Tabernero J, Elez E, et al. A phase Ib dose-escalation study of encorafenib and cetuximab with or without alpelisib in metastatic BRAF-mutant colorectal cancer. *Cancer Discov*. 2017. doi:10.1158/2159-8290.CD-16-0795
48. Corcoran RB, Andre T, Atreya CE, et al. Research article combined BRAF, EGFR, and MEK inhibition in patients with BRAFV600E-mutant colorectal cancer. *Cancer Discov*. 2018. doi:10.1158/2159-8290.CD-17-1226
49. Marisa L, de Reyniès A, Duval A, et al. Gene Expression Classification of Colon Cancer into Molecular Subtypes: Characterization, Validation, and Prognostic Value. *PLoS Med*. 2013. doi:10.1371/journal.pmed.1001453
50. Jorissen RN, Gibbs P, Christie M, et al. Metastasis-associated gene expression changes predict poor outcomes in patients with Dukes stage B and C colorectal cancer. *Clin Cancer Res*. 2009. doi:10.1158/1078-0432.CCR-09-1431
51. Smith JJ, Deane NG, Wu F, et al. Experimentally Derived Metastasis Gene Expression Profile Predicts Recurrence and Death in Patients With Colon Cancer. *Gastroenterology*. 2010. doi:10.1053/j.gastro.2009.11.005

CHAPTER 2

2

Collagen-rich stroma in aggressive colon tumors induces mesenchymal gene expression and tumor cell invasion

Thomas T. Vellinga, Sjoerd den Uil, Inne H.M. Borel Rinkes, Dieuwke Marvin, Bas Ponsioen, Adrian Alvarez-Varela, Szabolcs Fatrai, Cornelia Scheele, Danny A. Zwijnenburg, Hugo Snippert, Louis Vermeulen, Jan-Paul Medema, Hein Stockmann, Jan Koster, Remond J.A. Fijneman, Johan de Rooij, Onno Kranenburg

Oncogene. 2016 Oct 6;35(40):5263-5271

Abstract

Gene expression-based classification systems have identified an aggressive colon cancer subtype with mesenchymal features, possibly reflecting epithelial-to-mesenchymal transition (EMT) of tumor cells. However, stromal fibroblasts contribute extensively to the mesenchymal phenotype of aggressive colon tumors, challenging the notion of tumor EMT. To separately study the neoplastic and stromal compartments of colon tumors we have generated a Stroma Gene Filter (SGF). Comparative analysis of stromahigh and stromalow tumors shows that the neoplastic cells in stromahigh tumors express specific EMT drivers (ZEB2, TWIST1, TWIST2) and that 98% of differentially expressed genes are strongly correlated with them. Analysis of differential gene expression between mesenchymal and epithelial cancer cell lines revealed that Hepatocyte Nuclear Factor 4α (HNF4α), a transcriptional activator of intestinal (epithelial) differentiation, and its target genes are highly expressed in epithelial cancer cell lines. However, mesenchymal-type cancer cell lines expressed only part of the mesenchymal genes expressed by tumor-derived neoplastic cells, suggesting that external cues were lacking. We found that collagen-I dominates the extracellular matrix in aggressive colon cancer. Mimicking the tumor microenvironment by replacing laminin-rich Matrigel with collagen-I was sufficient to induce tumor specific mesenchymal gene expression, suppression of HNF4α and its target genes, and collective tumor cell invasion of patient-derived colon tumor organoids. The data connect collagen-rich stroma to mesenchymal gene expression in neoplastic cells and to collective tumor cell invasion. Targeting the tumor-collagen interface may therefore be explored as a novel strategy in the treatment of aggressive colon cancer.

Introduction

Gene expression profiling has recently been used to identify distinct molecular subtypes in colon cancer.[4, 12, 25, 26, 31, 33, 34, 38] Of particular interest are the molecular subtypes with a high propensity to form distant metastases, which couples specific aspects of tumor biology to metastasis and survival. Several independent studies have shown that metastasis-prone colon cancer is characterized by atypical gene expression patterns reflecting I) a more primitive stem-like phenotype[25, 34] and II) a mesenchymal phenotype[21, 33, 38]. Recent data indicate that the stem-like and mesenchymal tumor subtypes are highly related[12, 35], which is in line with the notion that epithelial-mesenchymal-transition (EMT) of tumor cells generates aggressive stem-like cancer cells.[17, 24, 46] Until recently, one aspect of colon cancer biology has remained relatively underexposed in the various classification studies: the gene expression profiles in these studies were generated from RNA that was isolated from unsegregated tumor tissue. This raises the possibility that some of the classifier-genes may be predominantly expressed in the stromal compartment and that stromal cells need to be taken into account when interpreting the differences in biology that are reflected by the differences in gene expression. For instance, colon tumors with microsatellite instability (MSI) are characterized by inflammatory gene expression,[35] reflecting the high levels of infiltrating immune cells in such tumors.[2, 32] Moreover, two recent studies have shown that stromal cells extensively contribute to the mesenchymal phenotype of poor prognosis colon tumors and to their signature-based identification. [7, 18] Indeed, a high content of tumor stroma, as judged by histology, had previously been associated with early relapse in colon cancer.[27, 28] Together, these studies challenge the notion that tumor cell EMT is the biological basis for the aggressive tumor phenotype. However, neither study has provided insight into the tumor cell-specific differences in gene expression in stroma^{high} versus stroma^{low} tumors.[7, 18] Therefore, we set out to examine the link between high stromal content and tumor cell EMT in aggressive colon cancer. We confirm that the mesenchymal nature of aggressive colon tumors is to a large extent determined by tumor stroma. We further show that the neoplastic compartment of stroma^{high} tumors is characterized by expression of a specific set of mesenchymal genes that is distinct from that expressed by stromal cells. We identify collagen-I as a causal link between high stromal content, mesenchymal gene expression in tumor cells, and collective tumor cell invasion.

Materials and methods

Experimental Design

To assess the contribution of stromal cells and tumor EMT to the mesenchymal phenotype of poor prognosis colon cancer, a stroma gene filter (SGF) was generated. The SGF was used to separate the gene sets that are predominantly expressed in the neoplastic and stromal compartments of colon tumors. In addition, we used gene expression profiles from previously classified cell lines. Comparative analysis of mesenchymal protein expression in tumor and stromal cells was performed on a large tissue micro-array. For *in vitro* experiments we used patient-derived organoid cultures and a recently developed system for studying colon cancer EMT.[5, 13, 22, 40]

Bioinformatics analyses

All bioinformatics analyses were performed using the genomics analysis and visualization platform (r2.amc.nl). For details see Supplemental Materials and Methods.

Organoid culture

Colon cancer organoids were established and cultured as described.[5, 13, 22, 40] In accordance with the local ethical committee on human experimentation (protocol #09-145). Informed consent was obtained from all patients.

Collagen-invasion assay

Tumor organoids were cultured either in Matrigel (standard protocol) or in collagen-I (1.5 mg/ml mixed with standard culture medium; Ibidi). To avoid interaction with the plastic/glass bottom of the plate, a bottom layer of 2 mg/ml collagen-I dissolved in PBS was generated. A drop of organoid-containing collagen was placed on top of the bottom layer. After 2 hours polymerization at 37 degrees standard culture medium was added. For the supplemental movies standard culture medium was conditioned for 24 hours on freshly isolated cancer associated fibroblasts and filtered before use (stimulates invasion). The RNA used in RT-qPCRs was extracted from organoids cultured in either Matrigel or Collagen-I in standard culture medium. Data shown is a representation of 3 independent experiments with depicted the mean and s.e.m., the student t test (unpaired, 2-tailed) was performed to analyze statistically significant differences between groups.

Immunofluorescence

Organoids in collagen-I were fixed with 4% formaldehyde for 20 min at room temperature followed by permeabilization with 2% Triton X-100 for 1h. Lumican staining was performed overnight with an anti-Lumican antibody (ab168348, Abcam) and Alexa-568-conjugated secondary antibody (Invitrogen, A-11011). Nuclei were counterstained with DAPI. Stained

coverslips were analyzed using a Leica SP8 confocal microscope. Images were analyzed using ImageJ software (NIH).

Immunohistochemistry

TMA sections were constructed from formalin-fixed and paraffin-embedded (FFPE) tumor tissue of 386 stage II and III colon cancer patients, as described earlier.[5, 13, 22, 40] TMA slides were deparraffinized and rehydrated, and after antigen retrieval in a microwave incubated with antibodies directed against HTR2B (Sigma, HPA012867) 1:400 or SPARC (Invitrogen, 33-550) 1:300 for 1 hour at room temperature. The secondary antibodies were from htVision (ImmunoLogic). For Versican staining, antigens were retrieved by microwaving for 30 min at 90W in 10 mM citrate buffer solution (pH 6.0). Primary mouse anti-versican antibody (clone 2-B-1, Seikagaku, Tokyo, Japan) was incubated at a 1:300 dilution in phosphate-buffered saline containing 1 % bovine serum albumin and 0.1 % Tween 20 (Sigma-Aldrich, St. Louis, MO, USA) at 4°C overnight, and subsequently detected by a horseradish peroxidase– coupled anti-mouse polymer (Envision, Dako, Heverlee, Belgium) followed by incubation with diaminobenzidine (Dako). For Lumican staining, antigens were retrieved by autoclaving in 10 mM Tris/1 mM EDTA buffer (pH 9.0). The primary rabbit anti-lumican antibody (HPA001522; Atlas Antibodies, Stockholm, Sweden) was incubated at a dilution of 1:50 in antibody diluent (Dako) overnight at 4°C. Staining was detected by incubation with a horseradish peroxidase–coupled anti-rabbit polymer and incubation with diaminobenzidine (Dako). All sections were counterstained with Mayer hematoxylin. Sections were glass covered and scanned for digital immunohistochemical evaluation as described earlier.[5, 13, 22, 40]

EMT assay

L145 colonospheres expressing either GFP or mCherry were co-cultured with the EMT-inducing cell line 'Differentiated Tumor Cell line-1' (DTC1) for 48 hours.[5, 13, 22, 40] FACS sorting of GFP or mCherry positive cells was performed prior to analysis (RT-qPCR) of the expression of mesenchymal and epithelial markers.

RTqPCR

Total RNA was isolated from tumor organoids according to the manufacturer's protocol (RNeasy Mini Kit, Qiagen). cDNA was synthesized using iScriptcDNA Synthesis Kit (Bio-Rad Laboratories). Amplification was performed in an iCyclerthermocycler (Bio-Rad Laboratories) using iQ SYBR Green Supermix (Bio-Rad Laboratories). mRNA expression levels were quantified using iCycler software (Bio-Rad Laboratories) and were normalized to rpl13a.

Statistical Analysis

For the various statistical tests used in the bioinformatics analyses see the respective section in the Supplementary Methods. The chi-square test was used to assess the association of expression values of Lumican, Versican and SPARC in the tumor and stroma compartments, as quantified by immunohistochemistry. The student's t-test was used to assess the statistical significance of differences in RT-qPCR values.

Results

A stroma gene filter

To identify the source of mesenchymal gene expression in relapse-prone colon tumors we identified all genes that are predominantly expressed by human tumor stroma. Transplantation of human tumors into mice leads to the replacement of human tumor stroma with that of mouse origin. Therefore, we analyzed expression profiles generated from 39 primary colorectal tumors and their paired xenografts[20] and identified a set of 3105 genes whose expression was significantly lower upon transplantation ($p<e-6$; Figure 1a and Supplementary Table S1). This list contains genes that I) are predominantly expressed by stromal cells and II) genes that are expressed in tumor cells but require the presence of human stroma. To identify the subset of genes that are predominantly expressed by stromal cell types we used gene expression profiles generated from FACS- or Laser Capture Microdissection (LCM)-purified tumor-derived fibroblasts and immune cells.[6, 30] Of the 3105 'down-in-xenograft' genes approximately half (1576 genes; Supplementary Table S1) were predominantly expressed by stromal fibroblasts, immune cells, or both (Figure 1b and c). Thus, expression of these genes is largely lost in xenografts *and* is predominantly expressed in purified stromal cell types. We refer to this gene list as the 'stroma gene filter' (SGF). The remaining genes of the 'down-in-XG' list (1529 genes) were highly expressed in tumor cells, but in a human stroma-dependent manner, as their expression is lost in xenografts (Figure 1c).

To further validate the SGF we compared its expression to an independently generated and recently published 141-gene stroma signature, called Estimate.[48] There was an excellent correlation between the Estimate gene set and the SGF in three independent large colon tumor datasets (Figure 1d). [19, 25, 26, 39] The SGF was significantly higher expressed in mesenchymal-type (CCS3) and stem-like colon tumor subtypes than in the other subtypes (Figure 1d, inset and Supplementary Figure S1). This is line with the recent findings that stromal gene expression defines such tumors[7, 18] and that the mesenchymal and stem-like molecular subtypes are highly related.[35]

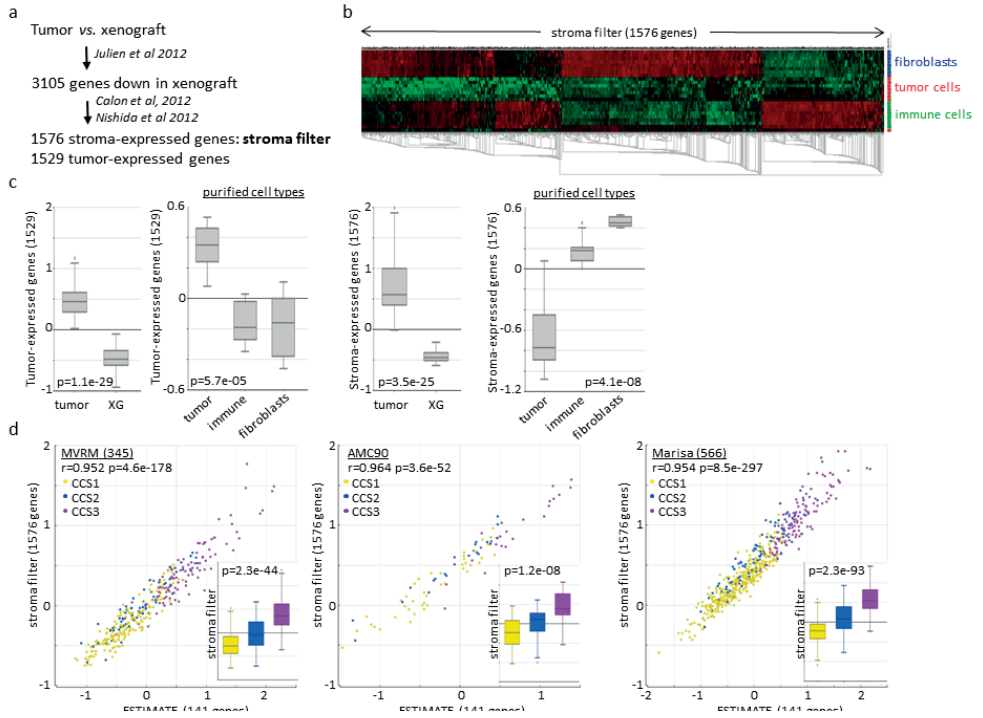

Figure 1

High expression of stromal genes in mesenchymal-type colon cancer.

(a) Strategy for the generation of the Stroma Gene Filter (SGF). (b) Heatmap of the expression of SGF genes in purified colon cancer cell types using dataset GSE39395. Red denotes high expression; Green denotes low expression. (c) Gene expression profiles generated from FACS- or Laser Capture Micro-dissection-purified tumor cell subtypes (GSE39395; GSE35602) were used to separate the genes that are significantly down-regulated in tumor xenografts (3105 genes; E-MTAB-991) into two separate categories: First, genes that are predominantly expressed by tumor cells (1529 genes, left two panels). Second, genes that are predominantly expressed by stromal cells (1576 genes, right two panels). The latter is referred to as the SGF. (d) Expression of the 1576 SGF genes and the 141 genes making up the Estimate stroma-indicator were condensed into a single metagene expression value in R2. The dotplots show the correlation of SGF expression (all stroma-derived genes) with the stroma signature in relation to tumor subtypes in three large tumor cohorts. The inset shows expression values of the SGF in the different tumor subtypes. Yellow: epithelial, CCS1; Blue: MSI, CCS2; Purple: Mesenchymal-like, CCS3.

A tumor cell-specific mesenchymal gene expression program in stroma^{high} tumors

Stroma-expressed genes[48] can separate colon tumor cohorts into subgroups with markedly different disease-free survival times (Figure 2a, see also[7, 18]). The stroma^{high} group contained the vast majority of previously classified mesenchymal-type (>90%) and stem-like (>95%) tumors (Figure 2b), further connecting high stromal gene expression to recurrence-prone colon cancer subtypes. This raises the question whether the mesenchymal nature of

such tumors is due to high stromal content, to tumor cell EMT, or to both. To address this, we identified the gene expression differences between the stroma^{high} and stroma^{low} tumor subgroups (p<e-6; 2534 genes; Supplementary Table S2). Next, we used the SGF to distinguish between tumor-expressed (1631) and stroma-expressed (903) genes (Figure 2b and Supplementary Table S2). Of the 1631 tumor-expressed genes, 925 were enriched in the stroma^{high} tumors and 706 were enriched in the stroma^{low} tumors. To interpret the biology reflected by these gene lists we used the DAVID functional annotation tool.[15, 16] These analyses revealed that the tumor compartment of the stroma^{high} group was enriched in gene ontology (GO)-terms reflecting tumor cell adhesion and migration (Supplementary Table S3), while the stroma^{low} group was enriched in GO-terms reflecting tumor metabolic and biosynthetic processes (Supplementary Table S3). Although EMT was not present in the list of enriched GO-terms in the stroma^{high} group we found that the core EMT-inducing transcription factors ZEB2, TWIST1 and TWIST2 were among the top 15% of genes that were highly expressed by tumor cells in stroma^{high} tumors, as were TGFβ1 and TGFβ2 (highlighted in Supplementary Table S2). To gain further insight into a possible relationship between high stromal content and EMT in the tumor compartment we analyzed which of the 1631 genes that were differentially expressed in the tumor compartment of stroma^{high} and stroma^{low} tumors were correlated with the three tumor-specific EMT drivers (ZEB2/TWIST1/TWIST2; Supplementary Table S4). Strikingly, almost all of these genes (1597; 98%) were highly significantly correlated with the ZEB2/TWIST1/TWIST2 gene set (p<e-6), either in a positive fashion (910 genes; reflecting a mesenchymal phenotype) or in a negative fashion (687 genes; reflecting an epithelial phenotype) (Figure 2b and Supplementary Table S4). Without exception, the 910 genes reflecting a mesenchymal tumor cell phenotype were high in the stroma^{high} subgroup, whereas all 687 genes reflecting a more epithelial phenotype were high in the stroma^{low} subgroup (Figure 2b and c). Finally, the 910 mesenchymal genes identified a poor prognosis subgroup of colon tumors containing 92% (93/101) of the tumors that were previously classified as CCS3 and 93% (125/134) of the stroma^{high} tumors (Figure 2d and e).

Together, these data show that separation of colon tumors on the basis of stromal gene expression links high stromal content to poor prognosis and a tumor compartment that is characterized by mesenchymal gene expression, increased cell-matrix adhesion, and tumor cell migration.

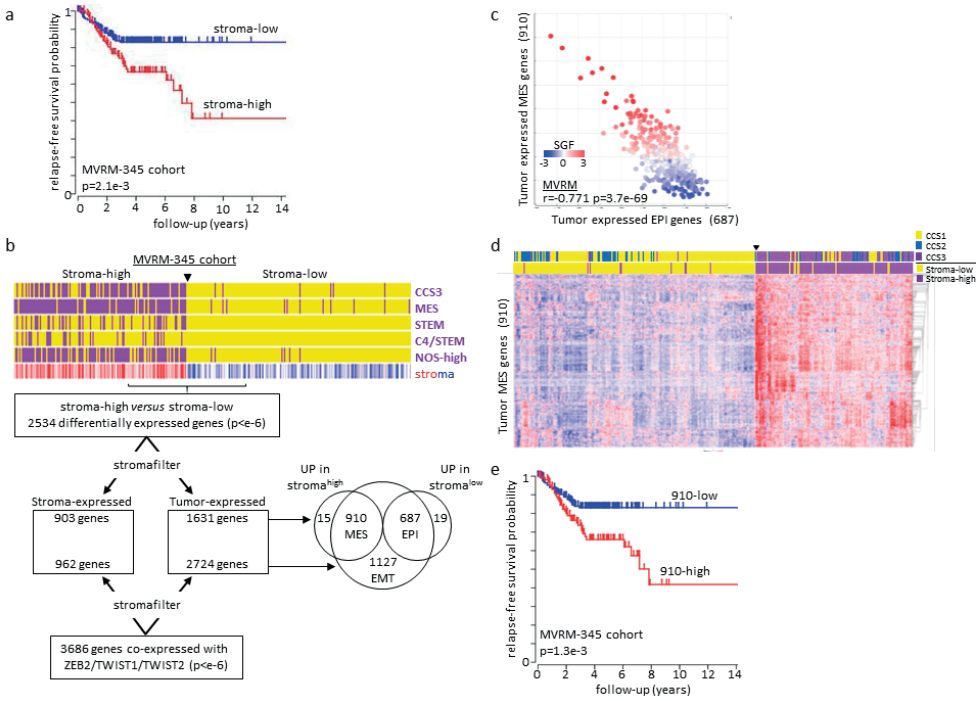

Figure 2

Identification of a mesenchymal gene expression program in the tumor compartment of stroma-high colon tumors.

(a) The 141-gene Estimate signature was used to cluster the 345 tumors of the MVRM cohort (batch-corrected datasets GSE14333, GSE17536, GSE17537) into two groups: those with low and high expression of stromal genes. The Kaplan Meier curve shows the differences in disease-free survival between the generated groups. (b) The tumors in the MVRM cohort were clustered into subgroups using published gene sets. Tumors that were classified as 'stem' and 'mesenchymal'-like tumors by each of these signatures are indicated in purple. NOS refers to Nanog/Oct4/Sox2. The plot shows the distribution of such tumors over the stroma-high and stroma-low tumor subgroups. Expression of the SGF in each of the tumors is color coded from blue (low) to red (high). All significantly differentially expressed genes between stroma-high and stroma-low tumors were identified with R2 and the SGF was used to discriminate between genes that are predominantly expressed by tumor cells (1631 genes) and by stromal cells (903 genes). The list of 1631 differentially expressed genes in tumor cells was compared to a list of all genes significantly co-expressed with ZEB2, TWIST1 and TWIST2 in the tumor compartment (2724 genes; Supplementary Table S6). 1597/1634 genes (98%) was correlated with ZEB2/TWIST1/TWIST2 expression. Without exception, all mesenchymal genes (910) were high in the stroma-high subgroup and all epithelial genes (687) were high in the stroma-low group. (c) Dot-plot showing the inverse correlation between the tumor-expressed epithelial and mesenchymal gene sets in relation to stromal content (blue=low; red=high). (d) The 910 tumor cell-expressed mesenchymal genes were used to cluster the 345 tumors of the MVRM cohort into two subgroups. The previous Estimate- and CCS-based classification of the same tumors is shown on the top. (e) The Kaplan Meier curve shows the differences in disease-free survival between the two groups generated in (d).

Mesenchymal gene expression in cancer-associated fibroblasts and in tumor cells after EMT

A surprising finding was that the mesenchymal gene expression programs in stromal cells and tumor cells were so clearly separable, yet highly correlated. One of the markers that is used to identify mesenchymal-type colon cancers on histology is ZEB1,[26, 34] which is part of the SGF (Supplementary Table S1) and is predominantly expressed by stromal cells.[18] Therefore, we analyzed how ZEB1 and N-cadherin expression levels in colon tumor cells after EMT in relation to expression of these genes in cancer-associated fibroblasts (CAFs). CAFs were freshly isolated from colon tumors and were expanded in vitro. We recently developed a co-culture system in which differentiated tumor cells (DTCs) induce EMT in colonosphere cultures (Supplementary Figure S2a).[11] This resulted in classical features of EMT, including loss of E-cadherin (CDH1) expression, increased expression of CDH2, ZEB1, ZEB2, SNAI1, and VIM and deposition of FN1 at the colonosphere/DTC interface (Supplementary Figure S2b-d). However, RT-qPCR analysis showed that the expression of CDH2, VIM and FN1 in tumor cells after EMT was still ~50-500-fold lower than expression of these genes in multiple CAF cultures (Supplementary Figure S2e). These results show that small amounts of stromal fibroblasts could easily mask the differential expression of classical mesenchymal markers in the neoplastic compartment when analyzing EMT in unsegregated tumor material.

Identification of stroma^{high} colon tumors by mesenchymal genes expressed in cancer cell lines

If an EMT program is active in the tumor compartment it may also be identifiable in (stroma-free) colon cancer cell lines. We made use of the Broad panel of colon cancer cell lines that had previously been classified into molecular subtypes.[26] We identified 917 genes that were significantly differentially expressed between epithelial (CCS1-type; n=27) and mesenchymal (CCS3-type; n=19) cell lines of the Broad panel (Supplementary Table S5; ANOVA $p<0.01$). Of these, 305 genes were higher in CCS3 cell lines and 612 were higher in CCS1 cell lines. Applying the SGF to these gene sets revealed that the majority (196; 64%) of the 305 mesenchymal genes and almost all (602/612) of the epithelial genes were predominantly expressed in the tumor compartment of unsegregated tumors. In human colon tumors there was a highly significant correlation between the cell-line derived mesenchymal gene set (n=196), the tumor-expressed mesenchymal gene set (n=910) and the Estimate stroma-identifier (Figure 3a). Together the data firmly connect mesenchymal gene expression in the neoplastic compartment to a stroma-high context.

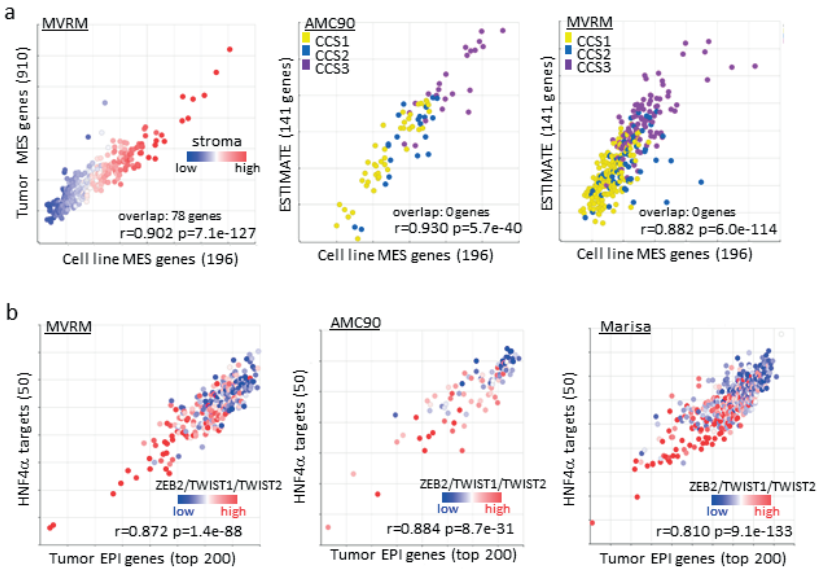

Figure 3

Tumor-specific mesenchymal gene expression is positively correlated with stroma and negatively with HNF4α target genes.

(a) First dotplot shows the correlation between tumor-expressed mesenchymal gene sets I) identified by applying the SGF to gene expression data of unsegregated tumors and II) identified in previously classified tumor cell lines. Second two dotplots show the correlation between tumor cell line-derived mesenchymal genes and the Estimate stroma identifier in two large colon tumor cohorts. (b) Transcription factor binding site analysis of the genes differentially expressed between CCS1 and CCS3 tumor cell lines identified HNF4α target genes to be overrepresented in CCS1 cell lines (Supplementary Table S6). The dotplots show the positive correlation of expression of the identified 50 HNF4α target genes with a previously identified set of 200 genes reflecting epithelial differentiation,[10] in relation to the tumor-specific expression of EMT drivers in three large colon tumor cohorts.

HNF4α target genes and colon cancer differentiation

Transcription factor binding site analysis of the promoters of the 917 genes differentially expressed between CCS1 and CCS3 cell lines revealed that genes with promoters containing binding sites for Hepatocyte Nuclear Factor 4-alpha (HNF4α were most significantly enriched (Supplementary Figure S3 and Supplementary Table S6). The vast majority of HNF4α target genes (50/56) were overexpressed in CCS1-type cell lines (Supplementary Figure S3). Interestingly, HNF4α is a transcriptional activator of genes inducing intestinal (epithelial) differentiation.[3, 23, 42] In addition, HNF4α suppresses mesenchymal gene expression in hepatocytes[36] and inhibits EMT and metastasis in colon cancer.[47] Furthermore, proteogenomic analysis of The Cancer Genome Atlas (TCGA) colon cancer cohort shows that mesenchymal-type colon tumors express very low levels of

HNF4α[49] We found that expression of the 50 HNF4α target genes derived from CCS1-type cell lines, were strongly and significantly correlated with a signature reflecting epithelial differentiation[10], and inversely correlated with expression of the tumor-specific EMT drivers ZEB2, TWIST1 and TWIST2 (Figure 3b), completely in line with the experimental data on HNF4α function as an inducer of epithelial differentiation genes and a suppressor of mesenchymal genes[3, 23, 36, 42, 47].

Co-expression of mesenchymal markers in tumor and stromal cells

The data so far indicate that mesenchymal gene expression in the tumor compartment correlates with high stromal content. To further validate this on tissue sections we analyzed expression of HTR2B on tissue microarrays (TMAs) containing a large series of 386 stage II and III colon tumors.[1] HTR2B is a marker of the mesenchymal subtype which is exclusively expressed by tumor cells and is part of an immunohistochemistry-based mini-classifier.[26]

Figure 4

VUmc-386 Tissue microarray	SPARC P-value	Versican P-value	Lumican P-value
HTR2B	<0.001	<0.05	<0.05

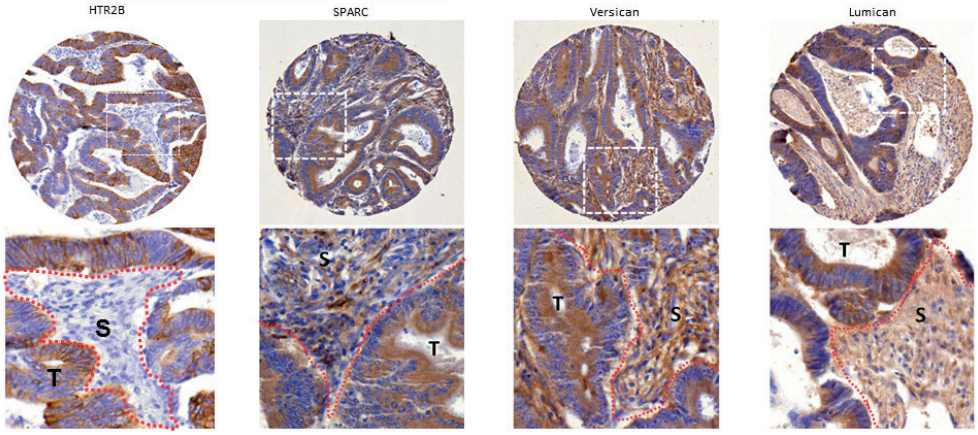

Figure 4

Co-expression of mesenchymal markers in tumor and stromal cells.

Representative TMA examples of colon tumors expressing high levels of HTR2B, VCAN, LUM and SPARC in both the tumor and stromal compartment. Significance of co-expression of these three mesenchymal markers in tumor- and stromal compartments is shown in Table 1.

Among the stainings that were previously performed on these TMAs, we searched for proteins whose expression was associated with a mesenchymal phenotype and correlated significantly with the expression of HTR2B. We found that SPARC, Versican (VCAN) and Lumican (LUM), all markers of the core EMT program defined by systems analysis[44] were

significantly co-expressed with HTR2B (all p values <0.05). In contrast to HTR2B, which is exclusively expressed by tumor cells, SPARC, VCAN and LUM are expressed by both tumor cells and stromal cells. Separate scoring of SPARC, VCAN and LUM in tumor cells and stromal cells revealed a highly significant positive correlation of the staining for each of these markers between the neoplastic and stromal compartments (Supplementary Table 1 and Figure 4). These results support the concept that the neoplastic cells in mesenchymal-type tumors express mesenchymal genes in a high-stroma context.

Table 1

VUmc-386	SPARC-tumor		Versican-tumor		Lumican-tumor	
Tissue microarry	Chi-square	P-value	Chi-square	P-value	Chi-square	P-value
SPARC-stroma	51.411	<0.001	8.061	0.528	9.606	0.383
Versican-stroma	11.095	0.269	83.610	<0.001	74.837	<0.001
Lumican-stroma	13.684	0.134	26.444	0.002	81.769	<0.001

Concordant expression of mesenchymal genes in the neoplastic and stromal compartments of colon tumors.

Expression of SPARC, Lumican (LUM) and Versican (VCAN) in the tumor and stromal compartments of 386 colon tumors were analyzed by immunohistochemistry and scored in a blinded fashion. Correlations of the staining scores for each of the markers in both compartments were subsequently analyzed by using the chi-square test.

Collagen-I promotes mesenchymal gene expression, suppresses HNF4α gene expression and stimulates tumor cell invasion

To gain insight into the relationship between stroma and tumor cell EMT we analyzed the GO-terms enriched in recurrence-prone colon tumors in more detail. 'Cell adhesion' and 'extracellular matrix (ECM)' were the GO terms that were most significantly enriched in those tumors. Collagen-I is among the most highly enriched genes in recurrence-prone tumors (Figure 5a). Collagens are predominantly produced by stromal cells, including CAFs and macrophages. To study the impact of collagen on the behavior of colon cancer cells we used the recently developed organoid technology.[37] Colon cancer organoids are usually grown in Matrigel[37] which largely consists of laminin and sheet-forming collagen IV, but lacks collagen-I. CRC organoids that are grown in Matrigel can readily be expanded and passaged but they do not grow invasively (Figure 5b and Supplementary Movie S1), not even in the presence of cancer-associated fibroblast (CAF)-conditioned medium. However, when embedded in collagen-I the CRC organoids adopt an invasive phenotype with tumor cells invading the surrounding collagen matrix (Figure 5b and c and Supplementary Movie S2). Interestingly, most single tumor cells detaching from the tumor bulk did not survive, but larger groups of tumor cells survived detachment and invaded the collagen matrix collectively (Figure 5c and d). Strikingly, RTqPCR analysis

showed that culturing organoids in collagen-I alone strongly induced the expression of the mesenchymal genes previously identified via IHC: LUM, SPARC and HTR2B as well as core EMT transcription factors ZEB1, TWIST1 and TWIST2, and tumor specific mesenchymal genes CFL2, RIT1 and FRMD6 (Figure 5e and Supplementary Table S6, highlighted genes). Next to the induction of a mesenchymal program collagen-I also suppressed the expression of HNF4α and its target genes CLRN3, GPA33, LGALS4, MYO7B and NR1I2 (Figure 6 and Supplementary Table S6, highlighted genes). These results identify collagen-I as a causal link between high stromal content, (tumor specific) mesenchymal gene expression and collective tumor cell invasion.

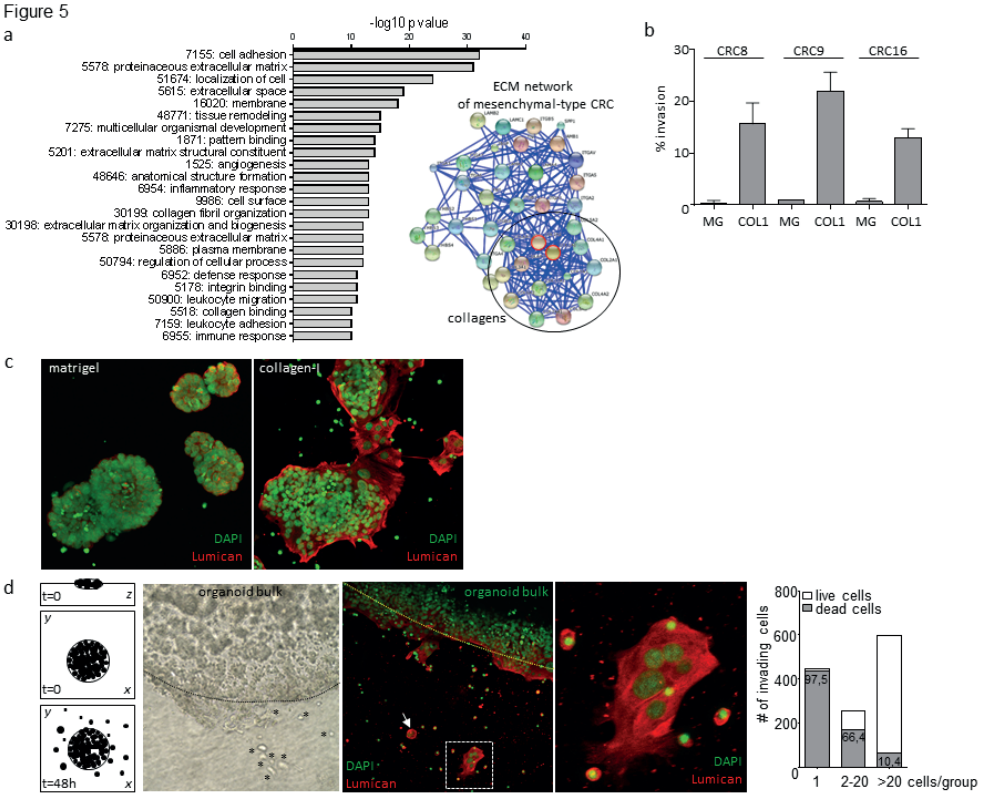

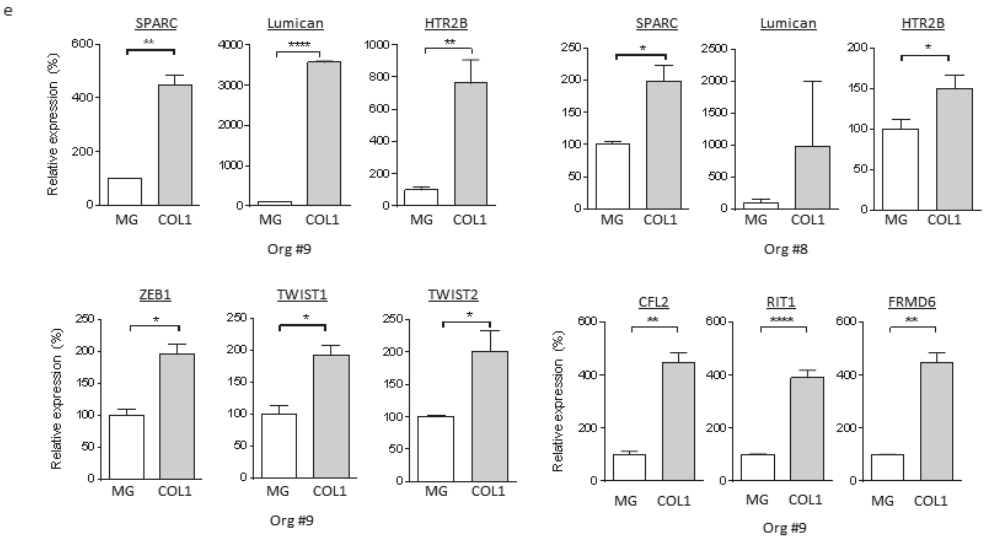

Figure 5

Collagen-I promotes mesenchymal gene expression, downregulates HNF4α and stimulates collective tumor cell invasion.

(a) Gene Ontology terms most significantly associated with mesenchymal-type tumors. The extracellular matrix in such tumors is shown as a STRING-generated network. The collagen-I chains are encircled. (b) Colon cancer organoid cultures derived from three patients were grown in Matrigel or collagen-I. Matrix invasion was quantified through morphometric analysis of the area of tumor cells outside the spherical organoid bulk. (c) Organoids were cultured either in Matrigel or in collagen-I. The organoid growth pattern and the expression of lumican was then assessed by immunofluorescence and confocal microscopy analysis. Nuclei were counterstained with DAPI. (d) A drop of collagen-I containing an organoid-initiated tumor-bulk was applied to a collagen-I base layer and was further cultured in CAF-conditioned medium for two days. Groups of tumor cells invaded the collagen base in a three-dimensional manner. Organoid invasion and expression of lumican was then assessed by immunofluorescence and confocal microscopy analysis. Nuclei were counterstained with DAPI. The number of live and dead cells outside the original collagen drop was then quantified in 36 different fields covering 672 z-positions in total. Cells with highly condensed DNA were considered dead. Dotted lines show the border between the collagen drop and the collagen-base.
(e) RNA was isolated from organoids 8 and 9 cultured in either matrigel or collagen-I for 4 days. Expression of the indicated genes was then analyzed by RT-qPCR. * $p<0.05$; ** $p<0.01$; **** $p<0.0001$

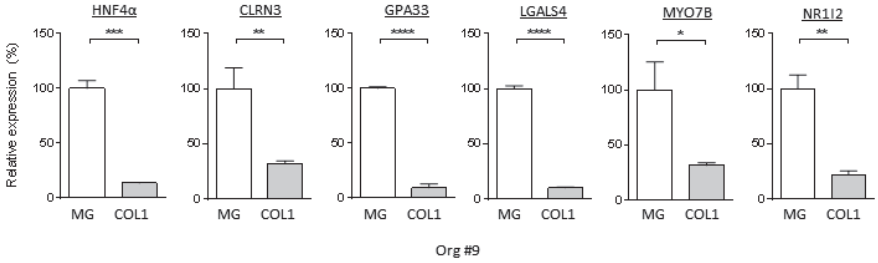

Figure 6

Collagen-I downregulates HNF4α and its target genes.

RNA was isolated from organoid 9 cultured in either matrigel or collagen-I for 4 days. Expression of the indicated genes was then analyzed by RT-qPCR. * p<0.05; ** p<0.01; *** p<0.001; **** p<0.0001..

Discussion

Multiple classification studies have reported the identification of a 'mesenchymal' colon cancer subtype, which has largely been interpreted to reflect tumor EMT. [4, 21, 26, 33, 38] More recently, this has been challenged by two reports showing that the mesenchymal nature of this tumor subgroup is largely due to the tumor stroma and that stromal genes contribute to their signature-based identification. [7, 18] Our study unifies both viewpoints by showing that the neoplastic compartment of stroma-high tumors is characterized by a distinct mesenchymal gene expression program which, similar to stroma-derived gene sets, can identify aggressive colon tumors. In fact, virtually all genes that were differentially expressed in the neoplastic compartments of stroma^{high} and stroma^{low} tumors were significantly correlated with tumor cell-expressed EMT drivers: All 910 mesenchymal genes were highly expressed in stroma^{high} tumors and all 687 epithelial genes were highly expressed in stroma^{low} tumors. Perhaps surprisingly, gene ontology and gene set enrichment analyses failed to identify EMT as a defining feature of this 910/687 gene set. This may be due to the fact that 'classical' mesenchymal genes such as CDH2, ZEB1 and FN1 were excluded from the tumor-specific gene list, through application of the stroma filter. Indeed, while these genes are clearly expressed in tumor cells after EMT, the level of expression was still one-to-several orders of magnitude lower than that in CAFs. Second, many genes in the 910/687 gene set are simply not annotated as 'EMT genes' despite their close association with ZEB2/TWIST1/TWIST2, presumably because experimentally derived gene sets reflecting EMT not necessarily overlap with mesenchymal gene expression in tumors in cancer patients. Indeed, systems analysis of EMT has shown that there is surprisingly little overlap between the mesenchymal gene expression programs following EMT in different experimental model systems.[44] The link between stroma and tumor cell EMT is further strengthened by the finding that TWIST1-positive cells are primarily localized within the stroma of human colon tumors.[8] In addition, IHC studies on human tumors and analysis of spontaneous intestinal tumors in mice have further demonstrated that EMT is a real and sometimes widespread phenomenon in colon cancer.[8, 9, 17, 41] Major basement membrane (BM) components are laminins and the sheet-forming collagen IV, while fibrillar collagens such as collagen-I make up the stromal matrix. Localized loss of BM integrity is associated with EMT and correlates with disease progression.[41] An immediate consequence of the loss of BM integrity is exposure of tumor cells to the underlying collagen-I-rich stromal matrix. Our data identify collagen-I as a causal link between high stromal content, (tumor specific) mesenchymal gene expression and collective tumor cell invasion. We cannot exclude that collagen-I also induces single cell migration, but that the experimental conditions do not allow the survival of such cells. The results support a model in which increased contact of tumor cells with the stromal matrix promotes EMT and local tumor cell invasion. TGFβ was recently identified as an important tumor cell-produced cytokine acting on nearby CAFs to secrete factors that promote metastasis and

tumor-initiating capacity.[6, 7] While TGFβ fails to induce EMT in most colon cancer models – at least in part because the pathway is frequently inactivated to allow tumor initiation – it is also one of the most potent inducers of collagen expression and deposition,[43] providing an additional link between TGFβ signaling, stroma biology, and tumor cell invasion. Non-TGFβ signaling pathways that promote EMT in colon cancer cells include WNT5A activation of FZD2,[13] Jagged activation of NOTCH,[5, 9] and hypoxia.[14] Importantly, WNT5A, and NOTCH ligands are predominantly expressed by stromal cells and act on tumor cells to promote metastasis.[5, 13, 22, 40] Interestingly, a recent report identified collagen stiffness as a key factor driving EMT by inducing TWIST1 entry into the nucleus of breast cancer cells.[45] Another important factor regulating EMT in neoplastic cells is the activity of the HNF4α transcription factor, a powerful suppressor of mesenchymal gene expression.[36, 47] Proteogenomic characterization of colon cancer shows that the mesenchymal subtype ('*C*') is characterized by low protein and RNA levels of HNF4α and the absence of HNF4α amplification, while collagens and SPARC are highly expressed in C-type cancers.[49] High HNF4α expression may therefore reduce the aggressive phenotype of colon tumors by promoting epithelial differentiation[3, 23, 42] and by suppressing mesenchymal gene expression[36, 47] in the neoplastic compartment.

The reciprocal interaction of stromal cell types, the extracellular matrix, and neoplastic cells is highly complex and most likely varies between tumors. The challenge therefore is to identify the most important and general aspects of these interactions in the context of metastatic colon cancer progression. Indeed, therapeutic targeting of the central nodes in tumor-ECM-stroma signaling is considered to have great potential in the treatment of aggressive cancer types.[29] Novel molecular diagnostic tools are needed to identify the tumors that may benefit from such treatment. The tumor specific mesenchymal gene expression program identified in this study could help developing such tools.

References

1 Belt EJ, Fijneman RJ, van den Berg EG, Bril H, Delis-van Diemen PM, Tijssen M *et al*. Loss of lamin A/C expression in stage II and III colon cancer is associated with disease recurrence. Eur J Cancer 2011; 47: 1837-1845.

2 Boissiere-Michot F, Lazennec G, Frugier H, Jarlier M, Roca L, Duffour J *et al*. Characterization of an adaptive immune response in microsatellite-instable colorectal cancer. Oncoimmunology 2014; 3: e29256.

3 Boyd M, Bressendorff S, Moller J, Olsen J, Troelsen JT. Mapping of HNF4alpha target genes in intestinal epithelial cells. BMC Gastroenterol 2009; 9: 68.

4 Budinska E, Popovici V, Tejpar S, D'Ario G, Lapique N, Sikora KO *et al*. Gene expression patterns unveil a new level of molecular heterogeneity in colorectal cancer. The Journal of pathology 2013; 231: 63-76.

5 Caiado F, Carvalho T, Rosa I, Remedio L, Costa A, Matos J *et al*. Bone marrow-derived CD11b+Jagged2+ cells promote epithelial-to-mesenchymal transition and metastasization in colorectal cancer. Cancer research 2013; 73: 4233-4246.

6 Calon A, Espinet E, Palomo-Ponce S, Tauriello DV, Iglesias M, Cespedes MV *et al*. Dependency of colorectal cancer on a TGF-beta-driven program in stromal cells for metastasis initiation. Cancer Cell 2012; 22: 571-584.

7 Calon A, Lonardo E, Berenguer-Llergo A, Espinet E, Hernando-Momblona X, Iglesias M *et al*. Stromal gene expression defines poor-prognosis subtypes in colorectal cancer. Nature genetics 2015.

8 Celesti G, Di Caro G, Bianchi P, Grizzi F, Basso G, Marchesi F *et al*. Presence of Twist1-positive neoplastic cells in the stroma of chromosome-unstable colorectal tumors. Gastroenterology 2013; 145: 647-657 e615.

9 Chanrion M, Kuperstein I, Barriere C, El Marjou F, Cohen D, Vignjevic D *et al*. Concomitant Notch activation and p53 deletion trigger epithelial-to-mesenchymal transition and metastasis in mouse gut. Nature communications 2014; 5: 5005.

10 Emmink BL, Laoukili J, Kipp AP, Koster J, Govaert KM, Fatrai S *et al*. GPx2 suppression of H2O2 stress links the formation of differentiated tumor mass to metastatic capacity in colorectal cancer. Cancer research 2014; 74: 6717-6730.

11 Fatrai S, van Schelven SJ, Ubink I, Govaert KM, Raats D, Koster J *et al*. Maintenance of Clonogenic KIT(+) Human Colon Tumor Cells Requires Secretion of Stem Cell Factor by Differentiated Tumor Cells. Gastroenterology 2015; 149: 692-704.

12 Guinney J, Dienstmann R, Wang X, de Reynies A, Schlicker A, Soneson C *et al*. The consensus molecular subtypes of colorectal cancer. Nature medicine 2015; 21: 1350-1356.

13 Gujral TS, Chan M, Peshkin L, Sorger PK, Kirschner MW, MacBeath G. A noncanonical Frizzled2 pathway regulates epithelial-mesenchymal transition and metastasis. Cell 2014; 159: 844-856.

14 Hongo K, Tsuno NH, Kawai K, Sasaki K, Kaneko M, Hiyoshi M *et al*. Hypoxia enhances colon cancer migration and invasion through promotion of epithelial-mesenchymal transition. The Journal of surgical research 2013; 182: 75-84.
15 Huang da W, Sherman BT, Lempicki RA. Systematic and integrative analysis of large gene lists using DAVID bioinformatics resources. Nature protocols 2009; 4: 44-57.
16 Huang da W, Sherman BT, Zheng X, Yang J, Imamichi T, Stephens R *et al*. Extracting biological meaning from large gene lists with DAVID. Current protocols in bioinformatics / editoral board, Andreas D Baxevanis [et al] 2009; Chapter 13: Unit 13 11.
17 Hwang WL, Yang MH, Tsai ML, Lan HY, Su SH, Chang SC *et al*. SNAIL regulates interleukin-8 expression, stem cell-like activity, and tumorigenicity of human colorectal carcinoma cells. Gastroenterology 2011; 141: 279-291, 291.
18 Isella C, Terrasi A, Bellomo SE, Petti C, Galatola G, Muratore A *et al*. Stromal contribution to the colorectal cancer transcriptome. Nature genetics 2015.
19 Jorissen RN, Gibbs P, Christie M, Prakash S, Lipton L, Desai J *et al*. Metastasis-Associated Gene Expression Changes Predict Poor Outcomes in Patients with Dukes Stage B and C Colorectal Cancer. ClinCancer Res 2009; 15: 7642-7651.
20 Julien S, Merino-Trigo A, Lacroix L, Pocard M, Goere D, Mariani P *et al*. Characterization of a large panel of patient-derived tumor xenografts representing the clinical heterogeneity of human colorectal cancer. ClinCancer Res 2012; 18: 5314-5328.
21 Loboda A, Nebozhyn MV, Watters JW, Buser CA, Shaw PM, Huang PS *et al*. EMT is the dominant program in human colon cancer. BMCMedGenomics 2011; 4: 9.
22 Lu J, Ye X, Fan F, Xia L, Bhattacharya R, Bellister S *et al*. Endothelial cells promote the colorectal cancer stem cell phenotype through a soluble form of Jagged-1. Cancer Cell 2013; 23: 171-185.
23 Lussier CR, Babeu JP, Auclair BA, Perreault N, Boudreau F. Hepatocyte nuclear factor-4alpha promotes differentiation of intestinal epithelial cells in a coculture system. Am J Physiol Gastrointest Liver Physiol 2008; 294: G418-428.
24 Mani SA, Guo W, Liao MJ, Eaton EN, Ayyanan A, Zhou AY *et al*. The epithelial-mesenchymal transition generates cells with properties of stem cells. Cell 2008; 133: 704-715.
25 Marisa L, de RA, Duval A, Selves J, Gaub MP, Vescovo L *et al*. Gene expression classification of colon cancer into molecular subtypes: characterization, validation, and prognostic value. PLoSMed 2013; 10: e1001453.
26 Melo DSE, Wang X, Jansen M, Fessler E, Trinh A, de Rooij LP *et al*. Poor-prognosis colon cancer is defined by a molecularly distinct subtype and develops from serrated precursor lesions. NatMed 2013; 19: 614-618.
27 Mesker WE, Junggeburt JM, Szuhai K, de HP, Morreau H, Tanke HJ *et al*. The carcinoma-stromal ratio of colon carcinoma is an independent factor for survival compared to lymph node status and tumor stage. Cell Oncol 2007; 29: 387-398.
28 Mesker WE, Liefers GJ, Junggeburt JM, van Pelt GW, Alberici P, Kuppen PJ *et al*. Presence of a high amount of stroma and downregulation of SMAD4 predict for worse survival for stage I-II colon cancer patients. Cell Oncol 2009; 31: 169-178.

29 Miles FL, Sikes RA. Insidious changes in stromal matrix fuel cancer progression. Molecular cancer research : MCR 2014; 12: 297-312.

30 Nishida N, Nagahara M, Sato T, Mimori K, Sudo T, Tanaka F *et al*. Microarray analysis of colorectal cancer stromal tissue reveals upregulation of two oncogenic miRNA clusters. Clinical cancer research : an official journal of the American Association for Cancer Research 2012; 18: 3054-3070.

31 Perez-Villamil B, Romera-Lopez A, Hernandez-Prieto S, Lopez-Campos G, Calles A, Lopez-Asenjo JA *et al*. Colon cancer molecular subtypes identified by expression profiling and associated to stroma, mucinous type and different clinical behavior. BMCCancer 2012; 12: 260.

32 Phillips SM, Banerjea A, Feakins R, Li SR, Bustin SA, Dorudi S. Tumour-infiltrating lymphocytes in colorectal cancer with microsatellite instability are activated and cytotoxic. The British journal of surgery 2004; 91: 469-475.

33 Roepman P, Schlicker A, Tabernero J, Majewski I, Tian S, Moreno V *et al*. Colorectal cancer intrinsic subtypes predict chemotherapy benefit, deficient mismatch repair and epithelial-to-mesenchymal transition. IntJCancer 2013.

34 Sadanandam A, Lyssiotis CA, Homicsko K, Collisson EA, Gibb WJ, Wullschleger S *et al*. A colorectal cancer classification system that associates cellular phenotype and responses to therapy. NatMed 2013; 19: 619-625.

35 Sadanandam A, Wang X, de Sousa EMF, Gray JW, Vermeulen L, Hanahan D *et al*. Reconciliation of classification systems defining molecular subtypes of colorectal cancer: interrelationships and clinical implications. Cell Cycle 2014; 13: 353-357.

36 Santangelo L, Marchetti A, Cicchini C, Conigliaro A, Conti B, Mancone C *et al*. The stable repression of mesenchymal program is required for hepatocyte identity: a novel role for hepatocyte nuclear factor 4alpha. Hepatology 2011; 53: 2063-2074.

37 Sato T, Stange DE, Ferrante M, Vries RG, van Es JH, Van den BS *et al*. Long-term expansion of epithelial organoids from human colon, adenoma, adenocarcinoma, and Barrett's epithelium. Gastroenterology 2011; 141: 1762-1772.

38 Schlicker A, Beran G, Chresta CM, McWalter G, Pritchard A, Weston S *et al*. Subtypes of primary colorectal tumors correlate with response to targeted treatment in colorectal cell lines. BMCMedGenomics 2012; 5: 66.

39 Smith JJ, Deane NG, Wu F, Merchant NB, Zhang B, Jiang A *et al*. Experimentally derived metastasis gene expression profile predicts recurrence and death in patients with colon cancer. Gastroenterology 2010; 138: 958-968.

40 Smith K, Bui TD, Poulsom R, Kaklamanis L, Williams G, Harris AL. Up-regulation of macrophage wnt gene expression in adenoma-carcinoma progression of human colorectal cancer. British journal of cancer 1999; 81: 496-502.

41 Spaderna S, Schmalhofer O, Hlubek F, Berx G, Eger A, Merkel S *et al*. A transient, EMT-linked loss of basement membranes indicates metastasis and poor survival in colorectal cancer. Gastroenterology 2006; 131: 830-840.

42 Stegmann A, Hansen M, Wang Y, Larsen JB, Lund LR, Ritie L *et al*. Metabolome, transcriptome, and bioinformatic cis-element analyses point to HNF-4 as a central regulator of gene expression during enterocyte differentiation. Physiol Genomics 2006; 27: 141-155.

43 Tabibzadeh S. Homeostasis of extracellular matrix by TGF-beta and lefty. Frontiers in bioscience: a journal and virtual library 2002; 7: d1231-1246.

44 Thomson S, Petti F, Sujka-Kwok I, Mercado P, Bean J, Monaghan M *et al*. A systems view of epithelial-mesenchymal transition signaling states. ClinExpMetastasis 2011; 28: 137-155.

45 Wei SC, Fattet L, Tsai JH, Guo Y, Pai VH, Majeski HE *et al*. Matrix stiffness drives epithelial-mesenchymal transition and tumour metastasis through a TWIST1-G3BP2 mechanotransduction pathway. Nature cell biology 2015.

46 Wellner U, Schubert J, Burk UC, Schmalhofer O, Zhu F, Sonntag A *et al*. The EMT-activator ZEB1 promotes tumorigenicity by repressing stemness-inhibiting microRNAs. Nature cell biology 2009; 11: 1487-1495.

47 Yao HS, Wang J, Zhang XP, Wang LZ, Wang Y, Li XX *et al*. Hepatocyte nuclear factor 4alpha suppresses the aggravation of colon carcinoma. Molecular carcinogenesis 2015.

48 Yoshihara K, Shahmoradgoli M, Martinez E, Vegesna R, Kim H, Torres-Garcia W *et al*. Inferring tumour purity and stromal and immune cell admixture from expression data. Nature communications 2013; 4: 2612.

49 Zhang B, Wang J, Wang X, Zhu J, Liu Q, Shi Z *et al*. Proteogenomic characterization of human colon and rectal cancer. Nature 2014; 513: 382-387.

Supplementary information

Bioinformatics analysis

All relevant datasets were uploaded into R2 for subsequent analysis. The MVRM dataset is compiled of three distinct datasets (GSE14333, GSE17536, GSE17537). The Marisa, GSE39582 and the AJCCIIAMC90 dataset, GSE33113. Batch effects were diagnosed by Principle Component Analysis. ComBat was used to correct for the non-biological effects between the three groups. The option 'Find differential expression between groups' was used to create the 'down-in-xenograft' gene list and to distinguish between genes preferentially expressed by tumor- and stromal cells types, using a single gene p value (Anova) cut-off of <e-6. False Discovery Rate (fdr) was used to correct p values for multiple testing.

To visualize expression of particular gene sets in distinct tumor subgroups the option 'relate two tracks' was used. Condensation of gene set expression into single values per tumor was performed with the 'View Gene Set' option and storing the obtained values as a track for subsequent analysis.

All dotplots visualizing the comparative expression of gene sets were created using the 'relate two tracks option'. Pearson correlation (r) values and accompanying p-values were obtained by selecting the xy plot option.

The generation of tumor subgroups on the basis of differential expression of gene sets was performed using the k-means option (10x100 draws). The settings were as follows: Transform: zscore. Minimum number of present calls: 1. Floor data at 16. Minimal expression range at 48. Minimal maximum expression at 68. No sample or gene filters were applied unless specified in the text.

Survival differences between groups were visualized in Kaplan Meier curves and p values were generated with the log rank test. Correction for multiple testing was done with the Bonferroni method.

Overlap between gene sets was identified with the web-based GeneVenn tool (http://genevenn.sourceforge.net/).

Gene ontology and analysis of enrichment of KEGG pathways in gene sets was performed with the Database for Annotation, Visualization and Integrated Discovery (DAVID) v6.7.[14, 15]

Visualization of the extracellular matrix network was performed with the web-based STRING functional protein association networks tool (http://string-db.org/).

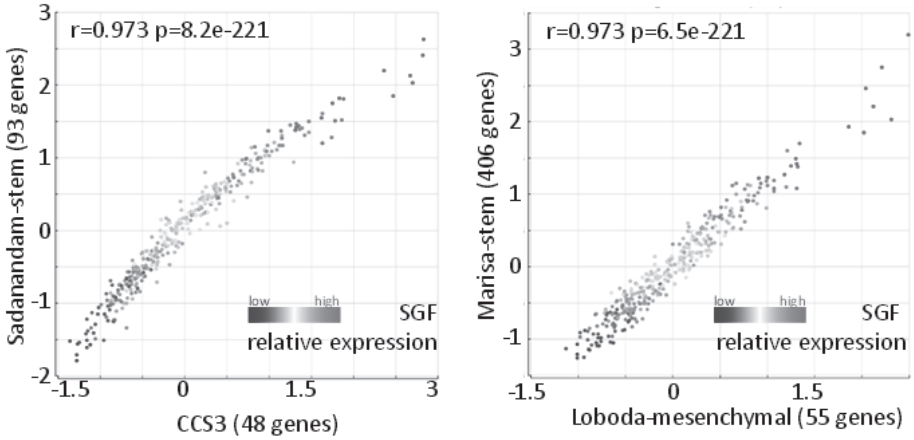

Supplementary Figure S1. Expression of gene sets identifying stem-like and mesenchymal-type colon tumors are strongly correlated.

Expression of published gene sets positively identifying mesenchymal- type tumors and stem-like tumors in the MVRM cohort were condensed into single 'meta-gene' expression values for each gene set and every tumor. Expression of two gene sets identifying stem-like tumors was then correlated to two gene sets identifying mesenchymal-type tumors in relation to expression of the SGF (blue = low; red = high).

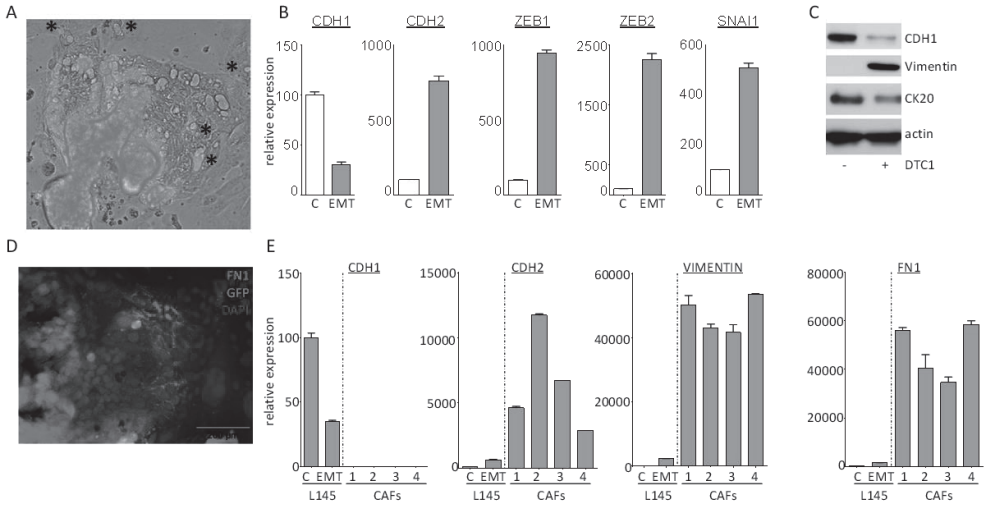

Supplementary Figure S2. Expression of mesenchymal markers in tumor cells following EMT in relation to CAFs.

(a) Epithelial-mesenchymal transition was induced in mCherry-expressing L145 patient-derived colonospheres by co-culturing them with differentiated tumor cell line-1 (DTC1).[11] Three days after co-culture, the colonosphere architecture was lost and cells started to detach from the spheroids. (b) mCherry-positive cells were FACS-sorted from the co-culture and were analyzed for expression of the indicated epithelial and mesenchymal markers by RT-qPCR and (c) western blotting. (d) Three days after co-culturing L145-GFP with DTC1 cells, the co-cultures were analyzed by immunofluorescence for GFP (L145) and fibronectin (FN1). Nuclei were stained with DAPI (blue). (e) Expression of the indicated mesenchymal markers in tumor cells before and after EMT was tested by RT-qPCR, in relation to expression of the same genes in 4 independent Cancer Associated Fibroblasts cultures (CAFs).

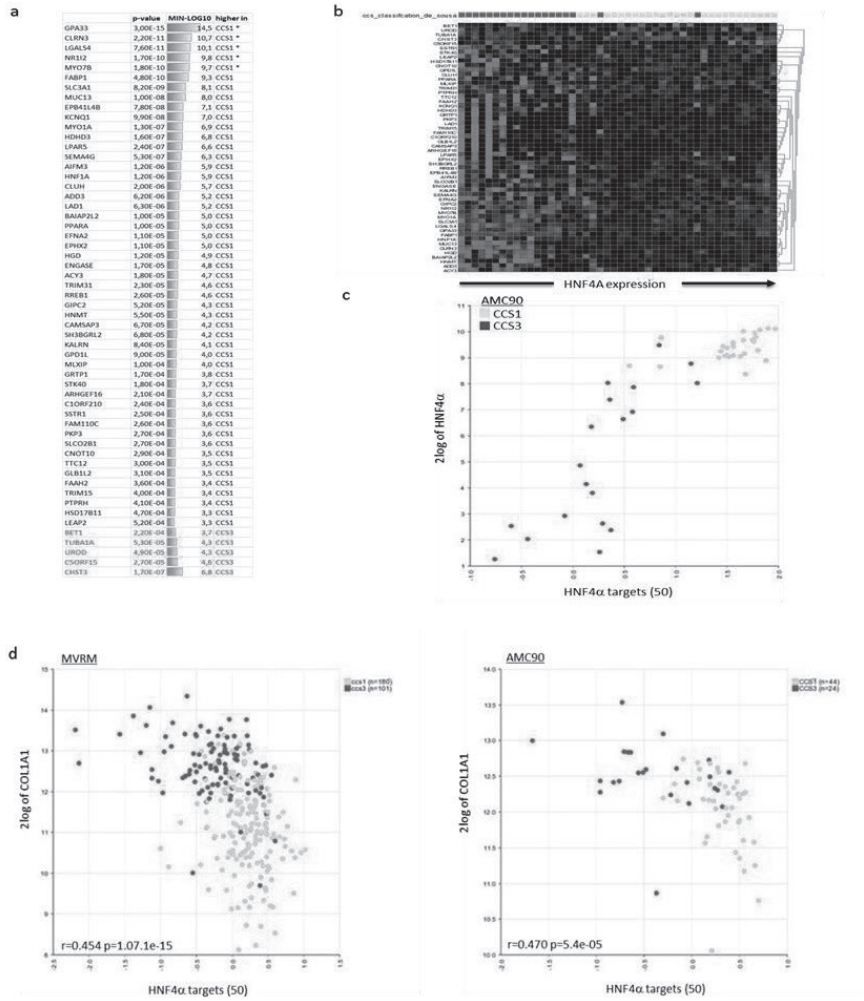

Supplementary Figure S3. HNF4α targets are highly expressed in CCS1 tumors and show an inverse correlation with collagen-I expression.

(a) List of HNF4α target genes ordered to expression levels in CCS1 tumors. (b) Heatmap of the expression of HNF4α target genes in CCS1 and CCS3 tumors in the AMC90 colon tumor cohort. (c) Dotplot shows the correlation between HNF4α and its targets in the AMC90 colon tumor cohort. (d) Dotplots show the correlation between collagen-I and HNF4α targets in two large colon tumor cohorts.

Supplemental tables

can be downloaded at https://www.nature.com/articles/onc201660#supplementary-information

CHAPTER 3

3

Dasatinib inhibits fibroblast-led invasion and regenerative capacity of colorectal cancer organoids in collagen type I

Thomas T. Vellinga, Cornelia Veelken, Inge Ubink, Kirsten K.J. Verheij, Niek A. Peters, Susanne van Schelven, André Verheem, Peter Friedl, Inne H.M. Borel Rinkes, Onno Kranenburg

Submitted

Abstract

Colorectal cancers (CRC) can be classified into four consensus molecular subtypes (CMS1-4). Patients with CMS4 CRC have the highest chance of developing metastases and have the poorest prognosis. CMS4 tumours are characterised by a high stromal content and an extracellular matrix dominated by collagen type I. Here we show that collagen-I induces a CMS4-like gene expression program in human CRC organoids. We identify dasatinib as a candidate CMS4-targeting drug based on its affinity for tyrosine kinases highly expressed in CMS4. We show that dasatinib has a strong and long-lasting inhibitory effect on the regenerative potential of CRC organoids. Furthermore, it limits and reverses interface migration of three-dimensional CRC organoid cultures in fibrillar collagen. In a co-culture system, fibroblasts directly interact with CRC organoids, and induce formation of invasive multicellular strands and detachment of cancer cell clusters from the organoids, reminiscent of invasion and local dissemination found in CRC resection specimens. Dasatinib treatment reduces the number of fibroblasts, disrupts heterotypic tumour cell-fibroblast interactions and induces apoptosis and regression in established invasion zones. With these combined effects, dasatinib impairs both the onset and progression of invasion and the detachment of cell clusters. These results indicate that stromal fibroblasts stimulate invasion, promote survival of invading tumour cells, and assist invasive cluster formation. By targeting tyrosine kinases that are expressed on both tumour cells and cancer-associated fibroblasts, dasatinib could interfere with the invasive phenotype of colorectal cancer in desmoplastic stroma. We therefore propose that dasatinib may have clinical utility in the treatment of stroma-rich mesenchymal-type CRC (CMS4).

Introduction

The development of distant metastases is the most important determinant of survival in patients with colorectal cancer (CRC) and most other types of cancer. Despite improvements in surgical procedures, chemotherapy, and local radiation techniques, prognosis of patients with metastatic CRC remains poor, with five-year overall survival of only 15%.[1] To improve the outcome for patients with CRC, prevention of dissemination and outgrowth of metastases is crucial. Current adjuvant chemotherapy regimens reduce the risk of distant recurrence after primary CRC surgery in patients with stage III disease from 50% to 35%, which means that only 15% of these patients benefit from adjuvant treatment.[2] Thus, there is an urgent need for novel treatment strategies that eliminate residual disease or prevent its outgrowth. The Consensus Molecular Classification system distinguishes four molecular subtypes of colorectal cancer (CMS1-4), based on recurrent patterns of gene expression. CMS4 is frequently referred to as the 'mesenchymal subtype', and is characterized by a high stromal content and expression of gene signatures reflecting epithelial-to-mesenchymal transition and a more stem-like phenotype. CMS4 tumours have the highest propensity to form metastases.[3-5] The processes of invasion and metastases in CRC are incompletely understood. Increasing evidence suggests that the tumour microenvironment plays an active role in tumour progression. High stromal content is associated with poor prognosis in CRC[4-6], and the type and constitution of stroma further predict outcome.[7] CMS4 cancers are particularly rich in desmoplastic stroma.[8] We have previously shown that collagen type I dominates the extracellular matrix (ECM) of CMS4 CRC, and that interaction with collagen-I induces mesenchymal gene expression and collective tumour cell invasion in human colorectal cancer organoids.[9] To search for potentially effective CMS4-targeting drugs, we explored the effects of collagen-I on CRC organoids and identified signalling intermediates potentially associated with CRC invasion. We selected existing FDA-approved tyrosine kinase inhibitors based on their affinity for kinases that are highly expressed in CMS4, and further explored the c-Src inhibitor dasatinib as a potentially effective inhibitor of CMS4 biology. Indeed, dasatinib strongly suppressed migration of organoids on a collagen-I matrix, and three-dimensional fibroblast-led invasion in collagen-I. Our results suggest that dasatinib could have clinical utility in the treatment of stroma-rich mesenchymal-type CRC.

Materials and Methods

Cell culture

The patient-derived CRC organoids p8t, p9t, p19ta, p19tb, p9t, and p26t were established as part of a living biobank of CRC[10], and were kindly provided by the HUB foundation (hub4organoids.eu). The patient-derived CRC organoids HUB-02-B2-028 (TOR8), HUB-02-B2-031 (TOR9) and HUB-02-B2-040 (TOR10) were established at the Hubrecht Institute, within biobanking protocol HUB-Cancer TcBio#12-093 that was approved by the medical ethical committee of the University Medical Center Utrecht. Organoids were cultured in Matrigel (Corning, 356231) with basal medium 2+ containing advanced-DMEM/F12 (Life Technologies, 12634028), supplemented with penicillin (100 U/ml) and streptomycin (100 µg/ml; PAA), Hepes (10 mM, Lonza, BE17-737E)), Glutamax (400 µM, Life Technologies, 35050038), B27 (0.2X, Life Technologies, 17504044), N-Acetyl-L-cysteine (1mM, Sigma-Aldrich, A9165-5G), Noggin (10%), A83-01 (500 nM, Biovision, 1725-1) and SB202190 (10 µM, Sigma-Aldrich, S7067) at 37°C and 5% CO_2.

Human lung fibroblasts MRC5 were maintained in cell culture containing Dulbecco's modified Eagle medium (DMEM; Gibco/Thermo Fisher Scientific), supplemented with 10% fetal calf serum (FCS; Sigma Aldrich), penicillin (100 U/ml) and streptomycin (100 µg/ml), L-glutamine (2 mM; Gibco/Thermo Fisher Scientific), and sodium pyruvate (1 mM; Gibco/Thermo Fisher Scientific) at 37°C and 5% CO_2.

Colony formation assay

Organoids were dissociated into single cells with TrypLE™ Express (Thermo Fisher Scientific). Cell viability was assessed with trypan blue staining, and 500 or 1000 viable single cells were plated in 100ul 1.5 mg/ml collagen (10 mg/ml collagen-I (Ibidi, Martinried, Germany) mixed with BM2+, pH buffered with NaOH). Dasatinib (Sellenckchem, S1021) was diluted in DMSO to a stock concentration of 50uM, and further diluted in BM2+ medium. Plated cells were treated with 100nM dasatinib or 0.002% DMSO, starting 2 days after plating the cells, during 14 days. Medium was refreshed twice per week. Colonies were counted with light microscopy (EVOS, Thermo Fisher Scientific). The experiments were performed in triplicate, and repeated three times for each cell line. For secondary colony formation assays, the colonies from one of the assays of p9t were dissociated into single cells. Cells were counted and viability was assessed with trypan blue; 500 viable cells were plated in 1.5mg/ml collagen-I. Cells from colonies treated with dasatinib were divided in two groups: one group received no further treatment; the second group was again treated with 100nM dasatinib. The experiment was performed in triplicate.

Collagen matrix interface migration assay

For gene expression analysis and matrix invasion assays, Matrigel was replaced by 1.5 mg/ml collagen-I (10 mg/ml collagen-I (Ibidi, Martinsried, Germany) mixed with BM2+, pH buffered with NaOH). To stimulate collagen-I interface migration, a bottom layer of 2 mg/ml collagen-I dissolved in phosphate-buffered saline was created and allowed to polymerise at room temperature for one hour. Droplets of collagen (5-10ul) with organoids were placed on top of this layer and also allowed to polymerise at room temperature for one hour, after which BM2+ medium with dasatinib (100nM; Sellenckchem, S1021) or DMSO (0.002%) was added and cells were placed in an incubator at 37°C. Micrographs were taken with the EVOS inverted microscope.

To study whether dasatinib reverses the invasive phenotype observed on a collagen-I matrix interface, organoids were cultured in Matrigel until they reached a size of 0.75-5.0 mm^3 and then plated in collagen-I. Dasatinib treatment was started after five days, when invasive sheets had formed on the matrix interface.

Co-culture invasion assay

Organoids and MRC5 fibroblasts were co-cultured in a 3D rat-tail type I collagen matrix (5 mg/ml; Corning, REF 3542495) to test the effects of dasatinib on CRC organoid growth, invasion and interaction with fibroblasts. Organoids were cultured in Matrigel until they reached a size of 0.75-5.0 mm^3. Matrigel was dissolved with ice cold PBS and organoids were transferred to a 15ml falcon tube, followed by three washing steps with 10ml ice cold PBS and centrifugation in between (5 min, 111g, 4°C). Organoids were resuspended and kept on ice in BM2+ medium until embedding in collagen. MRC5 cells from 2D culture (80% confluency) were detached using Trypsin /EDTA (0.075%/2mM, Thermo Fisher Scientific) in PBS followed by addition of medium containing 10% FCS. Cells were spun down, resuspended in BM2+ and counted. Acidic collagen-I stock solution was mixed with 10x PBS, Milli-Q, and 1N NaOH to a final concentration of 5mg/ml at pH 7.4. 100-150 organoids and 4000 MRC5 fibroblasts were mixed with the collagen and plated as drops (80 µl) in a 24-well plate and maintained at 37°C for 30 min until polymerization. For long-term culture, BM2+ medium, supplemented with 2.5% FCS to induce fibroblast elongation and maintain cell vitality, was added. Medium was refreshed at day 3 and every second consecutive day with the addition of dasatinib (final concentration: 100 nM) or DMSO (final concentration: 0.002%). At day 3, 7 and 12 after embedding, samples were fixed (4% PBS-buffered paraformaldehyde; 30 min at 21 °C), washed with excess PBS (5x5 min) and stained for microscopy.

Immunofluorescence

For epifluorescence microscopy of CRC invasion in 3D, samples were stained with DAPI and AlexaFluor548-phalloidin (18h at 4°C) and washed with PBS (5x5 min). Samples for

confocal microscopy of 3D invasion were incubated in blocking buffer (PBS/10% normal goat serum/0.1% BSA/0.1% Triton X-100; Sigma) for 2 h at 20°C, followed by incubation with rabbit monoclonal anti-vimentin (MA5-14564; Thermo Fisher Scientific) and mouse monoclonal anti-p120 antibody (BD610133, BD Biosciences) in blocking buffer overnight (4 °C on a shaking platform), washing with PBS (5x5 min) and incubation with secondary pre-absorbed goat anti-rabbit or anti-mouse IgG coupled to AlexaFluor -488 or 647 (Invitrogen/Thermo Fisher Scientific), DAPI and AlexaFluor568-phalloidin in blocking buffer (18h at 4°C). After washing in PBS (5x5 min), samples were placed in a 3D glass chamber filled with PBS and analysed by bright-field and confocal microscopy. For confocal imaging of interface migration, samples were incubated with 1% w/v bovine serum albumin, 1% v/v dimethylsulfoxide and 0.2% v/v Triton X-100 in PBS (PBD02T) (4h at 20°C) followed by incubation with AlexaFluor488-phalloidin and DAPI in blocking buffer (18h, 4°C) followed 5x5 min washing in PBD02T.

Imaging of 3D organoid co-cultures

Growth and invasion from overviews of multiple organoids were visualized with bright-field and epifluorescence microscopy (Leica DMI6000B, 5x/0.12 air objective, 20µm inter slice distance, 400-1000µm z-size, tile scan of 20-30 images). Images were composed from multiple fields by automatic stitching. Confocal microscopy (Zeiss LSM880 scanner; 40x/1.0 NA water-immersion objective) was performed with sequential single-channel scanning (5µm inter-slice distance). For bright-field time-lapse microscopy, organoids and fibroblasts were embedded in collagen-I as described above and recorded starting on day 2 for 30h (Okolab 2.0, 37 °C , 5% CO_2, 10x objective).

Image analysis

Images were analysed with ImageJ/Fiji (version 1.51). Collagen matrix interface migration was analysed by measuring the surface area of the migratory sheet of the largest organoid in a collagen droplet relative to the total surface area of the organoid structure including the migratory sheet. 3D collagen invasion was quantified using maximum intensity projections (standard deviation) from 3D image stacks, as the number of invasive organoids and the percentage of invasive strands with detached clusters. The frequency of interaction between CRC cells and fibroblasts were manually counted using the phalloidin signal along the cell-cell interface. Apoptosis in invasion zones was detected as nuclear fragmentation from the DAPI signal. Fibroblasts were recognized by DAPI signal as elongated single nuclei. Unless stated otherwise, data represent three independent collagen cultures from one batch of organoids, including a total of 300-450 organoids. For the analysis of co-cultures (number of organoids, percentage of invasive strands with detached clusters or apoptotic tip, number of fibroblasts) at day 12, 6-8 replicates from two independent experiments representing 600-1,200 organoids were used. Graphs were created with GraphPad Prism version 7.02.

Luminex assay

Organoids were dissociated into single cells. Half of the cells were cultured in basement medium extract (Cultrex® Pathclear Reduced Growth Factor BME type 2, #3533-001-02) and the other half were cultured in collagen-I as described for the collagen matrix invasion assay. After three days medium was removed from the cells and immediately frozen down to -80°C. Medium was refreshed and again removed and frozen down four days later (seven days after first seeding the cells). CXCL1 and CXCL8 concentrations were measured using an in-house developed and validated (ISO9001 certified) multiplex immunoassay based on Luminex technology (xMAP, Luminex Austin TX USA). The assay was performed as described[11]. In short, samples were incubated with antibody-conjugated MagPlex microspheres for one hour at room temperature with continuous shaking, followed by one hour incubation with biotinylated antibodies, and 10 min incubation with phycoerythrin-conjugated streptavidin diluted in high performance ELISA buffer (HPE, Sanquin the Netherlands). Acquisition was performed with the Biorad FlexMAP3D (Biorad laboratories, Hercules USA) in combination with xPONENT software version 4.2 (Luminex). Data was analyzed by 5-parametric curve fitting using Bio-Plex Manager software, version 6.1.1 (Biorad).

Bioinformatical analyses and statistics

Total RNA was isolated from tumour organoids according to manufacturer's protocol (RNeasy Mini Kit, Qiagen, Hilden, Germany). Affymetrix microarray analyses were performed by the Department of Oncogenomics, Amsterdam Medical Centre. Fragmentation of RNA, labelling, hybridization to Human Genome U133 Plus 2.0 microarrays and scanning were performed following the manufacturer's protocol (Affymetrix, Thermo Fisher Scientific). All bioinformatics analyses were performed using R2: Genomics Analysis and Visualization Platform (r2.amc.nl). To visualize expression of particular gene sets in distinct sample subgroups the option 'relate two tracks' was used. Condensation of gene set expression into single values per tumour/sample was performed with the 'View Gene Set' option and by storing the obtained values as a track for subsequent analysis. Dot plots visualizing the comparative expression of gene sets were created using the 'relate two tracks option'. Pearson correlation (r) values and accompanying p-values were obtained by selecting the xy plot option. The generation of tumour subgroups on the basis of differential expression of gene sets was performed using the k-means option (10x100 draws). Survival differences between groups were visualized in Kaplan Meier curves and p values were generated with the log rank test. Correction for multiple testing was done with the Bonferroni method. Overlap between gene sets was identified with the web-based GeneVenn tool (http://genevenn.sourceforge.net/). Data from invasion assays were analysed with Mann-Whitney test, ANOVA, or multiple t-test, as appropriate. P-values below 0.05 were considered statistically significant.

Results

Interaction with type I collagen induces gene expression associated with CMS4 in human colorectal cancer organoids.

Three different human CRC organoid lines (p8t, p9t, and p26t) were grown in either Matrigel or collagen type I for seven days. Matrigel mainly consists of laminin, collagen type IV and entactin, similar to the basement membrane of a healthy colon, whereas collagen type I more closely resembles the interstitial ECM surrounding invading tumour cells that have breached the basement membrane.[12] We used microarray gene expression profiling to identify differences in gene expression between organoids cultured in reconstituted type I collagen and Matrigel (Figure 1a, Supplemental Table 1). We selected the 250 genes that were most significantly upregulated in collagen-I (COL250), and analysed the expression of these genes in a composite cohort of colorectal tumours (n=3232) that were used to develop the CMS classification.[3] Expression of the COL250 gene set was significantly correlated with expression of signature genes that identify the mesenchymal subtype CMS4, and inversely correlated with expression of signature genes identifying the canonical epithelial subtype CMS2 (Figure 1b). We next used the COL250 gene set to cluster the CMS-3232 cohort[3] into three groups (low, intermediate, or high expression of COL250) by k-means clustering (Supplemental Figure 1a). The COL250-high group consisted almost exclusively of tumours that had previously been classified as CMS4 (Figure 1c). A subset of CMS1 tumours also clustered in the COL250-high group, while nearly all CMS2 and CMS3 tumours were assigned to the low or intermediate groups. High expression of the COL250 gene set was associated with shorter disease-free and overall survival (Supplemental Figure 1b,c). These data indicate that switching the extracellular matrix from Matrigel to collagen type I induces a CMS4-like phenotype in human colorectal organoids.

To gain insight into the mechanisms that drive collagen-I-induced gene expression changes in organoids, we searched for functional protein association networks by using STRING (string-db.org). This analysis revealed that collagen-I-induced genes form a network around the non-receptor tyrosine kinase c-Src (Figure 1d). c-Src activates multiple signal transduction pathways involved in proliferation, survival, angiogenesis and migration/invasion of cancer cells.[13] c-Src activation results in increased expression of interleukin-8 (IL-8, CXCL8).[14] Indeed, IL-8 was the most significantly upregulated gene (p=2.84E-6) in collagen-I compared with matrigel culture (Figure 1e). The structurally related chemokine CXCL1 (GRO1-alpha) was also upregulated in collagen-I (p= 1.12E-3). To validate these findings, we measured the production of these chemokines by three independent CRC organoid lines in BME and collagen-I with a luminex assay.

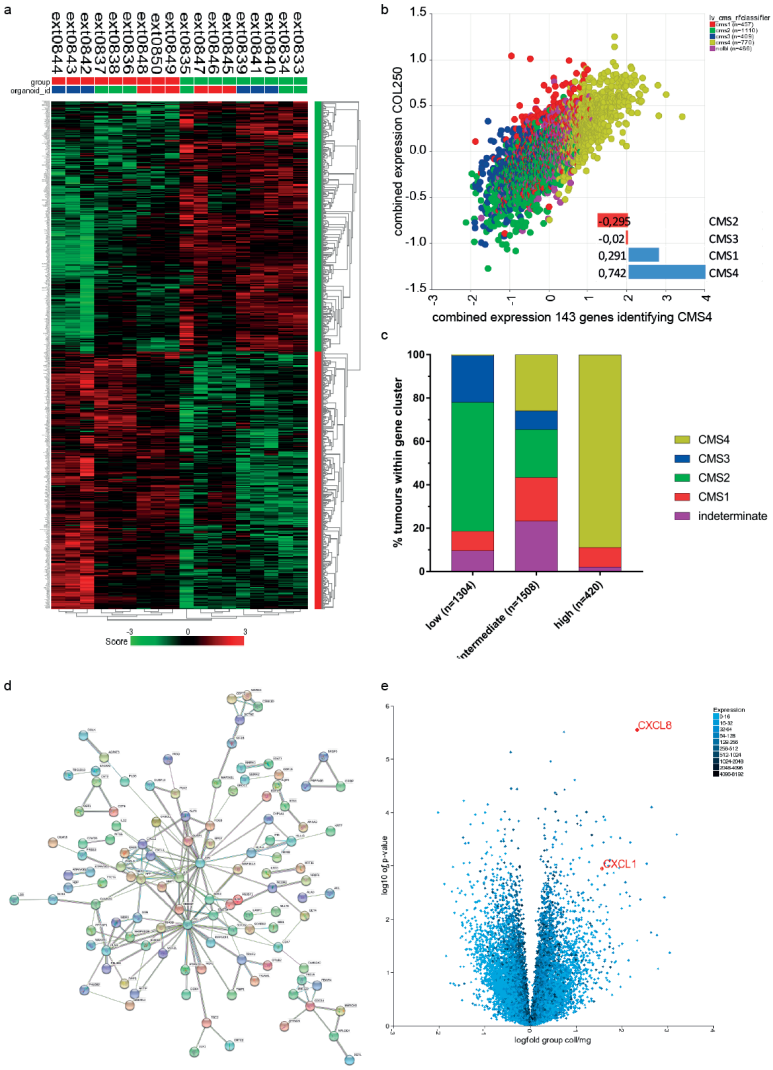

Figure 1

Collagen-I induced gene expression changes

a. Heatmap showing the 601 genes that were differentially expressed (ANOVA p<0.01) between cultures in matrigel and collagen-I. Colour codes: group – red = collagen-I, green = matrigel; organoid ID – blue = organoid p9t, green = organoid p8t, blue = organoid p26t.
b. Scatterplot showing the expression of CMS4 signature genes related to expression of COL250 genes in the CMS-3232 cohort. Inset: Pearson correlation (r-value) of CMS1-4 signature gene sets with the COL250 gene set.
c. Distribution of 3232 CMS classified tumours amongst the COL250 clusters.
d. STRING network analysis identifies activation of a protein network around c-Src upon culturing in collagen-I.
e. Volcano plot of ANOVA p-value versus fold change of gene expression from organoids cultured in collagen-I or in Matrigel. CXCL8 and CXCL1 are highlighted.

After three days, the CXCL8 concentration in medium from organoid TOR9 was 3.5 times higher in collagen-I culture, compared with BME culture, and after seven days it was 11 times higher (Supplemental Table 2). No change in CXCL8 production was observed in the other organoid cultures. CXCL1 concentrations were elevated in medium from all three tested organoids (TOR8, TOR9 and TOR10). After three days, concentrations were 9 times, 13 times and 3 times higher respectively in collagen-I compared with BME cultures. After seven days, TOR9 even produced 96 times more CXCL1 in collagen-I than in BME. Thus, the collagen-I induced upregulation of gene expression corresponds with increased production of the chemokines CXCL1 and CXCL8 in collagen-I compared with BME.

Dasatinib as a candidate CMS4-targeting drug

To search for potential therapeutic targets in CMS4 CRC we focussed on the human kinome. We identified fifty-five kinases that are positively correlated with the CMS4 signature genes in two independent colon cancer cohorts (GSE39582[15] n=566, and TCGA[16] n=276; single gene p-values <e-6; Supplemental Table 2). Twenty-two of these were tyrosine kinases (TK), to which we refer as the 22TK panel (Supplemental Table 2). TKs are attractive therapeutic targets and a large number of approved TK inhibitors (TKIs) are available for the treatment of cancer and other diseases. We made use of a dataset reporting on the quantitative dissociation constants (*K*d) of drug-target interactions for 72 distinct kinase inhibitors[17]. Two kinases from the 22TK panel (ROR1, ROR2) were missing in the dataset and could not be analysed. The *K*ds of each of the 72 kinase inhibitors for the remaining 20 TKs are shown in Supplemental Table 3. The most potent inhibitor was foretinib, which binds 18 of the 20 queried CMS4 TKs with a *K*d lower than 300 nM. The twenty-five most efficient 22TK inhibitors contained eight FDA-approved anti-cancer drugs, which are not currently indicated for the treatment of colon cancer: foretinib, dasatinib, cediranib, sorafenib, pazopanib, vandetanib, nilotinib, and imatinib (Table 1).

Table 1

	# targets		selectivity score	Kd for CMS4-associated tyrosine kinases																			
	all	<300	σ (3 uM)	KIT	PDGFRA	PDGFRB	FLT1	DDR2	KDR	AXL	TIE1	FGR	FYN	HCK	BTK	EPHA3	EPHA7	FER	FES	FGFR1	ITK	JAK1	JAK3
Foretinib	18	17	0,4404	2,5	4,5	0,96	3,8	3,6	12	0,093	0,79	40	88	15	76	1	2,5	37	110	690	69		
Dasatinib	13	9	0,2668	0,81	0,47	0,63	5000	3,2	2900			0,5	0,79	0,35	1,4	0,093				3700			640
Vandetanib	15	6	0,2358	260	230	88	260	320	820	250	1500	270	360	360	1700	2000	2400			560			
Pazopanib	14	6	0,215	2,8	4,9	2	14	98	14		700	1600	2700	5700				2700	1400	990			6900
Sorafenib	15	7	0,1684	28	62	37	31	6,6	59	4500	68	7800	8400	8500		1900	5300			2800			7300
Cediranib	15	8	0,1632	0,38	0,41	0,32	0,74	48	1,1	490	290	1100	1200	590	4300	3700	620			53			
Nilotinib	9	5	0,1244	29	180	73		33			1000	320	1600	390		110							
Imatinib	6	4	0,057	13	31	14		15				2400	3100										

Affinity of eight FDA-approved TKIs for 20TKs correlated with CMS4.

When plotting the inhibition profiles of these eight drugs onto the human kinome, we found excellent overlap between the targets of foretinib and dasatinib and the CMS4 22TK panel (Figure 2a). Dasatinib is a potent inhibitor of c-Src and the expression of a gene signature predicting sensitivity to dasatinib[18] was significantly upregulated by embedding organoids in collagen-I (Figure 2b). Based on this overlap, and the superior

selectivity score of dasatinib compared with foretinib (0.27 versus 0.44, respectively (Table 1)), we selected dasatinib for further studies.

Dasatinib reduces clone formation and inhibits two-dimensional sheet migration of CRC organoids

We performed colony-formation assays to test the effect of dasatinib on regenerative capacity of organoids grown in three-dimensional (3D) collagen type I, and found a consistent reduction of colony formation by ~50% in two different organoid lines (p9t and p19tb, Figure 3a). After re-plating the resulting colonies in a second colony-formation assay, we found that, even in the absence of continued drug exposure, the regenerative capacity of dasatinib-treated cancer cells was strongly and significantly impaired (Figure 3b). We recently showed that collagen-I induces emigration of cell sheets from human CRC organoids along the interface of two collagen-I matrix layers.[9] Treatment with 100 nM dasatinib (concentration based on [19]) inhibited sheet migration invasion between collagen layers in three different organoid lines (Figure 3c). Moreover, treatment with dasatinib was sufficient to reverse the migratory phenotype: upon dasatinib treatment, we observed a marked reorganisation at the invasive front, leading to the formation of a sharply demarcated epithelial barrier (Figure 3d). This treatment effect may be more clinically relevant, as in patients, local cancer cell invasion will have occurred before initiation of dasatinib therapy.

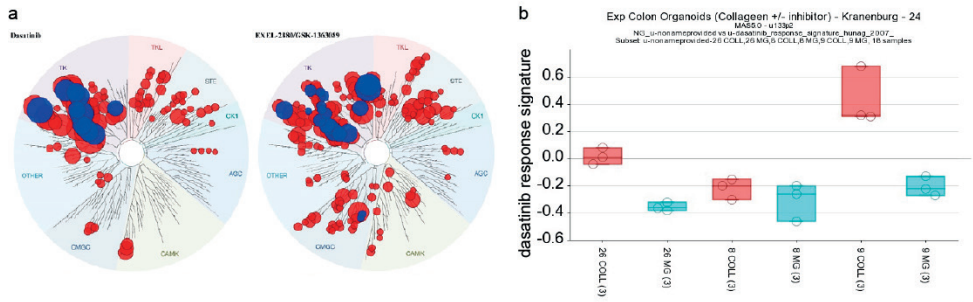

Figure 2

Identification of dasatinib as a potential anti-CMS4 drug

a. Activity spectra of dasatinib and foretinib (EXEL-2880) mapped on the human kinome. The size of each red spot reflects the dissociation constant of each drug for specific kinases. Larger spots indicate lower *K*d and more efficient inhibition. Kinases from the 22TK panel are highlighted in blue. Images generated using TREEspot™ Software Tool and reprinted with permission from KINOMEscan®, a division of DiscoveRx Corporation, © DISCOVERX CORPORATION 2010.

b. Expression of gene signature of genes positively correlated with dasatinib response[18] in organoids p26t, p8t and p9t in collagen-I and matrigel matrix.

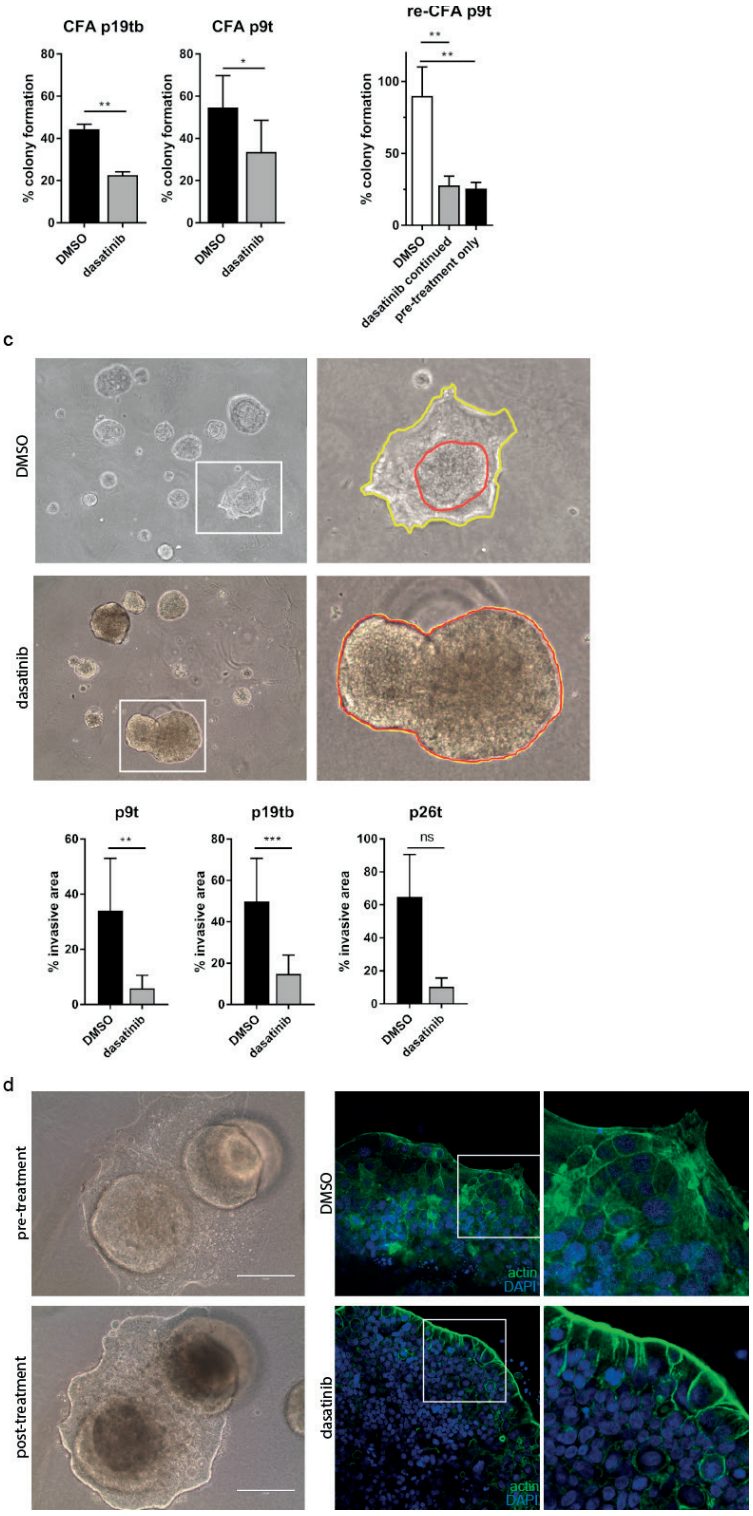
CFA p19tb
CFA p9t
re-CFA p9t
% colony formation
DMSO
dasatinib
dasatinib continued
pre-treatment only
c
DMSO
dasatinib
p9t
p19tb
p26t
% invasive area
ns
d
pre-treatment
post-treatment
actin
DAPI

Figure 3

Dasatinib inhibits and reserves two-dimensional organoid invasion on collagen-I

a. Colony formation assays (CFA) with p19tb and p9t treated with dasatinib (100nM). Bars represent mean plus standard deviation (SD) of combined results from repeated experiments (p19tb n=2, p9t n=3), **p=0.0043, *p=0.0188 (Mann Whitney test).
b. Secondary CFA with p9t after pre-treatment with dasatinib in the first CFA, with and without continued TKI treatment. Bars represent mean plus standard deviation (SD), **DMSO vs dasatinib continued p=0.0016, DMSO vs pre-treatment only p=0.0013 (one-way ANOVA, multiple comparisons test).
c. Dasatinib inhibits spreading of 3D organoids on the collagen-I matrix interface. Representative images of the collagen matrix interface migration assay with organoid p26t are shown (top = DMSO-treated, bottom = dasatinib-treated). The yellow line delineates the total surface area of the organoid, the red line surrounds the non-invasive organoid structure. The percentage of invasive area relative to the total surface area of the organoid is quantified in the graphs (p9t: n=5-6 organoids per condition, p19tb: n=9-10 organoids per condition, p26t: n=3 organoids per condition), bars represent mean plus standard deviation (SD), **p=0.0043, ***p=0.0003, ns=not significant (Mann Whitney test).
d. Dasatinib reverses collagen-I interface migration. Left panel: micrographs showing invasive behaviour of organoid p9t after five days in collagen-I culture (top), upon which treatment was started; dasatinib treatment (100nM) resulted in reorganisation of the invasive front after five days (bottom). Right panel: confocal microscopy images showing differences in actin organisation at the invasive front of DMSO-treated organoids (top) compared with dasatinib-treated organoids (bottom).

Dasatinib inhibits fibroblast-led three-dimensional invasion in collagen-I

The ECM of CMS4 tumours is rich in dense stroma and cancer-associated fibroblasts.[4, 5] Collective invasion of tumour cells through the ECM requires track clearance by leader cells.[20] Fibroblasts can function as leader cells, guiding the directional invasion of tumour cell strands in a range of cancer types.[21] To study the role of fibroblasts in directing colorectal cancer cell invasion in collagen-I, we co-cultured p19ta organoids with MRC5 lung fibroblasts, which are considered to be activated fibroblasts[22]. Organoids embedded in 3D fibrillar collagen without fibroblasts showed continued growth but little invasion (mono-culture, Figure 4a). In co-culture with fibroblasts however, 17% of the organoids formed multicellular strand-like invasion zones (Figure 4a-c). Fibroblasts approached and physically connected to tumour organoids prior to onset of invasion (supplemental material online, movies 1-4), consistent with reports on fibroblast-led collective tumour cell invasion[23]. After twelve days of co-culture, the tips of the invasive strands were either connected to fibroblasts (50%) or lacked physical connections to fibroblasts (50%, Supplemental Figure 2a). Heterotypic interactions between fibroblasts and invasive cells emigrating from the CRC organoids contained high levels of F-actin and p120 catenin (Figure 4b), indicating cadherin-based cell-cell junctions between fibroblasts and tumour cells, as described[21].

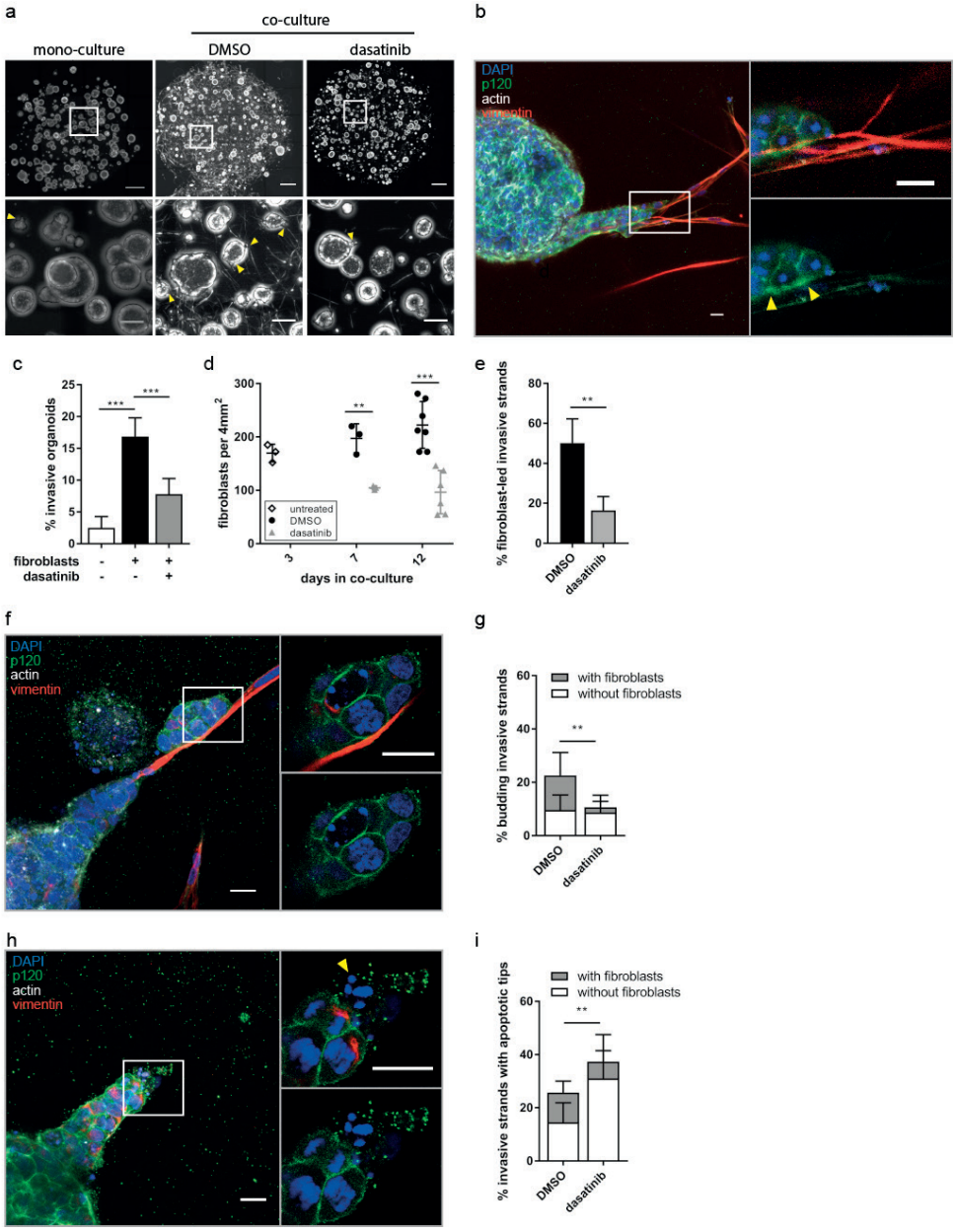

Figure 4

dasatinib inhibits fibroblast-induced invasion in three-dimensional collagen-I matrix

a. Top row: overview images of collagen-I matrices with p19ta mono-culture (left) and co-cultures of p19ta organoids with MRC5 fibroblasts without dasatinib treatment (middle) and with dasatinib treatment (right) after 12 days. Fluorescence shows F-actin (phalloidin) signal, scale bar = 200um. Bottom row: magnifications from top row, showing invasive strands emerging from the organoids (yellow arrow heads), scale bar = 1000um.

b. Confocal microscopy image showing interaction (intense p120 staining, yellow arrow heads) between an invasive organoid strand and a fibroblast. Scale bars = 20um.
c. Quantification of fibroblast-induced invasion at day 12, bars represent mean plus standard deviation (SD) based on combined results from two repeated experiments with 3-4 gels per condition, ***p<0.0001 (one-way ANOVA, multiple comparisons test).
d. Dasatinib reduces the total number of fibroblasts in the co-culture over time. Co-culture gels were fixed and analysed at three time points: at day 3 (before start of dasatinib/DMSO treatment), and at day 7 and day 12. **p=0.004, ***p=0.0002 (Multiple t-test, Statistical significance determined using the Holm-Sidak method, with alpha = 0.05)
e. Dasatinib reduces the percentage of fibroblast-associated invasive strands in co-culture. Bars represent mean plus standard deviation (SD) based on two repeated experiments with 3-4 gels per condition measured at day 12, **p=0.0012 (Mann Whitney test).
f. Confocal microscopy image showing budding of a tumour cluster from the invasive strand, guided by a fibroblast, scale bars = 20um.
g. Dasatinib decreases the number of invasive strands that show viable budding cells in co-culture. Bars represent mean plus standard deviation (SD) based on two repeated experiments with 3-4 gels per condition measured at day 12, ** p=0.0093, the reduction in budding events with fibroblasts was significant (two-way ANOVA with multiple comparisons).
h. Confocal microscopy image showing apoptotic nuclei (yellow arrow head) at the tip of an invasive strand, scale bars = 20um.
i. Dasatinib increases the percentage of invasive strands with apoptotic tips. Bars represent mean plus standard deviation (SD) based on two repeated experiments with 3-4 gels per condition measured at day 12, ** p=0.0081, the increase in apoptosis in strands without fibroblasts was significant (two-way ANOVA with multiple comparisons).

We next studied the effect of dasatinib on fibroblast-led 3D invasion. Treatment was started three days after establishment of the co-cultures, when invasion was initiated (Supplemental Figure 2b). Treatment with dasatinib reduced the number of fibroblasts with 44% from day 3 to day 12 while fibroblasts continued to proliferate in control culture (Figure 4d). CRC organoid invasion was reduced by 50% (Figure 4c) and 20% of the remaining invasive strands were connected to fibroblasts by day 12 (Figure 4e). In untreated co-cultures, release of 'budding' tumour cell clusters from invasive strands was observed in 23% of all invasive strands, and this rate was reduced by half by treatment with dasatinib (Figure 4f, g). Dasatinib further increased apoptotic events in the tips of the invasive strands, most prominently in strands lacking contact with fibroblasts (Figure 4h, i; 31% vs. 15% apoptosis, compared to DMSO). These data show that fibroblasts induce CRC invasion in 3D organoid culture. Interaction between fibroblasts and organoids trigger collective CRC cell invasion and budding, and both phenomena can be inhibited by dasatinib.

Discussion

In the present study we found that collagen-I, which is particularly abundant in CMS4 cancers[9], instigates an invasive, CMS4-like phenotype in patient-derived CRC organoids. This is in line with our previous data showing that the epithelial tumour cells in CMS4 cancers express a distinct set of mesenchymal genes.[9] We identified the TKI dasatinib as a potentially effective CMS4-targeting drug. Dasatinib is currently indicated for treatment of chronic myeloid leukaemia and acute lymphatic leukaemia. Our results show that many dasatinib targets are highly expressed in CMS4 CRC, and that it binds relatively few non-CMS4 targets. We found that dasatinib interferes with two major hallmarks of aggressive cancer behaviour in colorectal cancer organoids: cancer cell spread and regenerative capacity. Dasatinib inhibited – and even reversed – the invasive behaviour of colorectal cancer organoids in collagen-I by restoring epithelial integrity at the tumour-matrix interface. Our results are in line with previous studies documenting anti-invasive and anti-metastatic effects of dasatinib in pre-clinical models of pancreatic adenocarcinoma [19, 24], colon cancer cancer cell lines[25], thyroid carcinoma[20], and prostate cancer[26]. To study the interaction between tumour cells and fibroblasts in collagen-I-rich ECM, we developed a co-culture system. The presence of fibroblasts induced invasion of CRC organoids in a 3D collagen matrix, whereas in 3D mono-culture hardly any invasion occurred. This indicates that cancer cells require a track or an interface (as in our 2D interface model) to be able to migrate. The invasive tumour cell strands were either connected to fibroblasts or lacked contact with fibroblasts. This suggests that there are multiple potential mechanisms by which fibroblasts induce CRC invasion, including transient contact with tip cells to lead CRC invasion[21], formation of collagen tracks to enable autonomous CRC invasion[27], and/or paracrine signaling through cytokine release to induce ECM remodeling and invasion of CRC cells[28]. Treatment with dasatinib reduced the number of fibroblasts in the co-culture, reduced the number of invasive strands, and caused apoptosis of tumour cells located at the tips of the invasive strands. Based on these results we propose that stromal fibroblasts lead CRC invasion and promote survival of invading tumour cell strands and clusters. By targeting tyrosine kinases that are expressed on fibroblasts and/or on tumour cells, dasatinib abrogates the invasive phenotype of colorectal cancer organoids in desmoplastic stroma. Dasatinib was originally developed as an inhibitor of BCR-ABL and c-Src, but the spectrum of its high-affinity targets includes many pro-metastatic tyrosine kinases. To what extent inhibition of the various targets contributes to the observed treatment effects in our models is difficult to discern and most likely context-dependent, since many of its targets have proven pro-metastatic activity. In the context of CMS4 CRC – with collagen-I dominating the ECM – it is interesting to note that dasatinib is a potent inhibitor of the collagen-receptor DDR2. Elevated DDR2 expression in gastric cancer cells has been associated with increased peritoneal dissemination, and either knockdown of DDR2 or treatment with dasatinib reduced peritoneal metastasis formation in vivo.[29]

Similarly, in head and neck squamous cell carcinoma, DDR2 overexpression was found to stimulate migration and invasion, which could be inhibited by dasatinib.[30] The specific role of DDR2 and other members of the CMS4 22TK panel in colon cancer progression require further investigation.

Although dasatinib had an anti-metastatic effect in an *in vivo* model of pancreatic adenocarcinoma, treatment did not result in survival advantage, due to continued growth of the primary tumour.[19] Indeed, the concentration of dasatinib that was required to inhibit proliferation was markedly higher than the concentration required to inhibit c-Src.[19] Likewise, dasatinib monotherapy had little effect on growth of colorectal cancer xenografts.[31] Combination of dasatinib with chemotherapy may provide a promising treatment strategy, with chemotherapy targeting the actively proliferating tumour bulk and dasatinib targeting both the stromal fibroblasts and the invasive (non-proliferating) tumour cells. Two early clinical trials showed that addition of dasatinib to current standard chemotherapeutic regimens is safe.[32, 33] Furthermore, oxaliplatin treatment was associated with increased Src activity in liver metastases, and Src activation correlated with shorter relapse-free survival.[34] Dasatinib reversed resistance to oxaliplatin caused by high phospho-Src levels in vivo.[35] This study shows how new insights into the biology of CRC subtypes can guide the design of targeted therapies. Collectively, the results suggest a model in which the collagen-rich ECM and stromal fibroblasts promote mesenchymal gene expression and invasion of tumour cells, and that targeting these interactions could be an effective therapy for CMS4 CRC. Based on our findings that dasatinib has anti-invasive effects and limits the regenerative capacity of CRC organoids in collagen, and on clinical data showing that dasatinib can be safely combined with chemotherapy in CRC patients, we propose that this drug should be evaluated as a CMS4-targeting drug in clinical studies with pre-selected patients.

References

1. Hackl C, Neumann P, Gerken M, Loss M, Klinkhammer-Schalke M, Schlitt HJ. Treatment of colorectal liver metastases in Germany: a ten-year population-based analysis of 5772 cases of primary colorectal adenocarcinoma. *BMC Cancer* 2014, 14(1): 810.
2. Bockelman C, Engelmann BE, Kaprio T, Hansen TF, Glimelius B. Risk of recurrence in patients with colon cancer stage II and III: a systematic review and meta-analysis of recent literature. *Acta Oncol* 2015, 54(1): 5-16.
3. Guinney J, Dienstmann R, Wang X, de Reynies A, Schlicker A, Soneson C*, et al.* The consensus molecular subtypes of colorectal cancer. *Nat Med* 2015, 21(11): 1350-1356.
4. Calon A, Lonardo E, Berenguer-Llergo A, Espinet E, Hernando-Momblona X, Iglesias M*, et al.* Stromal gene expression defines poor-prognosis subtypes in colorectal cancer. *Nat Genet* 2015, 47(4): 320-329.
5. Isella C, Terrasi A, Bellomo SE, Petti C, Galatola G, Muratore A*, et al.* Stromal contribution to the colorectal cancer transcriptome. *Nat Genet* 2015, 47(4): 312-319.
6. Huijbers A, Tollenaar RA, v Pelt GW, Zeestraten EC, Dutton S, McConkey CC*, et al.* The proportion of tumor-stroma as a strong prognosticator for stage II and III colon cancer patients: validation in the VICTOR trial. *Annals of oncology : official journal of the European Society for Medical Oncology / ESMO* 2013, 24(1): 179-185.
7. Ueno H, Kanemitsu Y, Sekine S, Ishiguro M, Ito E, Hashiguchi Y*, et al.* Desmoplastic Pattern at the Tumor Front Defines Poor-prognosis Subtypes of Colorectal Cancer. *Am J Surg Pathol* 2017, 41(11): 1506-1512.
8. Calon A, Espinet E, Palomo-Ponce S, Tauriello DV, Iglesias M, Cespedes MV*, et al.* Dependency of colorectal cancer on a TGF-beta-driven program in stromal cells for metastasis initiation. *Cancer Cell* 2012, 22(5): 571-584.
9. Vellinga TT, den Uil S, Rinkes IH, Marvin D, Ponsioen B, Alvarez-Varela A*, et al.* Collagen-rich stroma in aggressive colon tumors induces mesenchymal gene expression and tumor cell invasion. *Oncogene* 2016, 35(40): 5263-5271.
10. van de Wetering M, Francies HE, Francis JM, Bounova G, Iorio F, Pronk A*, et al.* Prospective derivation of a living organoid biobank of colorectal cancer patients. *Cell* 2015, 161(4): 933-945.
11. de Jager W, te Velthuis H, Prakken BJ, Kuis W, Rijkers GT. Simultaneous detection of 15 human cytokines in a single sample of stimulated peripheral blood mononuclear cells. *Clin Diagn Lab Immunol* 2003, 10(1): 133-139.
12. Crotti S, Piccoli M, Rizzolio F, Giordano A, Nitti D, Agostini M. Extracellular Matrix and Colorectal Cancer: How Surrounding Microenvironment Affects Cancer Cell Behavior? *J Cell Physiol* 2017, 232(5): 967-975.
13. Wheeler DL, Iida M, Dunn EF. The role of Src in solid tumors. *The oncologist* 2009, 14(7): 667-678.
14. Trevino JG, Summy JM, Gray MJ, Nilsson MB, Lesslie DP, Baker CH*, et al.* Expression and activity of SRC regulate interleukin-8 expression in pancreatic adenocarcinoma cells: implications for angiogenesis. *Cancer Res* 2005, 65(16): 7214-7222.

15. Marisa L, de Reynies A, Duval A, Selves J, Gaub MP, Vescovo L, *et al.* Gene expression classification of colon cancer into molecular subtypes: characterization, validation, and prognostic value. *PLoS medicine* 2013, 10(5): e1001453.
16. Cancer Genome Atlas N. Comprehensive molecular characterization of human colon and rectal cancer. *Nature* 2012, 487(7407): 330-337.
17. Davis MI, Hunt JP, Herrgard S, Ciceri P, Wodicka LM, Pallares G, *et al.* Comprehensive analysis of kinase inhibitor selectivity. *Nat Biotechnol* 2011, 29(11): 1046-1051.
18. Huang F, Reeves K, Han X, Fairchild C, Platero S, Wong TW, *et al.* Identification of candidate molecular markers predicting sensitivity in solid tumors to dasatinib: rationale for patient selection. *Cancer Res* 2007, 67(5): 2226-2238.
19. Morton JP, Karim SA, Graham K, Timpson P, Jamieson N, Athineos D, *et al.* Dasatinib inhibits the development of metastases in a mouse model of pancreatic ductal adenocarcinoma. *Gastroenterology* 2010, 139(1): 292-303.
20. Haeger A, Krause M, Wolf K, Friedl P. Cell jamming: collective invasion of mesenchymal tumor cells imposed by tissue confinement. *Biochim Biophys Acta* 2014, 1840(8): 2386-2395.
21. Labernadie A, Kato T, Brugues A, Serra-Picamal X, Derzsi S, Arwert E, *et al.* A mechanically active heterotypic E-cadherin/N-cadherin adhesion enables fibroblasts to drive cancer cell invasion. *Nat Cell Biol* 2017, 19(3): 224-237.
22. Shimizu M, Takakuwa Y, Nitta S. Study of stimulation-secretion coupling in a flow culture system: periodic secretion of hepatocyte growth factor by interleukin-1 alpha-stimulated human embryonic lung fibroblasts. *Biochim Biophys Acta* 1995, 1244(2-3): 357-362.
23. Gaggioli C, Hooper S, Hidalgo-Carcedo C, Grosse R, Marshall JF, Harrington K, *et al.* Fibroblast-led collective invasion of carcinoma cells with differing roles for RhoGTPases in leading and following cells. *Nat Cell Biol* 2007, 9(12): 1392-1400.
24. Erami Z, Herrmann D, Warren SC, Nobis M, McGhee EJ, Lucas MC, *et al.* Intravital FRAP Imaging using an E-cadherin-GFP Mouse Reveals Disease- and Drug-Dependent Dynamic Regulation of Cell-Cell Junctions in Live Tissue. *Cell Rep* 2016, 14(1): 152-167.
25. Serrels A, Macpherson IR, Evans TR, Lee FY, Clark EA, Sansom OJ, *et al.* Identification of potential biomarkers for measuring inhibition of Src kinase activity in colon cancer cells following treatment with dasatinib. *Mol Cancer Ther* 2006, 5(12): 3014-3022.
26. Park SI, Zhang J, Phillips KA, Araujo JC, Najjar AM, Volgin AY, *et al.* Targeting SRC family kinases inhibits growth and lymph node metastases of prostate cancer in an orthotopic nude mouse model. *Cancer Res* 2008, 68(9): 3323-3333.
27. Drifka CR, Loeffler AG, Esquibel CR, Weber SM, Eliceiri KW, Kao WJ. Human pancreatic stellate cells modulate 3D collagen alignment to promote the migration of pancreatic ductal adenocarcinoma cells. *Biomed Microdevices* 2016, 18(6): 105.
28. Cao H, Eppinga RD, Razidlo GL, Krueger EW, Chen J, Qiang L, *et al.* Stromal fibroblasts facilitate cancer cell invasion by a novel invadopodia-independent matrix degradation process. *Oncogene* 2016, 35(9): 1099-1110.

29. Kurashige J, Hasegawa T, Niida A, Sugimachi K, Deng N, Mima K*, et al.* Integrated Molecular Profiling of Human Gastric Cancer Identifies DDR2 as a Potential Regulator of Peritoneal Dissemination. *Sci Rep* 2016, 6: 22371.
30. von Massenhausen A, Sanders C, Bragelmann J, Konantz M, Queisser A, Vogel W*, et al.* Targeting DDR2 in head and neck squamous cell carcinoma with dasatinib. *International journal of cancer Journal international du cancer* 2016, 139(10): 2359-2369.
31. Scott AJ, Song EK, Bagby S, Purkey A, McCarter M, Gajdos C*, et al.* Evaluation of the efficacy of dasatinib, a Src/Abl inhibitor, in colorectal cancer cell lines and explant mouse model. *PloS one* 2017, 12(11): e0187173.
32. Parseghian CM, Parikh NU, Wu JY, Jiang ZQ, Henderson L, Tian F*, et al.* Dual Inhibition of EGFR and c-Src by Cetuximab and Dasatinib Combined with FOLFOX Chemotherapy in Patients with Metastatic Colorectal Cancer. *Clinical cancer research : an official journal of the American Association for Cancer Research* 2017, 23(15): 4146-4154.
33. Strickler JH, McCall S, Nixon AB, Brady JC, Pang H, Rushing C*, et al.* Phase I study of dasatinib in combination with capecitabine, oxaliplatin and bevacizumab followed by an expanded cohort in previously untreated metastatic colorectal cancer. *Invest New Drugs* 2014, 32(2): 330-339.
34. Kopetz S, Morris VK, Parikh N, Overman MJ, Jiang ZQ, Maru D*, et al.* Src activity is modulated by oxaliplatin and correlates with outcomes after hepatectomy for metastatic colorectal cancer. *BMC Cancer* 2014, 14: 660.
35. Perez M, Lucena-Cacace A, Marin-Gomez LM, Padillo-Ruiz J, Robles-Frias MJ, Saez C*, et al.* Dasatinib, a Src inhibitor, sensitizes liver metastatic colorectal carcinoma to oxaliplatin in tumors with high levels of phospho-Src. *Oncotarget* 2016, 7(22): 33111-33124.

Supplementary information

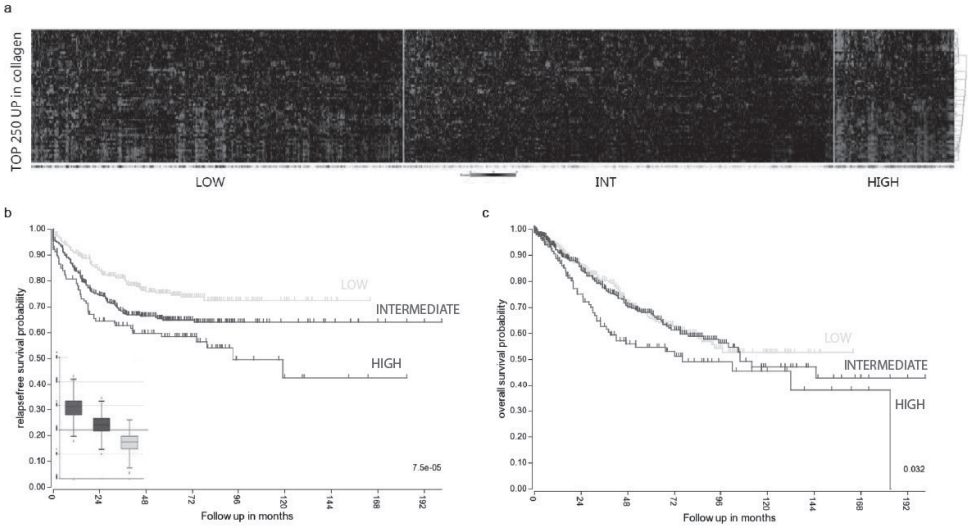

Supplemental Figure 1

a. Heatmap showing the expression of the 250 genes upregulated by collagen-I in the three clusters derived from k-means clustering.
b. Kaplan Meier curve of relapse-free survival based on clusters of COL250.
c. Kaplan Meier curve of overall survival based on clusters of COL250.

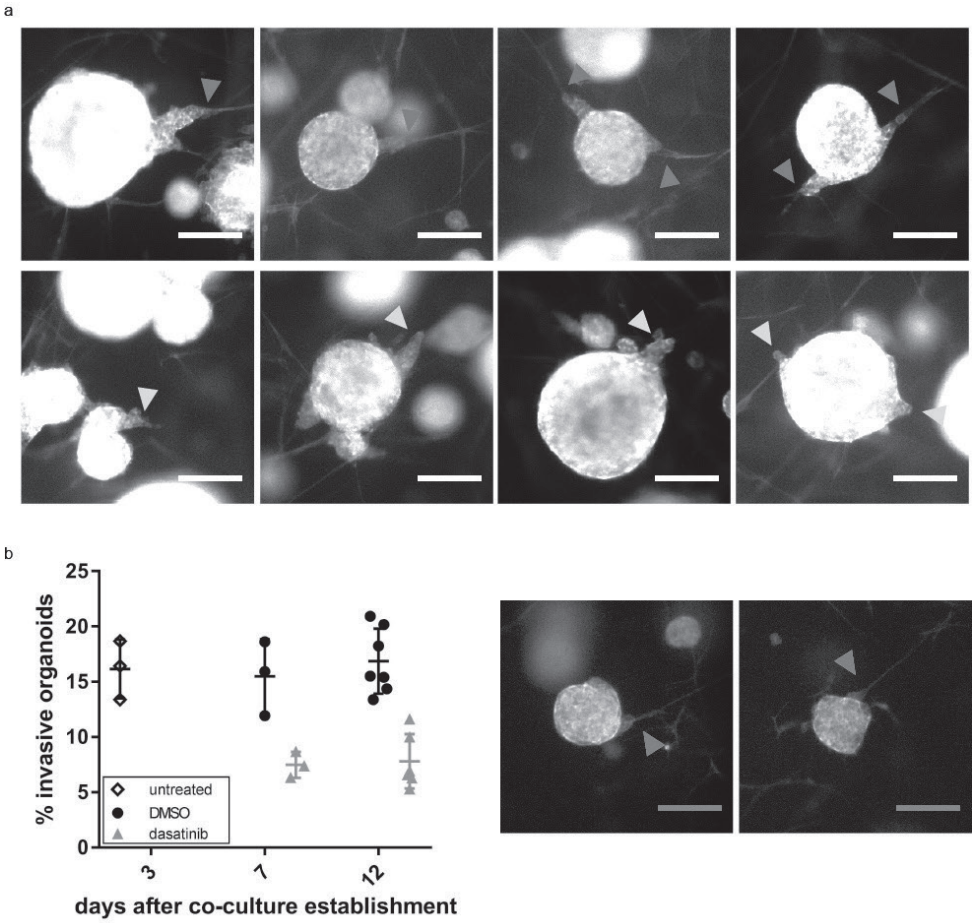

Supplemental Figure 2

a. Invasion of organoids p19ta in 3D collagen-I induced by fibroblasts; both guided by fibroblasts (green arrows, top row) and unguided (yellow arrows, bottom row) after 12 days. Fluorescence shows F-actin signal.

b. Fibroblast-led invasive strand formation over time. Co-cultures were fixed and analysed at three time points: at day 3 (before start of dasatinib treatment), day 7 and day 12. Images on the right show examples of fibroblast-led invasive strand formation at day 3, scale bar = 150 um.

CHAPTER 4

SIRT1/PGC1α-dependent increase in oxidative phosphorylation supports chemotherapy resistance of colon cancer

Thomas T. Vellinga, Tijana Borovski, Vincent C. J. de Boer, Szabolcs Fatrai, Susanne van Schelven, Kari Trumpi, Andre Verheem, Nikol Snoeren, Benjamin L. Emmink, Jan Koster, Inne H. M. Borel Rinkes and Onno Kranenburg

Clin Cancer Res. 2015 Jun 15;21(12):2870-9

Abstract

Purpose

Chemotherapy treatment of metastatic colon cancer ultimately fails due to the development of drug resistance. Identification of chemotherapy-induced changes in tumor biology may provide insight into drug resistance mechanisms.

Experimental design

We studied gene expression differences between groups of liver metastases that were exposed to pre-operative chemotherapy or not. Multiple patient-derived colonosphere cultures were used to assess how chemotherapy alters energy metabolism by measuring mitochondrial biomass, oxygen consumption and lactate production. Genetically manipulated colonosphere-initiated tumors were used to assess how altered energy metabolism affects chemotherapy efficacy.

Results

Gene ontology and pathway enrichment analysis revealed significant upregulation of genes involved in oxidative phosphorylation (OXPHOS) and mitochondrial biogenesis in metastases that had been exposed to chemotherapy. This suggested that chemotherapy induces a shift in tumor metabolism from glycolysis towards OXPHOS. Indeed, chemo-treatment of patient-derived colonosphere cultures resulted in an increase of mitochondrial biomass, increased expression of respiratory chain enzymes and higher rates of oxygen consumption. This was mediated by the histone deacetylase sirtuin-1 (SIRT1) and its substrate, the transcriptional co-activator PGC1α. Knockdown of SIRT1 or PGC1α prevented chemotherapy-induced OXPHOS and significantly sensitized patient-derived colonospheres, as well as tumor xenografts to chemotherapy.

Conclusion

Chemotherapy of colorectal tumors induces a SIRT1/PGC1α-dependent increase in OXPHOS that promotes tumor survival during treatment. This phenomenon is observed in chemotherapy-exposed resected liver metastases as well, strongly suggesting that chemotherapy induces long lasting changes in tumor metabolism that potentially interfere with drug efficiency. In conclusion, we propose a novel mechanism of tumor resistance that may be clinically relevant and therapeutically exploitable.

Introduction

Colon cancer is one of the most common and deadliest types of cancer. Mortality is mainly the consequence of metastatic growth in secondary organs like liver and lungs. Chemotherapeutic drugs that have proven to be effective in the treatment of metastatic colon cancer are 5-fluorouracil (5-FU), oxaliplatin and irinotecan which together prolong median survival from ~6 months to ~2 years [1]. However, most tumors are either intrinsically resistant to these drugs or acquire resistance during treatment. Consequently, disease progression following systemic therapy occurs in the vast majority of cases [1]. In order to rationally develop therapeutic approaches that can overcome drug resistance, it is essential to understand the underlying mechanisms. 'Omics' technologies are nowadays increasingly used to determine the (epi-)genetic underpinnings of drug resistance [2, 3]. In colon cancer this has resulted in the identification of gene signatures that can identify intrinsically drug-resistant tumor subtypes [4-7]. In the current study we use such technologies to study how drug resistance develops in colon cancer patients that are treated with chemotherapy. Normal, healthy cells mainly use OXPHOS for energy production. Cancer cells, however, face an impressive metabolic challenge due to rapid cell growth and frequent divisions, which forces them to adjust their energy metabolism in order to meet these demands [8]. The key event in this reprogramming is a switch in metabolism from OXPHOS towards aerobic glycolysis (Warburg effect) [9]. Tumor metabolism has received increased attention over the last decade, mainly in relation to proliferation and specific metabolic alterations. Only recently the metabolic state has been implicated in tumor drug resistance [10, 11]. Targeting tumor metabolism is now actively being studied as an alternative approach to overcome this problem. Drugs that limit the uptake of nutrients or interfere with their use in anabolic pathways have shown efficacy as resistance-modulating agents in several pre-clinical models [12-15]. However, the link between tumor metabolism and drug resistance is highly complex, it depends on multiple parameters such as oxygen and nutrient availability or the specific drugs that are being used, and the underlying mechanisms still remain to be elucidated[10]. In the present study we used transcriptomics data of liver metastases from chemotherapy-treated and chemo-naive colon cancer patients to identify a novel pathway of drug resistance, involving a change in energy metabolism. We show that upon chemotherapy, cancer cells shift their metabolism from glycolysis towards OXPHOS. This process is regulated via SIRT1-PGC1α signaling pathway and, as a consequence, increases the resistance of cells to chemotherapy.

Material and methods

Cell culture

Human colonosphere cultures were isolated from patients undergoing colon or liver resection of primary or metastatic adenocarcinoma and were propagated as described [16]. Briefly, colonospheres were cultured in advanced DMEM/F12 (Invitrogen) supplemented with 0,6% glucose (BDH Lab. Supplies), 2 mM L-glutamine (Biowhittaker), 9.6 μg/ml putrescin (Sigma), 6.3 ng/ml progesterone (Sigma), 5.2 ng/ml sodium selenite (Sigma), 25 μg/ml insulin (Sigma), 100 μg/ml apotransferrin (Sigma), 5 mMhepes (Gibco), 0,005 μg/ml trace element A (Cellgro), 0,01 μg/ml trace element B (Cellgro), 0,01 μg/ml trace element C (Cellgro), 100 μM β-mercaptoethanol (Merck), 10 ml antibiotic-antimycotic (Gibco), 4 μg/ml gentamicine (Invitrogen), 0.002% lipid mixture (Sigma), 5 μg/ml glutathione (Roche) and 4 μg/ml Heparin (Sigma). Growth factors (10 ng/ml b-FGF (Abcam)) were added to the cell culture medium freshly each week.

Flow cytometry

Mitotracker Green (Invitrogen) was added to the cultures at concentration of 300 nM for 30'. Colonospheres were washed with PBS and dissociated into single cell suspension using Accumax (Innovative Cell Technologies). Cells were resuspended in PBS containing 0.5 μg/ml propidium iodide (Sigma) to exclude dead cells and analyzed with flow cytometry (FACSCalibur, BD). Data were analyzed using Cell Quest Software (BD). Experiments were performed in triplicates, and the results are depicted as an average of at least three independent experiments. Data represented as mean ± SD.

Antibodies and reagents

The following antibodies were used for western blotting: anti-SIRT1 (Millipore), anti-cleaved caspase-3 and anti-cleaved PARP (Cell Signaling), MitoProfile Total OXPHOS Rodent WB antibody cocktail (Abcam), anti-β-actin (Novus Biologicals), HRP-labeled secondary antibodies(Dako). COX IV (Abcam) was used for immunohistochemistry. Oxaliplatin was obtained from Fresenius Kabi Oncology and 5-FU from TevaPharmachemie. For SIRT1 inhibition we used nicotinamide (Sigma), EX527 (Sigma) and TV6 (Cayman Chemical).

Lentiviral transduction

The shSIRT1 plasmids were obtained from the MISSION® shRNA TRC library (Sigma) [TRCN0000018979] and [TRCN0000018983]. shSCR plasmid (SHC002) was used as a control. The shPGC1α construct was a kind gift from Prof. P. Puigserver from the Dana-Farber Cancer Institute. Lentiviral particles were generated by transfecting 293T cells with pLKO and packaging vectors using Fugine (Roche). Transduced cells were selected with Puromycin (Sigma).

Immunohistochemistry

COX IV staining was performed on formalin-fixed paraffin embedded sections from colorectal liver metastasis. Samples were deparaffinized and rehydrated. Citrate buffer (pH6.0) was used for antigen retrieval. The primary anti-COX IV antibody was obtained from Abcam (ab14744, dilution 1:1000). The secondary antibody was from htVision (ImmunoLogic).

Quantitative Real Time Polymerase Chain Reaction

Total RNA was isolated according to the manufacturer's protocol (RNeasy Mini Kit, Qiagen) from colonosphere cultures or tissue samples. cDNA was synthesized using iScriptcDNA Synthesis Kit (Bio-Rad Laboratories). The amplification was performed in an iCyclerthermocycler (Bio-Rad Laboratories) using iQ SYBR Green Supermix (Bio-Rad Laboratories). mRNA expression levels were quantified using iCycler software (Bio-Rad Laboratories) and were normalized to B2M. The primers used for PGC1α were: Forward: GTAAATCTGCGGGATGATGG and Reverse: AATTGCTTGCGTCCACAAA. The primers used for RPL30 were: Forward: TTGCGCTTAGTAGTTCAATGG and Reverse: TGGTGAATTTGTGACGAATCC. All samples were analyzed in triplicates.

Animal experiments

Colonospheres were dissociated into single cell suspension with Accumax (Innovative Cell Technologies) and 5x104 cells stably expressing either SCR control or SIRT1shRNA were mixed with Matrigel (BD) at a 1:1 ratio and injected subcutaneously into the flanks of CBy.Cg-Foxn1nu/J mice. Tumor growth was measured every week and tumor volumes were calculated (V=axb2x0.5263), 'a' being the maximal width and 'b' maximal orthogonal width. Six weeks after the injection we started the chemo-treatment. Chemotherapy was administered intraperitoneally (i.p.) on weekly basis. Oxaliplatin (10 mg/kg) and 5-FU (100 mg/kg) were diluted in PBS. Control mice received PBS only. When tumors reached a volume of 1500 mm3 mice were sacrificed. For tumor analysis outliers (±>3 times SD from the mean) were excluded. For analysis of necrosis, the slides were digitized and analyzed via Aperio Imagescope (Leica Biosystems). The surface of necrotic areas (excluding the necrotic centre of the tumor) were measured and calculated as a percentage of the total area (excluding the necrotic centre). All experiments were performed in accordance with University of Utrecht institutional animal welfare guidelines.

Cell death analysis

Analysis of cell death was performed as follows: colonospheres were plated in 96-well plate and either treated or not with oxaliplatin (10 µg/ml) plus 5FU (10µg/ml) for 48h. Prior to the measurement, total cell population was labelled with DRAQ5™ (Abcam) and live cells were labelled with Calcein Green AM (Life Technologies). Fluorescence intensities were measured using the Arrayscan (ThermoScientific).The percentage of dead cells was

calculated by normalizing the levels of intensity to and expressed as a relative percentage of the plate-averaged vehicle treated control. Experiments were performed in triplicates, and the results display the average of at least three independent experiments. Data represented as mean ± SD.

Bioinformatics Analyses

We used our previously generated dataset containing gene expression profiles of 119 liver metastases [17] deposited at Array Access E-TABM-1112. The dataset was uploaded into the R2 microarray analysis and visualization platform (http://r2.amc.nl) and analyzed. Differential gene expression between tumor groups was performed with the 'Find differential expression between groups' option (single gene ANOVA $p<0.05$), and selecting each available clinical variable separately. To find differentially represented pathways in chemotherapy-treated versus non-treated tumors the resulting gene list was analyzed for Gene Ontology overrepresentation. In addition, differentially represented pathways were analyzed with the 'KEGG pathway finder' (Minimal t test $p<0.0001$).

OCR and ECAR measurement

The Seahorse XF96 Extracellular Flux Analyzer (Seahorse Biosciences) was used to obtain real-time measurements of oxygen consumption rate (OCR) and extracellular acidification rate (ECAR) in cells. Colonospheres treated with or without chemotherapy were harvested and dissociated to single cells using Accumax (Innovative Cell Technologies). Single cells were reconstituted in culture medium and seeded in 96-well Seahorse culture plates at a density of 40.000 cells/well. For analysis of ECAR, cells were reconstituted in Seahorse medium. Cells were allowed to settle for 1 hour prior to measurements. OCR and ECAR were analyzed using a 2 min mix followed by 3 min measurement cycle. Oligomycin (Sigma) was injected at a final concentration of 2 μM, carbonyl cyanide 4-(trifluoromethoxy) phenylhydrazone (FCCP, Sigma) at 3 μM, antimycin A (Sigma) at 5 μM and rotenone (Sigma) at 2 uM. Basal OCR is the mean OCR from 0, 5, 10, 15 min and maximal OCR is the mean OCR from 37, 42, 47 min. For ECAR measurements 2-deoxyglucose (Sigma) was injected at a final concentration of 100 mM. OCR and ECAR were normalized to protein or DNA content as measured using the BCA assay or Cyquant assay (Invitrogen). Data are presented as mean ± SEM.

Statistics

All values are presented as mean ± SEM or SD. The Student t test (unpaired, 2-tailed) or one way analysis of variance (ANOVA) was performed to analyze if differences between the groups are statistically significant. Differences with a P value of less than 0.05 were considered statistically significant.

Results

Chemotherapy of colorectal liver metastases induces lasting changes in gene expression

The majority of patients with metastatic colorectal cancer receive chemotherapy, either alone or in combination with surgery. To identify mechanisms that could underlie chemotherapy resistance we used gene expression profiles of 119 liver metastases of which 64 had received neo-adjuvant chemotherapy (i.e. prior to resection)[17]. Of all clinical variables tested, neo-adjuvant chemotherapy was by far most strongly associated with changes in gene expression (Supplementary table S2). Variables that were not correlated with significant changes in gene expression included various clinical scoring systems, tumor recurrence, tumor size and location, CEA levels, extent of resection and disease-free and overall survival (Supplementary table S2). We identified 481 genes whose expression was significantly ($p<0.05$) down-regulated and 613 genes whose expression was significantly up-regulated in chemotherapy-exposed tumors (Fig. 1A, Supplementary table S1). Interestingly, since the mean interval time between the last cycle of chemotherapy and resection of the metastases was 17 weeks (5-35), the observed gene signatures are persistent and long-lasting changes in gene expression.

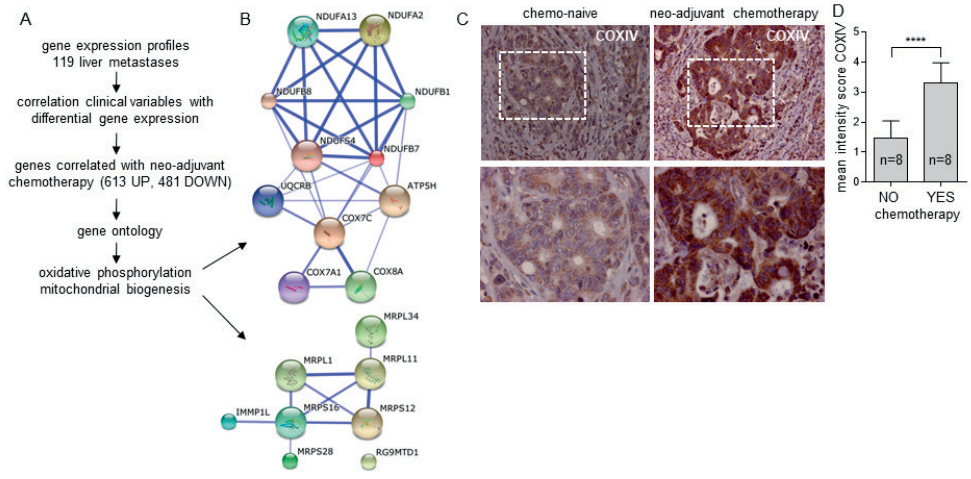

Figure 1

Chemotherapy of colon cancer liver metastases is associated with increased expression of genes involved in mitochondrial biogenesis and OXPHOS.

A, Overview of the study design. B, Analysis of the interaction between genes that were significantly upregulated in chemotherapy-treated tumors by using the Search Tool for the Retrieval of Interacting Genes/Proteins (STRING; string-db.org). The clusters reflecting OXPHOS and mitochondrial biogenesis are shown. C, Cytochrome c oxidase (COX IV) immunohistochemistry on paraffin-embedded tissue sections of liver metastasis either treated or not with neo-adjuvant chemotherapy. D, Quantification of the COX IV staining intensity (n=8 per group). Significance was determined with the Student's t test. ****$p<0.0001$.

Genes regulating mitochondrial biogenesis and OXPHOS are upregulated in chemotherapy-exposed liver metastases

To identify the biological pathways that are represented by the differentially expressed genes between chemotherapy-exposed and chemotherapy-naive tumors, we performed gene ontology analysis. This showed that the 'mitochondrial respiration chain' (GO0005746) was most significantly different between the two tumor groups (p=2.2e-5). In addition, the 'KEGG pathway finder' identified OXPHOS as the most significantly up-regulated pathway in chemotherapy-treated tumors (p=4.1e-4; Supplementary table S3). Similar results were obtained with Ingenuity Pathway Analysis (Supplementary table S3). The 14 differentially expressed OXPHOS pathway genes were all up-regulated in chemo-treated tumors. The electron transport chain consists of 5 distinct enzyme complexes. Chemo-treated metastases expressed high levels of multiple components of complexes I, III, IV and V (Supplementary table S4 and Fig. 1B). In addition, we found that mitochondrial biogenesis genes, in particular mitochondrial ribosomal proteins, like Mrpl11, Mrps16 and Mrps12, were also expressed to significantly higher levels in chemotherapy-treated tumors when compared to non-treated tumors (Supplementary table S4 and Fig. 1B). Next, we sought to validate the above results by performing immunohistochemistry analysis of the expression of COXIV, a component of mitochondrial complex IV and a frequently used marker for mitochondrial content, in pathological sections. For this, we used an independent series of colorectal liver metastases that had either received neo-adjuvant chemotherapy (n=8) or not (n=8). Indeed, we identified a markedly higher intensity of COXIV staining in sections from liver metastases that were treated with neo-adjuvant chemotherapy as compared to chemo-naive ones (Fig. 1C and Supplementary Fig. S1). Double-blind scoring of the stained sections confirmed that COXIV staining was significantly higher in treated compared to non-treated metastases (Fig. 1D). These findings establish that electron transport chain pathway is significantly upregulated in chemotherapy-treated liver metastases from two independent patient cohorts and that our gene expression findings can be translated to changes in actual protein levels of the electron transport chain.

Chemotherapy treatment induces oxidative energy metabolism in patient-derived colonospheres

Upregulation of mitochondrial biogenesis and electron transport chain pathways suggested that chemotherapy may alter energy metabolism in colorectal tumors by shifting cellular metabolism towards mitochondrial OXPHOS. To test this experimentally, we made use of a panel of colonosphere cultures established from primary colorectal tumors (CRC09, CRC16 and CRC29) and liver metastases (L145 and L167)[16]. First, we assessed how exposure of colonospheres to oxaliplatin and 5FU, the first line cytotoxic treatment for metastatic colorectal cancer, alters mitochondrial mass in these cells.

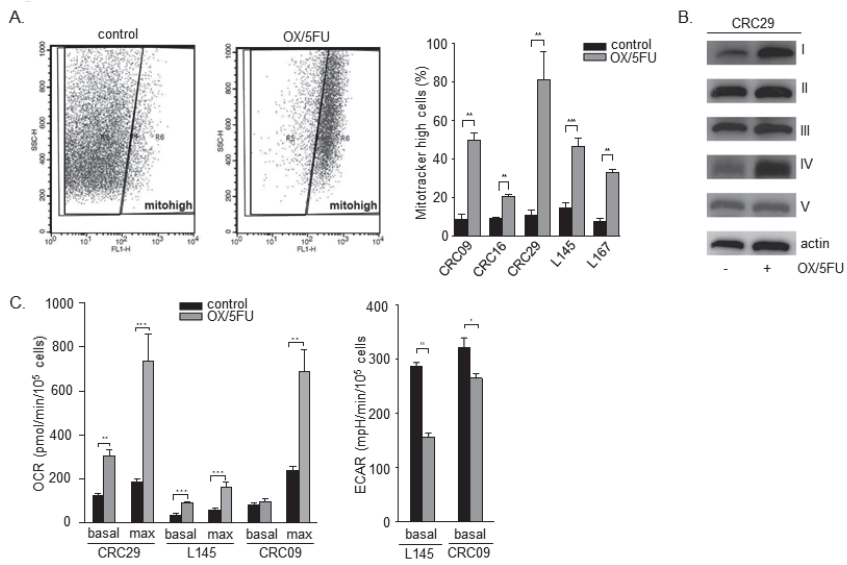

Figure 2

Chemotherapy increases OXPHOS in colonosphere cultures.

A, Colonosphere cultures derived from five distinct tumors were exposed to chemotherapy (oxaliplatin 10 µg/ml plus 5FU 10 µg/ml) for 72 hours. Mitotracker was used to determine chemotherapy-induced changes in mitochondrial content. FACSdot plots show an increase in mitotracker signal in colonosheres upon chemotherapy. Quantification of the FACS data is shown on the right. B, Colonosphere cultures were treated as in A for 48 hours. Western blot demonstrates an increase in OXPHOS enzymes after chemotherapy. C, Colonosphere cultures were treated as in A for 48 hours. The basal and maximal OCRs and basal ECARs were measured on the Seahorse Bioanalyzer. Significance was determined with the Student's t test. * $p<0.05$; ** $p<0.01$; *** $p<0.001$.

Control and drug-exposed colonospheres were stained with the fluorescent Mitotracker probe and mitochondrial content was determined by FACS analysis. Chemotherapy significantly increased mitochondrial mass in 5 distinct colonosphere cultures, irrespective of whether they were derived from primary tumors (n=3) or liver metastases (n=2) (Fig. 2A). Furthermore, similar to the upregulation of COXIV staining in chemotherapy treated tumors in vivo, protein levels of complex IV as well as complex I, II and III were strongly up-regulated following chemotherapy exposure (Fig. 2B), demonstrating that our colonosphere cultures reflected the changes we observed in vivo. Chemotherapy-induced increase in mitochondrial content and expression of OXPHOS enzymes suggested that chemotherapy-exposed tumor cells may switch from a glycolytic to a more oxidative energy metabolism. To test this directly, we determined oxygen consumption rates (OCR) and extracellular acidification rates (ECAR) of colonosphere cells by Seahorse analysis. Both basal and maximum OCRs were significantly increased in chemotherapy-treated colonopheres in three independent cultures (Fig. 2C). In parallel, ECAR was significantly

reduced. 2-deoxyglucose injection normalized the ECAR levels of both chemo-treated and non-treated cells to baseline levels. Both maximal and basal ECAR where reduced, demonstrating that the overall glycolytic capacity of the cells was reduced (Fig. 2D). Combined, lowered ECAR and enhanced OCR show that chemotherapy-treated colonospheres rely more on mitochondrial OXPHOS than non-treated ones.

Chemotherapy induces SIRT1 to promote oxidative energy metabolism

To identify potential regulators of the observed chemotherapy-induced metabolic changes, we re-analyzed the gene list that was upregulated in chemotherapy-treated tumors and searched for factors that could regulate mitochondrial biogenesis and/or OXPHOS.

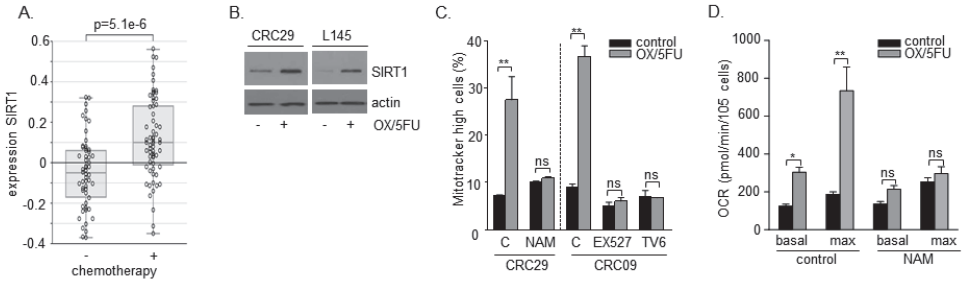

Figure 3

SIRT1 inhibition prevents chemotherapy-induced OXPHOS.

A, The gene expression profiles of 119 liver metastases [18] were used to analyse *SIRT1* expression in liver metastases that had been exposed to neo-adjuvant chemotherapy (n=64) and those that had not (n=55). The p-value was determined by one way analysis of variance (ANOVA). B, Colonosphere cultures were treated with oxaliplatin (10 µg/ml) plus 5FU (10µg/ml) for 24 hours. Western blot shows an increase in SIRT1 protein levels upon the treatment. C, The indicated colonosphere cultures were treated as in B for 48 hours, in the presence or the absence of the SIRT1 inhibitors nicotinamide (NAM; 30 mM), EX527 (30 µM) or TV6 (10 µM). Mitochondrial content was assessed as in Figure 2A. D, CRC29 colonospheres were treated with chemotherapy and NAM as in B for 48 hours. The basal and maximal OCRs were determined on the Seahorse Bioanalyzer. Significance was determined with the Student's t test. * p<0.05; **p<0.01; ***p<0.001.

We identified *SIRT1* as one of the most highly up-regulated genes in chemotherapy-treated tumors (top 5%; Supplementary table S1; Fig. 3A). *SIRT1* encodes sirtuin-1, a NAD+-dependent histone deacetylase which is activated in response to DNA damage and plays a key role in mitochondrial biogenesis [18,19]. None of the other Sirtuins (SIRT2-7) were enriched in chemotherapy-treated tumors. Treatment of colonosphere cultures with oxaliplatin and 5FU also greatly enhanced SIRT1 protein levels, thus demonstrating a causal relationship between chemotherapy and increased SIRT1 expression (Fig. 3B).

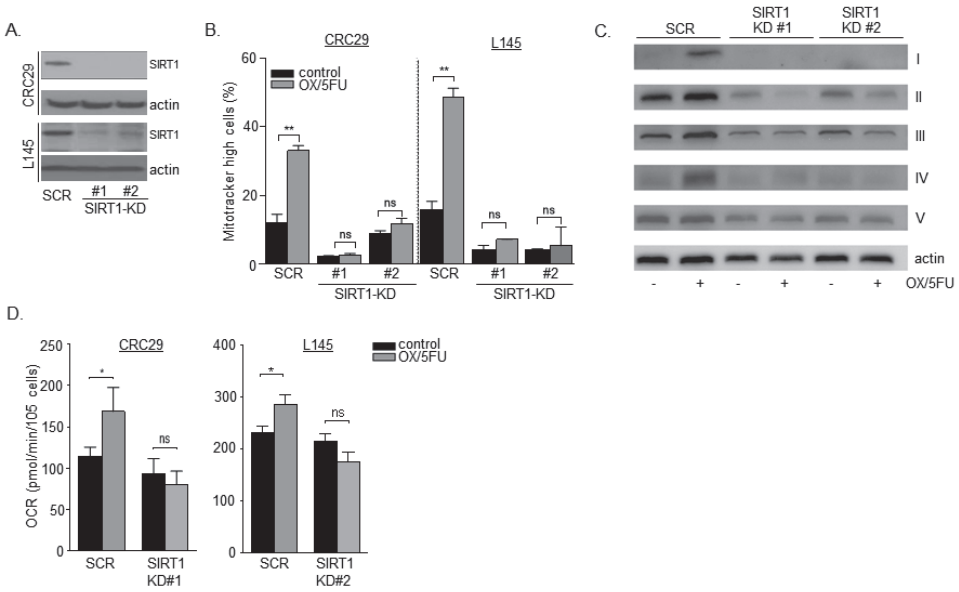

Figure 4

SIRT1 knockdown (KD) prevents chemotherapy-induced OXPHOS.

A, Colonosphere cultures were transduced with lentiviral vectors expressing two independent shRNAs targeting *SIRT1* or a control vector expressing a scrambled shRNA (SCR). SIRT1 protein levels in SCR and SIRT1 KD colonospheres were determined by Western blot analysis. B, SIRT1 KD and SCR colonospheres were treated with oxaliplatin (10 μg/ml) plus 5FU (10μg/ml) for 48 hours and mitochondrial content was analysed as in Figure 2A. C, SIRT1 KD and SCR colonosphere cultures were treated as in B. Expression levels of OXPHOS enzymes were measured by Western blot. D, SIRT1 KD and SCR colonopsheres were treated with chemotherapy as in B. The basal OCRs were measured on the Seahorse Bioanalyzer. Significance was determined with the Student's t test.*p<0.05; **p<0.01; ***p<0.001.

Next we analyzed whether inhibition of SIRT1 would interfere with the increase in mitochondrial mass triggered by chemotherapy. To this end we used the sirtuin inhibitors nicotinamide (NAM), EX-527 and Tenovin-6 (TV-6). All three compounds impaired the chemotherapy induced enhancement of mitochondrial mass (Fig. 3C). Importantly, NAM also completely prevented the increase in basal and maximal OCR (Fig. 3D). Next, we analyzed whether genetically ablating SIRT1 would impact chemotherapy-induced increase in mitochondrial mass. We suppressed SIRT1 in CRC29 and L145 colonospheres by expressing two independent short-hairpin RNAs (shRNAs) and used scrambled (SCR) hairpins as controls (Fig. 4A). Consistent with the SIRT1 inhibitor data, we found that SIRT1 knockdown (KD) prevented the chemotherapy-induced elevation in mitochondrial mass (Fig. 4B). Furthermore, expression of complex I-IV was upregulated by drug treatment, but was not induced in SIRT1 KD cells (Fig. 4C). Because NAM suppressed the increase in OCR upon drug-treatment, we performed similar Seahorse experiments in cells with KD

of SIRT1. Eliminating SIRT1 expression did not impact OCR in non-treated cells, whereas in chemotherapy treated cells OCR was greatly reduced (Fig. 4D), again demonstrating that SIRT1 is required for the induction of mitochondrial OXPHOS by chemotherapy. SIRT1 controls mitochondrial biogenesis by deacetylating and activating PGC1α, which is a master regulator of mitochondrial function [20]. PGC1α has been shown to be essential for directing the transcriptional program for enhancing mitochondrial biogenesis and function [21]. To test whether indeed mitochondrial biogenesis is activated in chemotherapy-treated colonospheres via SIRT1, we expressed shRNAs directed against PGC1α in CRC29 culture which resulted in efficient suppression of PGC1α protein expression (Fig. 5A). Again, chemotherapy caused an increase in mitochondrial mass and stimulated expression of OXPHOS enzymes in control cells, but in colonospheres where

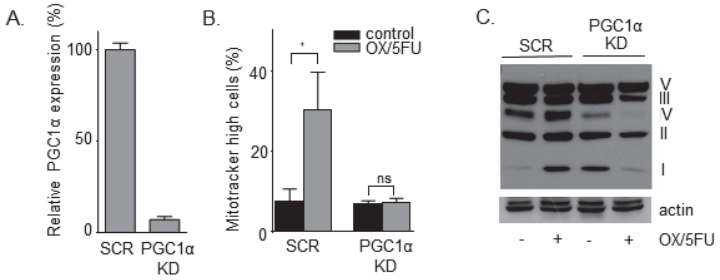

Figure 5

PGC1α knockdown (KD) prevents chemotherapy-induced OXPHOS.

A, CRC29 colonosphere cultures were transduced with a lentiviral vector expressing shRNA targeting PGC1α or a control vector expressing a scrambled shRNA (SCR). PGC1α mRNA levels were determined by qRT-PCR analysis. B, PGC1α KD and SCR colonospheres were treated with oxaliplatin (10 μg/ml) plus 5FU (10μg/ml) for 48 hours and mitochondrial content was analysed as in Figure 2A. Significance was determined with the Student's t test. *$p<0.05$. C, PGC1α KD and SCR colonosphere cultures were treated as in B. Protein levels of OXPHOS enzymes were measured by Western blot.

PGC1α was suppressed, both mitochondrial mass and expression of OXPHOS enzymes were not induced by chemotherapy treatment (Fig. 5B and 5C). Combined these findings demonstrate that both SIRT1 and PGC1α are necessary for triggering mitochondrial biogenesis in response to chemotherapy in patient-derived colonosphere cultures.

SIRT1 and PGC1α protect colon cancer cells against chemotherapy

In addition to mitochondrial biogenesis, SIRT1 is involved in multiple DNA repair processes and both SIRT1 and PGC1α play a role in the defense against reactive oxygen species (ROS) generated in high amounts by chemotherapy [22]. Furthermore, chemotherapy-induced DNA damage greatly increases the ATP demand [23]. Therefore we studied whether

suppression of SIRT1 or PGC1α would affect the sensitivity of cancer cells to chemotherapy. Strikingly, already after 16 hours of chemotherapy treatment of PGC1α KD cells, cleaved PARP and cleaved caspase-3 were detected, whereas in control cells only after 48 hours low levels of cleaved products became apparent (Fig. 6A).

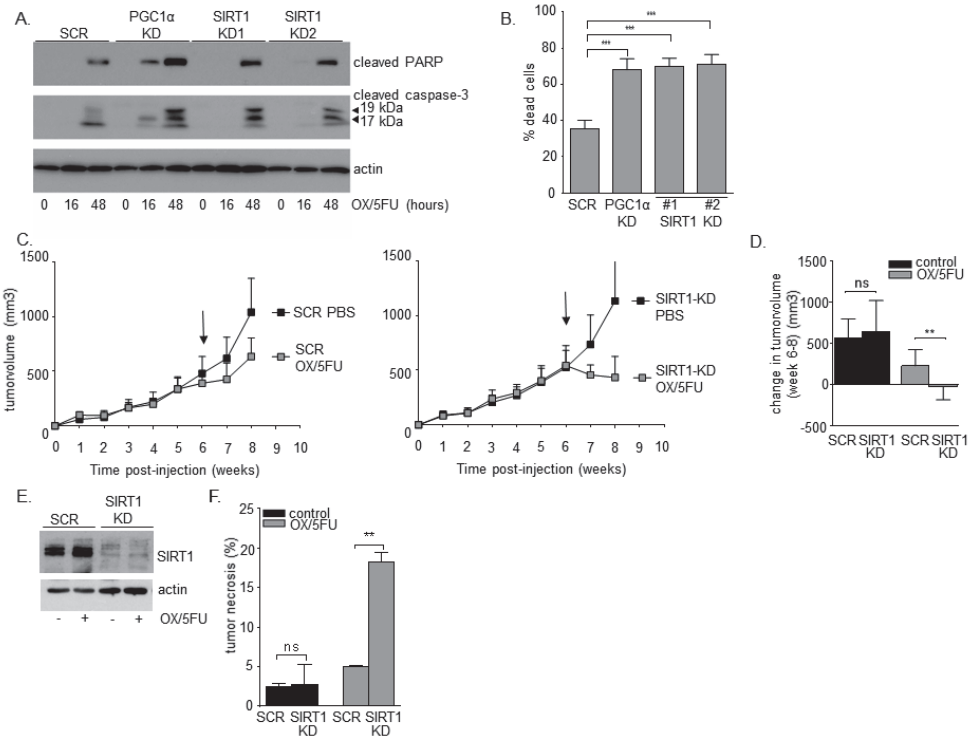

Figure 6

SIRT1 and PGC1α protect colon cancer cells against chemotherapy.

A, SIRT1 KD, PGC1α KD and SCR colonospheres were treated with chemotherapy for 16h and 48h. Cleaved PARP and cleaved caspase-3 levels were determined by western blot. Arrowheads indicate the 17 and 19 kDa cleaved forms of caspase-3. B, SIRT1 KD, PGC1α KD and SCR colonospheres were treated with chemotherapy for 48 hours and percentage of dead cells were measured by cytotoxicity assay, as described in Materials and Methods. C, SIRT1 KD and SCR colonospheres were injected subcutaneously into nude mice. From 6 weeks on, mice were treated with oxaliplatin plus 5FU or PBS as described in Materials and Methods. The experiment was terminated when the humane endpoint was reached (1500 mm^3tumor volume). The tumor growth curves are plotted as mean ± SEM (n = 9 per group). Arrows indicate start treatment. D, Absolute change in tumor volume from start treatment (week 6) till stop treatment (week 8). E, SIRT1 protein levels in SIRT1 KD and SCR tumors were determined by Western blot analysis. F, Quantification of the necrotic areas in tumor tissue sections from SIRT1 KD and SCR tumors as described in Material and Methods. Significance was determined with the Student's t test. * $p<0.05$; ** $p<0.01$; *** $p<0.001$.

Also in SIRT1 KD cells, drug treatment resulted in markedly increased levels of both cleaved PARP and cleaved caspase-3 as compared to treated control cells (Fig. 6A). Increased levels of cleaved PARP and cleaved caspase-3 indicate that SIRT1/PGC1α KD cells might commit to a cell death program faster than control cells. Therefore, we analyzed cell death using Arrayscan analysis upon drug treatment. Exposure of control cells to chemotherapy for 48 hours resulted in ~35% cell death. Strikingly, in both PGC1α and SIRT1 KD cells, the percentage of cell death was two-fold higher (Fig. 6B), demonstrating that PGC1α and SIRT1 make the colonospheres more resistant to chemotherapy. Finally, to evaluate the impact of SIRT1 KD on tumor growth and chemo-sensitivity in vivo, control and SIRT1 KD colonospheres were subcutaneously injected in nude mice. Mice were treated with oxaliplatin in combination with 5FU 6 weeks after injection of cells. As shown in Fig. 6C, SIRT1 KD tumors had a marked regression in response to oxaliplatin/5FU treatment. By contrast, chemotherapy did not induce regression of control tumors. Overall effect of chemotherapy at the end of the experiment was significantly more pronounced in SIRT1 KD compared to control tumors (Fig. 6D). Western blot analysis showed that SIRT1 KD was maintained in the tumors throughout the entire experiment (Fig. 6E). Histochemical analysis of tumor tissue sections further showed that chemotherapy induced significantly more cell death resulting in tumor necrosis in SIRT1 KD tumors compared to control tumors (Fig. 6F). Collectively, these results demonstrate that chemotherapy induces a switch in energy metabolism of tumor cells from glycolysis to OXPHOS via SIRT1/PGC1α and this protects cells from cytotoxic damage.

Discussion

Preventing disease progression by overcoming drug resistance is a major goal in medical oncology. In the present study we have identified OXPHOS and the SIRT1/PGC1α pathway as an important contributor to therapy resistance and a potential therapeutic target. Cells may rapidly adapt their metabolic pathways in response to changes in the microenvironment, including the availability of growth factors, nutrients and oxygen [24]. Our data indicate that genotoxic stress also alters energy metabolism. We show that colonospheres engage in a SIRT1/PGC1α-dependent reversion of the Warburg effect, shifting from glycolysis to OXPHOS in response to chemotherapy that subsequently improves their survival. This is in line with the previous reports correlating an increased mitochondrial, oxidative pathway to chemoresistance of tumor cells. Metabolic characterization of glioma cells revealed an enhanced oxidative metabolism in drug resistant cells compared to their drug-sensitive counterparts [25]. Importantly, we show that tumors of chemotherapy-treated cancer patients show lasting gene expression changes that reflect activation of the OXPHOS program. This strongly suggests that chemotherapy-induced gene expression alterations could potentially underlie tumor resistance in a long run, making our data clinically

relevant. Why would cancer cells switch their metabolism back to OXPHOS? Under normal conditions the amount of ATP produced through aerobic glycolysis is sufficient to support tumor cell growth and basal DNA repair activity. However, cellular demand is greatly increased following chemotherapy as many enzymes involved in DNA repair, drug efflux and drug detoxification require ATP to function [26, 27]. For cells, OXPHOS is the most efficient way to generate ATP, thus it is not surprising that cancer cells would switch back to this pathway in times of high demand. The role of SIRT1 in cancer is still controversial as evidence for both tumor promoting and suppressing activities have been found and the impact of SIRT1 on cell viability seem to be highly context-dependent [28]. In the present report we show that all tumor-derived colonosphere cultures and xenografts in which SIRT1 (or PGC1 α) were suppressed, were significantly sensitized to drug treatment. This is in line with the previously published data showing that SIRT1 KD sensitized Saos2 osteosarcoma cells to doxorubicin although this study did not identify increased OXPHOS as the critical downstream SIRT1 effector pathway[29]. Likewise, high expression of PGC1α in melanoma cells causes an increase in oxidative energy metabolism, increased expression of ROS-detoxifying enzymes and resistance to ROS-inducing drugs[30]. Upon PGC1α inhibition, such OXPHOS-dependent melanoma cells reverted to a glycolytic energy metabolism[31]. Mechanistically, chemotherapy-induced DNA damage results in increased expression of SIRT1, possibly via the multifunctional DNA repair protein and transcriptional co-activator APE1 [32, 33]. SIRT1-mediated de-acetylation reactions consume and require NAD+ as a substrate [34]. NAD+ levels rise when cells experience an energy deficit, for instance during fasting or exercise, and presumably also after chemotherapy-induced DNA damage[35]. Indeed, SIRT1 is recruited to sites of DNA damage and participates in several DNA repair processes 3[6, 18]. In addition, SIRT1 de-acetylates PGC1α, leading to its activation as a transcriptional co-activator [37]. PGC1α acts in concert with several transcription factors to stimulate the expression of genes involved in mitochondrial biogenesis and respiration, resulting in increased OXPHOS [38, 39]. Taken together our study provides insight into how colorectal tumors shift their energy metabolism when challenged with chemotherapy. We demonstrate OXPHOS to be upregulated in colon cancer cells via SIRT1/PGC1α upon treatment to foster their chemoresistance. Investigations targeting this program deserve further attention and may ultimately increase response rates to the treatment of colon cancer.

References

1. Lucas AS, O'Neil BH, Goldberg RM. A decade of advances in cytotoxic chemotherapy for metastatic colorectal cancer. Clinical colorectal cancer. 2011;10:238-44.
2. Longley DB, Allen WL, Johnston PG. Drug resistance, predictive markers and pharmacogenomics in colorectal cancer. Biochimica et biophysica acta. 2006;1766:184-96.
3. Crea F, Danesi R, Farrar WL. Cancer stem cell epigenetics and chemoresistance. Epigenomics. 2009;1:63-79.
4. Melo DSE, Wang X, Jansen M, Fessler E, Trinh A, de Rooij LP, et al. Poor-prognosis colon cancer is defined by a molecularly distinct subtype and develops from serrated precursor lesions. NatMed. 2013;19:614-8.
5. Roepman P, Schlicker A, Tabernero J, Majewski I, Tian S, Moreno V, et al. Colorectal cancer intrinsic subtypes predict chemotherapy benefit, deficient mismatch repair and epithelial-to-mesenchymal transition. IntJCancer. 2013.
6. Sadanandam A, Lyssiotis CA, Homicsko K, Collisson EA, Gibb WJ, Wullschleger S, et al. A colorectal cancer classification system that associates cellular phenotype and responses to therapy. NatMed. 2013;19:619-25.
7. Schlicker A, Beran G, Chresta CM, McWalter G, Pritchard A, Weston S, et al. Subtypes of primary colorectal tumors correlate with response to targeted treatment in colorectal cell lines. BMCMedGenomics. 2012;5:66.
8. Vander Heiden MG, Cantley LC, Thompson CB. Understanding the Warburg effect: the metabolic requirements of cell proliferation. Science. 2009;324:1029-33.
9. Warburg O. On the origin of cancer cells. Science. 1956;123:309-14.
10. Butler EB, Zhao Y, Munoz-Pinedo C, Lu J, Tan M. Stalling the engine of resistance: targeting cancer metabolism to overcome therapeutic resistance. Cancer research. 2013;73:2709-17.
11. Zhao Y, Butler EB, Tan M. Targeting cellular metabolism to improve cancer therapeutics. Cell death & disease. 2013;4:e532.
12. Cao X, Fang L, Gibbs S, Huang Y, Dai Z, Wen P, et al. Glucose uptake inhibitor sensitizes cancer cells to daunorubicin and overcomes drug resistance in hypoxia. Cancer chemotherapy and pharmacology. 2007;59:495-505.
13. Cufi S, Corominas-Faja B, Vazquez-Martin A, Oliveras-Ferraros C, Dorca J, Bosch-Barrera J, et al. Metformin-induced preferential killing of breast cancer initiating CD44+CD24-/low cells is sufficient to overcome primary resistance to trastuzumab in HER2+ human breast cancer xenografts. Oncotarget. 2012;3:395-8.
14. Maschek G, Savaraj N, Priebe W, Braunschweiger P, Hamilton K, Tidmarsh GF, et al. 2-deoxy-D-glucose increases the efficacy of adriamycin and paclitaxel in human osteosarcoma and non-small cell lung cancers in vivo. Cancer research. 2004;64:31-4.
15. Lu CW, Lin SC, Chien CW, Lin SC, Lee CT, Lin BW, et al. Overexpression of pyruvate dehydrogenase kinase 3 increases drug resistance and early recurrence in colon cancer. The American journal of pathology. 2011;179:1405-14.

16. Emmink BL, van Houdt WJ, Vries RG, Hoogwater FJ, Govaert KM, Verheem A, et al. Differentiated human colorectal cancer cells protect tumor-initiating cells from irinotecan. Gastroenterology. 2011;141:269-78.
17. Snoeren N, van Hooff SR, Adam R, van HR, Voest EE, Guettier C, et al. Exploring gene expression signatures for predicting disease free survival after resection of colorectal cancer liver metastases. PLoSONE. 2012;7:e49442.
18. Wang RH, Sengupta K, Li C, Kim HS, Cao L, Xiao C, et al. Impaired DNA damage response, genome instability, and tumorigenesis in SIRT1 mutant mice. Cancer Cell. 2008;14:312-23.
19. Knight JR, Milner J. SIRT1, metabolism and cancer. Current opinion in oncology. 2012;24:68-75.
20. Lagouge M, Argmann C, Gerhart-Hines Z, Meziane H, Lerin C, Daussin F, Messadeq N, et al.Resveratrol improves mitochondrial function and protects against metabolic disease by activating SIRT1 and PGC-1alpha. Cell. 2006;15:1109-22.
21. Puigserver P. Tissue-specific regulation of metabolic pathways through the transcriptional coactivator PGC1-alpha. Int. J Obes (Lond). 2005;29:S5-9.
22. Weijl NI1, Cleton FJ, Osanto S.Free radicals and antioxidants in chemotherapy-induced toxicity. Cancer Treat Rev. 1997;23:209-40.
23. Zhou Y, Tozzi F, Chen J, Fan F, Xia L, Wang J et al. Intracellular ATP levels are a pivotal determinant of chemoresistance in colon cancer cells. Cancer research. 2012;72:304-14.
24. Shlomi T, Benyamini T, Gottlieb E, Sharan R, Ruppin E. Genome-scale metabolic modeling elucidates the role of proliferative adaptation in causing the Warburg effect. PLoS computational biology. 2011;7:e1002018.
25 Oliva CR, Moellering DR, Gillespie GY, Griguer CE. Acquisition of chemoresistance in gliomas is associated with increased mitochondrial coupling and decreased ROS production. PLoS One. 2011;6:e24665.
26. Gottesman MM, Fojo T, Bates SE. Multidrug resistance in cancer: role of ATP-dependent transporters. NatRevCancer. 2002;2:48-58.
27. Osley MA, Tsukuda T, Nickoloff JA. ATP-dependent chromatin remodeling factors and DNA damage repair. Mutation research. 2007;618:65-80.
28. Deng CX. SIRT1, is it a tumor promoter or tumor suppressor? Int J Bio Sci. 2009;5:147-52.
29. Chu F, Chou PM, Zheng X, Mirkin BL, Rebbaa A. Control of multidrug resistance gene mdr1 and cancer resistance to chemotherapy by the longevity gene sirt1. Cancer research. 2005;65:10183-7.
30. Vazquez F, Lim JH, Chim H, Bhalla K, Girnun G, Pierce K, et al. PGC1alpha expression defines a subset of human melanoma tumors with increased mitochondrial capacity and resistance to oxidative stress. Cancer Cell. 2013;23:287-301.
31. Lim JH, Luo C, Vazquez F, Puigserver P. Targeting Mitochondrial Oxidative Metabolism in Melanoma Causes Metabolic Compensation through Glucose and Glutamine Utilization. Cancer research. 2014;74:3535-45.

32. Chu F, Chou PM, Zheng X, Mirkin BL, Rebbaa A. Control of multidrug resistance gene mdr1 and cancer resistance to chemotherapy by the longevity gene sirt1. Cancer research. 2005;65:10183-7.
33. Antoniali G, Lirussi L, D'Ambrosio C, Dal Piaz F, Vascotto C, Casarano E, et al. SIRT1 gene expression upon genotoxic damage is regulated by APE1 through nCaRE-promoter elements. Molecular biology of the cell. 2014;25:532-47.
34. Canto C, Auwerx J. Targeting sirtuin 1 to improve metabolism: all you need is NAD(+)? Pharmacological reviews. 2012;64:166-87.
35. Canto C, Auwerx J. Caloric restriction, SIRT1 and longevity. Trends in endocrinology and metabolism: TEM. 2009;20:325-31.
36. Martin SG, Laroche T, Suka N, Grunstein M, Gasser SM. Relocalization of telomeric Ku and SIR proteins in response to DNA strand breaks in yeast. Cell. 1999;97:621-33.
37. Gerhart-Hines Z, Rodgers JT, Bare O, Lerin C, Kim SH, Mostoslavsky R, et al. Metabolic control of muscle mitochondrial function and fatty acid oxidation through SIRT1/PGC-1alpha. The EMBO journal. 2007;26:1913-23.
38. Zhong L, Mostoslavsky R. Fine tuning our cellular factories: sirtuins in mitochondrial biology. Cell metabolism. 2011;13:621-6.
39. Scarpulla RC. Metabolic control of mitochondrial biogenesis through the PGC-1 family regulatory network. Biochimica et biophysica acta. 2011;1813:1269-78.

Supplemental information

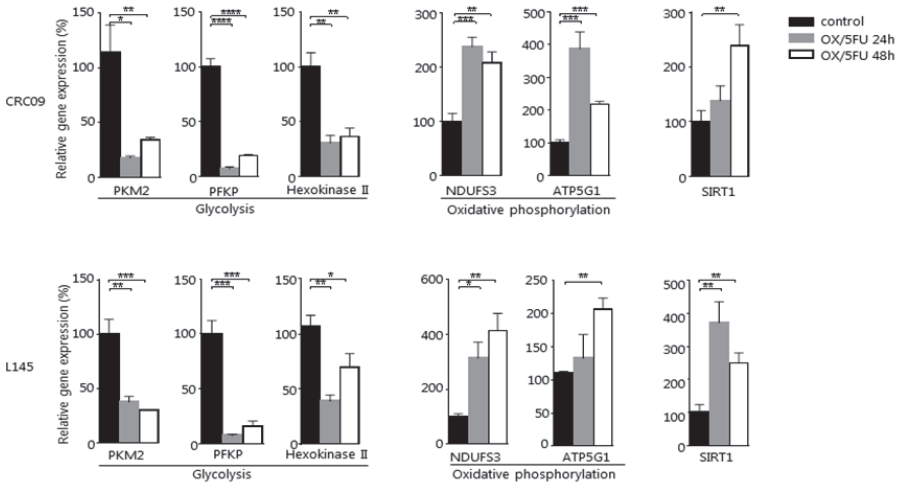

Supplementary figure S2

Expression changes of glycolytic and OXPHOS genes in response to chemotherapy.

RT-qPCR analysis of mRNA levels of genes encoding glycolytic enzymes (pyruvate kinase M2 (PKM2), Phosphofructokinase, platelet (PFKP) and Hexokinase II), OXPHOS enzymes (NADH dehydrogenase iron-sulfur protein 3 (NDUFS3) and ATP synthase lipid-binding protein (ATP5G1) a subunit of mitochondrial ATP synthase) and SIRT1.

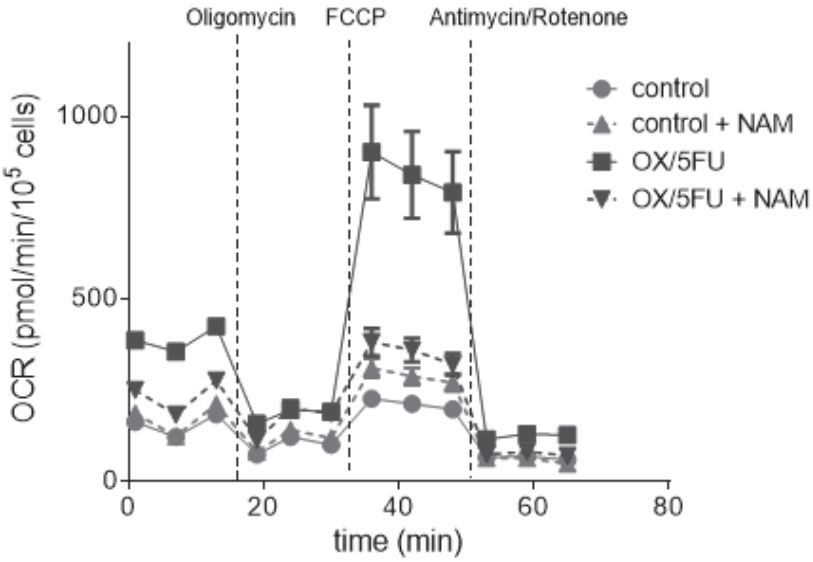

Supplementary figure S3

Oxygen consumption rates of colonospheres treated with chemotherapy +/- nicotinamide

Colonospheres were treated with oxaliplatin 10 µg/ml plus 5FU 10 µg/ml for 48 hours with or without nicotinamide (NAM) at a concentration of 30 nM. Oligomycin was injected at a final concentration of 2 µM, carbonyl cyanide 4-(trifluoromethoxy)phenylhydrazone (FCCP) at 3 µM, antimycin A at 5 µM and rotenone at 2 uM. Oxygen consumption rates were measured over time with the Seahorse.

Supplementary tables

The supplementary tables can be downloaded at:

http://clincancerres.aacrjournals.org/content/21/12/2870.figures-only

Supplementary table S1
Primers used for RT-qPCR analyses.

Supplementary table S2
Clinical variables associated with differences in gene expression among 119 resected liver metastases.

Supplementary table S3
613 genes whose expression was significantly upregulated and 481 genes whose expression was significantly ($p<0.05$) down-regulated in chemotherapy-treated tumors compared to chemo-naive tumors.

Supplementary table S4
KEGG pathway finder analysis and Ingenuity Pathway Analysis of upregulated genes in chemo-treated compared to chemo-naive tumors.

Supplementary table S5
P-values of expression levels of genes involved in mitochondrial dysfunction, ubiquinone synthesis and mitochondrial biogenesis upregulated in chemo-treated compared to chemo-naive tumors.

Supplementary table S6
(additional information regarding the calculation listed below)

ATP synthesis rates through glycolysis and OXPHOS.

The rates of ATP synthesized by glycolysis are as follows:

CRC09 (control): = ECAR= direct value from figure 2C: 321 pmoles/min/10^5 cells

CRC09 (chemo): = ECAR= direct value from figure 2C: 264 pmoles/min/10^5 cells

L145 (control): = ECAR = direct value from figure 2C: 285 pmoles/min/10^5 cells

L145 (chemo): = ECAR= direct value from figure 2C: 156 pmoles/min/10^5 cells

The rates of ATP synthesized by OXPHOS are as follows:

ATP synthesized by OXPHOS = OCR sensitive to oligomycin (= decline in basal OCR after oligomycin injection) x (P/O ratio of 2.5)

CRC09 (control): = 27 x 2.5 = 67.5 pmoles/min/10^5 cells

CRC09 (chemo): = 29 x2.5 = 72.5 pmoles/min/10^5 cells

L145 (control) = 26 x 2.5 = 65 pmoles/min/10^5 cells

L145 (chemo): = 42 x 2.5 = 105 pmoles/min/10^5 cells

CRC29 (control): = 57 x 2.5 = 142.5 pmoles/min/10^5 cells

CRC29 (chemo): = 208 x 2.5 = 520 pmoles/min/10^5 cells

Glycolysis is the predominant source of ATP production in non-treated colonospheres: pmoles of ATP for CRC09: 321 (glyc) versus 67.5 (OXPHOS) and for L145: 285 (glyc) versus 65 (OXPHOS). Furthermore chemotherapy increases ATP production via OXPHOS, while reducing ATP production via glycolysis.

CHAPTER 5

5

Lymphangiogenic gene expression is associated with lymph node recurrence and poor prognosis after partial hepatectomy for colorectal liver metastasis

Thomas T. Vellinga, Onno Kranenburg, Nicola Frenkel, Inge Ubink, Dieuwke Marvin, Klaas Govaert, Susanne van Schelven, Jeroen Hagendoorn and Inne H. M. Borel Rinkes

Ann Surg. 2017 Nov;266(5):765-771

Abstract

Objectives

To investigate the relevance of lymphangiogenic gene expression in primary and liver metastasis of colorectal cancer (CRC) and identify determinants of lymphatic invasion

Background

Lymphatic development promoting vascular endothelial growth factor C (VEGFC) is associated with poor outcome in primary CRC. For colorectal liver metastasis (CRLM), intrahepatic lymph invasion and lymph node metastasis are poor prognostic factors. Exact biological factors promoting lymphatic involvement remain elusive, just as the association with molecular subtypes of CRC.

Methods

We designed a lymphangiogenic gene set (VEGFC, Nrp-2, PDPN, LYVE-1, MRC1, CCL-21) and applied it to large datasets of CRC. Gene expression of the lymphangiogenic signature was assessed in resected CRLM specimens by Rt-QPCR. In vitro experiments were performed with colon cancer cell line Colo320 (high Nrp-2 expression) and human dermal microvascular lymphatic endothelial cells (LECs).

Results

Lymphangiogenic gene expression was associated with poor prognosis in both primary and liver metastasis of CRC. CRLM with high expression of consensus molecular subtype-4 identifier genes also exhibited high lymphangiogenic gene expression. Lymph node recurrence following CRLM resection was associated with high expression of VEGFC and Nrp-2. Blocking Nrp-2 significantly reduced invasion of Colo320 cells through an LEC monolayer.

Conclusions

Lymphangiogenic gene expression is correlated with worse prognosis and consensus molecular subtype-4 in both primary and liver metastatic CRC. VEGFC and Nrp-2 expression may be predictive of lymph node involvement in recurrence after resection of CRLM. Nrp-2, expressed on both tumor and LECs, may have a mechanistic role in lymphatic invasion and is a potential novel target in CRC.

Introduction

Colorectal Liver metastases (CRLM) ultimately occur in 60% of colorectal cancer patients [1]. While liver-directed treatment including partial hepatectomy may lead to cure in ~35% of cases, post-surgery recurrence still presents a formidable problem in the majority of patients and therapeutic efficacy remains low [2]. Therefore, molecular factors and genetic characteristics that can be used to predict, or exploited to treat, recurrence or progression of CRLM are needed. In primary CRC recent work has identified four Consensus Molecular Subtypes (CMS1-4) based on RNA expression analysis [3]. These molecular subtypes are reflections of differences in activity of specific signaling pathways. Where CMS1-3 have comparable prognosis, CMS4 has a statistically significant and clinically relevant worse prognosis. For CRLM these subtypes have not been defined so far. Another established prognostic marker in primary CRC is lymph node metastasis. In resectable CRLM, hepatic lymph node metastasis (i.e., lymph nodes in the hepatoduodenal ligament) was shown to be present in 15-28% of patients undergoing systematic hepatoduodenal lymph node dissection and to significantly worsen prognosis [4–7]. Moreover, intrahepatic lymphatic invasion is associated with decreased survival in resected CRLM [8]. Surprisingly, systematic hilar lymph node dissection is not a standard procedure during partial hepatectomy for CRLM. Interestingly, direct molecular evidence of lymphangiogenic or lymphatic metastasis-promoting pathways in CRLM is lacking. Vascular endothelial growth factor (VEGFC) is a major driver of lymphangiogenesis, lymphatic hyperplasia, and lymphatic metastasis [9] and is associated with lymph node metastasis and clinical outcome parameters in many cancer types [10]. VEGFC binds to VEGFR2 and VEGFR3 and activation of these receptors induces angiogenesis and lymphangiogenesis [11]. In primary CRC, VEGFC expression is clearly associated with shorter disease free/overall survival [12–14]. VEGFC mainly signals through VEGFR-3 to induce sprouting of lymphatic endothelial cells, with Neuropilin-2 (Nrp-2) acting as a co-receptor [15–17]. Blocking Nrp-2 inhibits the formation of functional lymphatic vessels within tumors and inhibits the development of metastasis. Importantly, this is partly independent of VEGF receptor activation [18]. This makes VEGFC and Nrp-2 the most important stimulants of lymphatic cancer dissemination documented to date. However, the relevance of lymphangiogenic gene expression in CRC and CRLM has not been investigated. In this study, we set out to find molecular factors that identify CRLM patients at risk for lymph node dissemination and provide data on the signaling pathways involved. Therefore, we devised a lymphangiogenic gene set and used unsupervised clustering analysis and show that this gene set is predictive of poor prognosis and of an aggressive mesenchymal molecular subtype in both primary CRC and CRLM. Second, using clinical follow up data from patients who had undergone partial hepatectomy for CRLM, we further validated the prognostic impact of VEGFC and Nrp-2 in post-resection lymph node recurrence. Last, we explored the potential mechanistic role of Nrp-2 in colorectal cancer cell invasion of lymphatic endothelium using in vitro

models and fluorescence microscopy. Taken together, these novel findings contribute to the characterization of aggressive CRC and provide a tool to select CRLM patients at high risk of developing lymph node recurrence. Surgically, these data may aid in identifying patients who may benefit from hilar lymphadenectomy during partial hepatectomy for colorectal liver metastasis. Oncologically, these data point to the VEGFC-VEGFR3 and Nrp-2 signaling pathways as potential targets in this patient population.

Material and methods

Bioinformatics analysis

For gene expression analysis we used the Guinney composite cohort (compiled of 18 CRC datasets), the Khambata-Ford cohort and our own previously generated dataset containing gene expression profiles of 119 CRLM deposited at Array Access E-TABM-1112 [3,19,20]. The datasets were uploaded into the R2 microarray analysis and visualization platform for subsequent analysis. Survival differences between groups were visualized using Kaplan Meier curves and p values were generated with the log rank test. Correction for multiple testing was done with the Bonferroni method. Composite values of expression of the lymphangiogenesis gene signature were generated by using the 'view geneset' option and storing the resulting values as a separate track. Expression of the lymphangiogenic signature within tumor subgroups (e.g. CMS1-4, or LM1-3) was analyzed by using the 'relate 2 tracks' option. The LA high/intermediate/low subgroups were generated by k-means clustering using the LA gene set. K-means clustering is a method for organizing gene expression data by clustering patients with similar gene expression of one gene or multiple genes (signature) in groups of high, (intermediate) and low expression.

Lymphangiogenic gene set

The lymphangiogenic gene set is a 6 gene signature, including the 2 main drivers of lymphangiogenesis, vascular endothelial growth factor C (VEGFC) and Neuropilin-2 (Nrp-2). The other 4 genes of the signature are all markers of lymph endothelial cells, including lymphatic vessel endothelial hyaluronan receptor 1 (LYVE-1), mannose receptor-C type 1 (MRC1), Chemokine (C-C motif) ligand 21 (CCL-21) and podoplanin (PDPN) [21].

Lymph node recurrence after partial hepatectomy for CRLM.

Our previous study involved 265 CRLM patients undergoing liver surgery [22]. Patients were categorized according to site of tumor recurrence. Of the 129 patients with post-hepatectomy recurrence, lymph node recurrence was present in 31 cases. Lymphanedectomy was not routinely performed at the time of initial hepatic surgery. 102 patients with post-hepatectomy recurrence had neo-adjuvant and/or adjuvant chemotherapy. Stored samples of the resected CRLM specimen were retrieved of these

patients. Inclusion for RNA extraction was based on bio-availability of patient material and informed consent. Total RNA was isolated according to the manufacturer's protocol (RNeasy Mini Kit, Qiagen).

Cell culture

Lymphatic endothelial cells were purchased from Lonza. HMVEC-dLyNeo-Der Lym Endo Cells, EGM-2MV, CC-2812. Colo320 cells were purchased from Sigma-Aldrich. Cells were cultured according to the manufacturers' protocol.

Immunofluorescence

Cells were fixed with 4% paraformaldehyde, permeabilized with 0,1% Triton X-100 in PBS, blocked with 1% BSA in PBS. After incubation with primary antibodies for 2h at RT, cells were washed 3xPBS and incubated with the secondary antibody for 30' at RT. Following the final washing step, cells were incubated with 5ug/ml DAPI.

Antibodies and reagents

For the Nrp-2 neutralization experiments we used the Nrp-2 antibody AF-2215 from R&D systems at a concentration of 20 µg/ml. For immunofluorescence and western blotting the Nrp-2 antibody from Santa Cruz was used (sc-13117). To track the colo320 cells during immunofluorescence they were stained with cell tracker orange (C2927), from Thermo Fisher Scientific. For PDPN western blotting we used PDPN antibody ab10288 from Abcam at 1/1000.

Matrigel invasion experiments

To test for invasion we used Corning Biocoat Matrigel Invasion Chambers, product #354480. For 8 hours LECs were allowed to form a monolayer, followed by seeding 200.000 colo320 cells on top. Colo320 cells were serum-starved for 8 hours. Medium in the top chamber was endothial growth medium (EGM). Medium in the bottom chamber was EGM + bulletkit minus VEGF and 1:1000 hepatocyte growth factor and 10% FBS were added. Colo320 cells were labeled with cell tracker orange, Thermo Fisher Scientific. After 22 hours membranes of the invasion chambers were harvested according to manufacturer's protocol. Subsequently the membranes were photographed by digital microscopy and uploaded into ImageJ. By using ImageJs threshold function the cells were selected. Next the number of cells was counted using analyze particles. All experiments were performed in triplicate. Data are representative of three independent experiments.

Quantitative Real Time Polymerase Chain Reaction

cDNA was synthesized using iScriptcDNA Synthesis Kit (Bio-Rad Laboratories). The amplification was performed in an iCyclerthermocycler (Bio-Rad Laboratories) using iQ SYBR Green Supermix (Bio-Rad Laboratories). mRNA expression levels were quantified

using iCycler software (Bio-Rad Laboratories) and were normalized to B2M. All patients provided informed consent for the use of their tumor material for research purposes.

Statistics

All values are presented as mean (SEM). Student t test (unpaired 2-tailed) was used to compare statistical differences between groups. Differences with a P-value<0.05 were considered statistically significant.

Results

Lymphangiogenic gene expression is associated with mesenchymal-type CRC and poor prognosis.

To study whether VEGFC expression was associated with a particular CMS we used a large composite cohort consisting of over three thousand primary CRC tumors [3]. Figure 1A shows that VEGFC expression is significantly higher in mesenchymal-like (CMS4) colon tumors than in any of the other subtypes. Furthermore, VEGFC expression alone is associated with a significantly shorter disease-free survival (p= 0.0021) (Fig. 1B). We generated a signature combining both factors that stimulate lymphangiogenesis and markers of lymph endothelial cells (VEGFC, Nrp-2, CCL21, LYVE1, MRC1, PDPN). This signature was subsequently used to identify 'lymphangiogenic-prone' tumors and to assess the potential relationship of its expression with survival. To this end, the tumors of the composite CMS cohort were clustered (k-means) into LymphAngiogenic LA-^{LOW}, LA-^{INTERMEDIATE}, and LA-^{HIGH} subgroups. These respective subgroups showed an increasing worse relapse free survival (Fig. 1C). Two relatively small CRC datasets in the r2 platform contain overall survival (OS) data: the Smith dataset, containing 232 tumors [23] and the AMC 90 set [24], comprised of 90 tumors. We divided these datasets into two clusters of respectively high and low expression of the LA signature. In the Smith dataset high LA expression is associated with significantly worse OS (p=0.011) and for the AMC 90 dataset there is a trend towards worse OS with high LA expression (p=0.157) (Supplemental Fig. S1A,B). Furthermore, the LA-^{HIGH} group largely consisted of mesenchymal-like (CMS4) tumors, whereas the LA-^{LOW} subgroup was mostly epithelial-like (CMS2, CMS3; Fig. 1D). This suggests that lymphangiogenic gene expression may be a previously unrecognized hallmark of poor-prognosis CMS4-type CRC. Next, we studied whether lymphangiogenic gene expression is associated with poor survival in patients with CRLM treated with an intentionally curative partial liver resection. To this end, we used a previously generated dataset containing gene expression profiles from resected liver metastases with clinical follow-up [19].

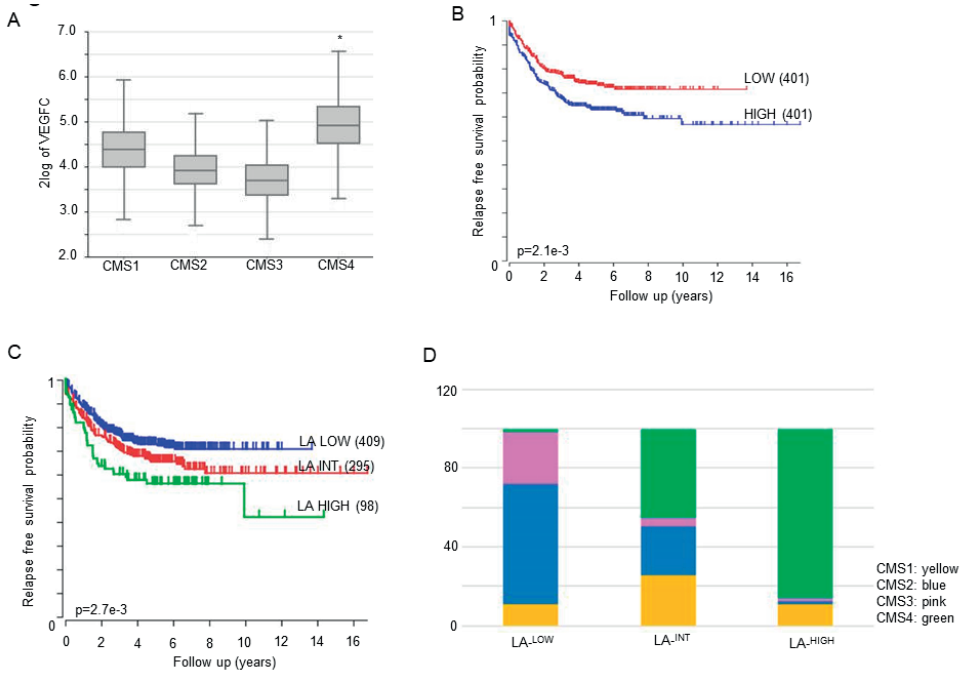

Figure 1

Lymphangiogenic gene expression is associated with mesenchymal-type CRC and poor prognosis.

(A) Box plot of VEGFC expression among the different consensus molecular subtypes (CMSs) in the Guinney composite cohort [3]. VEGFC is highest expressed in mesenchymal type CMS4. (B) Kaplan-Meier analysis of relapse free survival for CRC patients of the composite CMS cohort [3] according to VEGFC expression, the cutoff is median expression. (C) Kaplan Meier analysis of relapse free survival of the composite cohort according to expression of lymphangiogenic (LA) signature (based on k-means clustering). (D) Composite bar chart showing the distribution of the different CMSs in the LA-^{LOW}, LA-^{INT} and LA-^{HIGH} groups.

Consensus clustering identified three molecular subtypes (Liver Metastasis (LM) 1-3) in this dataset, including subtype LM3 associated with worse overall survival (p=1.5e-3) (Fig. 2A). Of these three LM subtypes, LM3 displayed a significantly higher expression of the lymphangiogenic signature (Fig. 2B). In line with this, we found that expression of the lymphangiogenic signature was strongly correlated with expression of CMS4-identfying signature genes in CRLM (r=0.830 p=2.0e-21) in an independently generated gene expression dataset [20] (Fig. 2C).

Lymph node recurrence following liver metastasis resection is associated with high expression of VEGFC and Nrp-2.

To validate the microarray data on patient material and relate to clinicopathological data we made use of our previously published paper concerning recurrence locations after hepatectomy for CRLM [22].

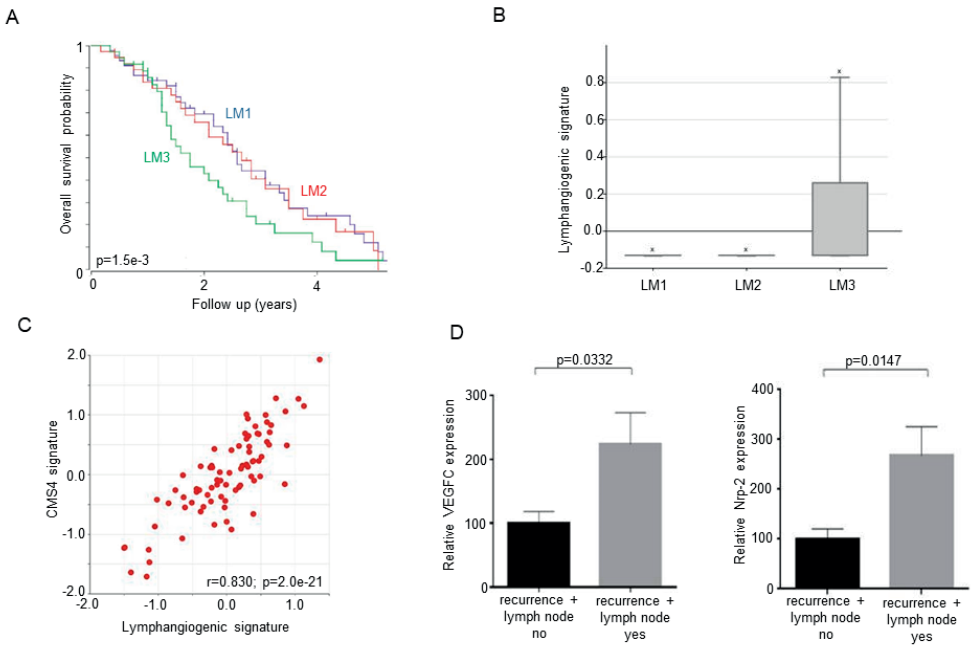

Figure 2

Lymph node recurrence following liver metastasis resection is associated with high expression of VEGFC and Nrp-2.

(A) Kaplan-Meier analysis of overall survival for CRLM patients treated with partial hepatectomy according to molecular subtype of the CRLM, as identified by k-means clustering. (B) Box plot of lymphangiogenic gene expression in CRLM. Lymphangiogenic gene expression is highest in poor prognosis CRLM subtype LM3. (C) Dot plot representing the correlation between the lymphangiogenic signature and the CMS4 signature in an independently generated gene expression dataset (r=0.830) [20]. (D) RT-qPCR analysis of VEGFC and Nrp-2 expression in CRLM. VEGFC and Nrp-2 are significantly higher expressed in CRLM of patients with lymph node involvement in their post-hepatectomy recurrence.

31 patients (24%) had recurrence with lymph nodes included in their recurrence locations. We extracted RNA from resected liver metastases of patients with lymph node involvement in their recurrence location (n=15) and from liver metastases of patients with recurrence and no lymph node involvement (n=15). RTqPCR analysis showed that the

levels of the main drivers of lymphangiogenesis and lymphatic invasion (VEGFC and Nrp-2) were significantly higher expressed in liver metastases that recurred *with* lymph node involvement than in those recurring *without* lymph node involvement (resp. p=0.0332 and p=0.0147) (Fig. 2D). The other 4 genes of the signature: PDPN, LYVE-1, MRC1 and CCL-21, all markers of lymphatic endothelial cells, were not significantly different between the two groups (Supplemental Fig. S2). Similar to VEGFC, Nrp-2 was highly expressed in primary CMS4-type tumors and high Nrp-2 expression was associated with decreased relapse free survival (p= 0.0001) (Fig. 3A, B).

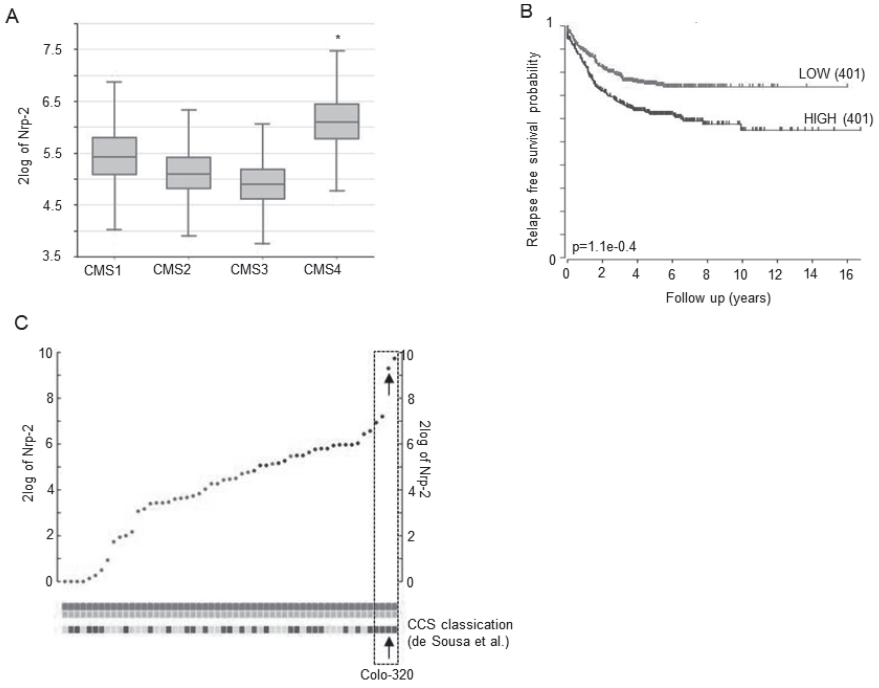

Figure 3

Nrp-2 is highly expressed in primary CMS4 tumors and associated with early relapse.

(A) Box plot of Nrp-2 expression in the different CMSs. Nrp-2 is highest expressed in mesenchymal type CMS4. (B) Kaplan-Meier analysis of relapse free survival for CRC patients of the composite CMS cohort [3] according to Nrp-2 expression, the cutoff is median expression. (C) Colorectal cell lines of the Cellline Cancer Encyclopedia (Broad Institute) sorted from low to high Nrp-2 expression. These cell lines have previously been classified into molecular subgroups according to the CCS classification. Colo320 is classified as poor prognosis subtype CCS3. (Yellow CCS1, blue CCS2, purple CCS3).

Nrp-2 mediates invasion of colon cancer cells through a monolayer of LECs.

To study the role of Nrp-2 in CRC invasion, we searched the Cellline Cancer Encyclopedia (Broad Institute) for (a) colorectal cancer cell line(s) expressing Nrp-2. These cell lines

have previously been classified into molecular subgroups [24]. We found that 4 out of 4 cell lines expressing the highest levels of Nrp-2 RNA were classified as mesenchymal (Fig. 3C). Based on these analyses we chose Colo320 as a model (mesenchymal-type) cell line in subsequent in vitro experiments. Western blot analysis confirmed Nrp-2 (but not PDPN) expression in Colo320 cells, while LECS expressed both markers (Supplemental Fig. S3). As expected [25], transwell assays showed the capacity of Colo320 cells to invade a basement membrane (BM) layer (Fig. 4A). Blocking Nrp-2 function with a neutralizing antibody (AF-2215, R&D systems, 20 µg/ml) did not affect the capacity of Colo320 cells to invade through BM. Next, we generated an additional barrier consisting of a monolayer of LECs on top of the BM. After the monolayer had reached confluency, Colo320 cells were seeded on top, either in the presence or absence of the Nrp2-neutralizing antibody or an isotype control antibody. Colo320 cells invaded through the LEC-monolayer and the BM, although with somewhat lower efficiency than through BM alone. The neutralizing Nrp-2 antibody almost completely prevented the invasion of Colo320 cells through the LEC-BM layer, while the isotype control antibody had no effect (Fig. 4B).

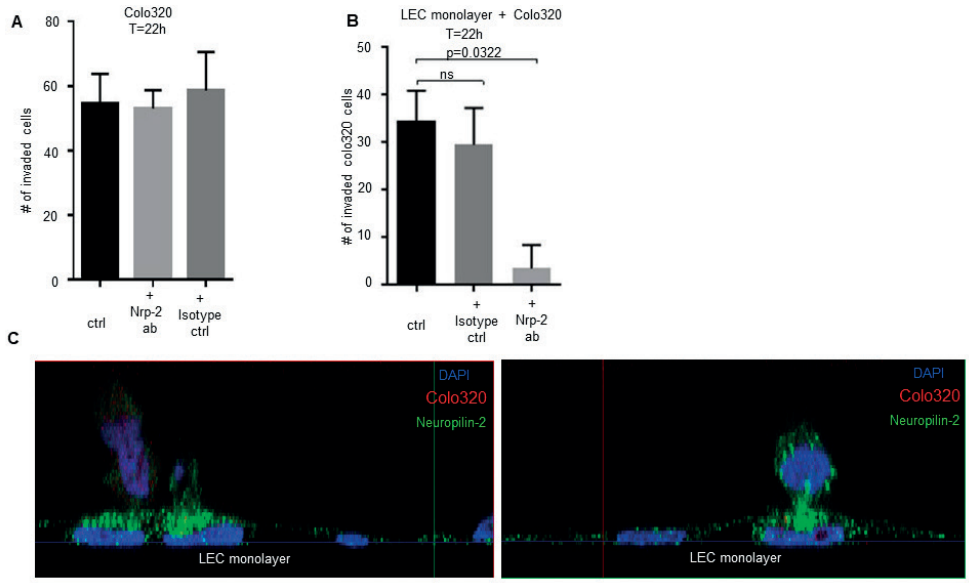

Figure 4

Nrp-2 mediates invasion of colon cancer cells through a monolayer of LECs.

(A) The percentage of invaded Colo320 cells in an invasion chamber assay. Ctrl, addition of Nrp-2 antibody or isotype control antibody. (B) The percentage of Colo320 cells that surpassed the LEC monolayer and matrigel layer of an invasion chamber assay. Nrp-2 antibody significantly impaired Colo320 invasion through a LEC monolayer (p=0.0322). (C) Immunofluorescence analysis of Nrp-2 in a LEC-Colo320 coculture. Data indicate higher Nrp-2 expression where colo320 cells interact with LEC.

To visualize the interaction between Colo320 cells and LECs immunofluorescence of a co-culture was performed. To distinguish the different cell types, Colo320 cells were stained with the fluorescent dye cell tracker orange. A confluent monolayer of LECs was created and orange Colo320 cells were placed on top. After 22 hours the coculture was fixed and stained with dapi and Nrp-2. 10% of the Colo320 cells interacted with the LEC bottom layer. Immunofluorescence analysis showed that Nrp-2 protein was localized to sites of interaction between colo320 cells and LECs (Fig. 4C).

Discussion

Although regional lymph node involvement in CRLM is a clinically relevant phenomenon [4–7] and intrahepatic lymphatic invasion predicts liver-lymph node metastasis [8], supporting molecular data on involved pathways and associated CRC subtypes does not exist. Using bioinformatics analysis in large gene expression datasets of both primary and liver-metastatic CRC, we here provide the first evidence that lymphangiogenic gene expression is a previously unrecognized feature of aggressive mesenchymal-type primary colorectal tumors, which is preserved in the liver-metastatic setting. We identified Nrp-2 and VEGFC as predictors of lymph node recurrence after liver surgery for CRLM. Our in vitro data point out to an important role of Nrp-2 in facilitating LEC invasion. The poor prognosis subtype in primary CRC, CMS4 is characterized by high expression of mesenchymal genes, epithelial to mesenchymal transition activation, transforming growth factor beta signaling and matrix remodeling [3]. K-means clustering analysis of our data identified 3 genetic subtypes in CRLM. Subtype LM3 is associated with worse prognosis and exhibits high expression of both the CMS4 identifier genes and the lymphangiogenic signature.

Nrp-2 and Nrp-1 make up the neuropilins, transmembrane glycoproteins that are activated by class III semaphorins and VEGFA/C. Nrp-2 is implicated in small lymphatic vessel development and is associated with lymphatic invasion in breast, papillary thyroid, clear renal cell and pancreatic cancer [17,26–28]. A large multi-institutional analysis of 1669 CRC patients showed the majority of patients (66%) had colorectal primaries with locoregional lymph node metastases [29]. Follow up of these patients identified as most frequent sites of metastasis the liver, followed by lymph nodes. This affirms the lymphatic system as a common metastatic route in CRC. The exact mechanism cancer cells use to enter the lymphatic system is unknown. VEGFC increases the delivery of cancer cells to lymph nodes [30]. In addition, our data pointed to Nrp-2 as an important factor in facilitating entry into the lymphatic system. Co-targeting of VEGFC and Nrp-2 could limit lymphatic dissemination and provide better containment for unresectable CRC metastases. Lymph nodes are the second most frequent site of CRC recurrence [29]. In CRLM hepatic lymph node invasion occurs in 15-28% [4–7]. Post partial hepatectomy 24% of patients develop recurrence that includes one or more lymph nodes. Ogura et al. demonstrated the value of

extended lymphadenectomy in CRC with isolated synchronous extraregional lymph node metastasis. Lymph node resection was associated with a significantly better prognosis[31]. A clinical consequence of our data could be that Nrp-2/VEGFC analysis allows us to select patients that may benefit from an added standard liver lymphadenectomy to the partial liver resection for their colorectal liver metastases. Alternatively such patients may also benefit from adjuvant lymph-angiogenesis targeting drugs (such as inhibitors of the VEGFR family, including VEGFR3) following liver resection.

References

1. Ruers, T. J. M. & Hagendoorn, J. Treatment dilemmas in patients with synchronous colorectal liver metastases. *Recent Results Cancer Res.* **196**, 37–49 (2012).
2. Araujo, R. L. C., Riechelmann, R. P. & Fong, Y. Patient selection for the surgical treatment of resectable colorectal liver metastases. *J. Surg. Oncol.* (2016). doi:10.1002/jso.24482
3. Guinney, J. *et al.* The consensus molecular subtypes of colorectal cancer. *Nat. Med.* **21**, 1350–1356 (2015).
4. Adam, R. *et al.* Is hepatic resection justified after chemotherapy in patients with colorectal liver metastases and lymph node involvement? *J. Clin. Oncol.* **26**, 3672–80 (2008).
5. Adam, R. *et al.* Concomitant Extrahepatic Disease in Patients With Colorectal Liver Metastases. *Ann. Surg.* **253**, 349–359 (2011).
6. Beckurts, K. T., Hölscher, a H., Thorban, S., Bollschweiler, E. & Siewert, J. R. Significance of lymph node involvement at the hepatic hilum in the resection of colorectal liver metastases. *Br. J. Surg.* **84**, 1081–4 (1997).
7. Laurent, C. *et al.* Impact of microscopic hepatic lymph node involvement on survival after resection of colorectal liver metastasis. *J. Am. Coll. Surg.* **198**, 884–891 (2004).
8. de Ridder, J. A. M., Knijn, N., Wiering, B., de Wilt, J. H. W. & Nagtegaal, I. D. Lymphatic Invasion is an Independent Adverse Prognostic Factor in Patients with Colorectal Liver Metastasis. *Ann. Surg. Oncol.* 638–645 (2015). doi:10.1245/s10434-015-4562-8
9. Tammela, T. & Alitalo, K. Lymphangiogenesis: Molecular Mechanisms and Future Promise. *Cell* **140**, 460–476 (2010).
10. Jain, RK, Fenton, B. T. Intratumoral Lymphatic Vessels: A Case of Mistaken Identity or Malfunction? *JNCI J Natl Cancer Inst* **94**, 417–421 (2002).
11. Ferrara, N., Gerber, H. P. & LeCouter, J. The biology of VEGF and its receptors. *Nat Med* **9**, 669–676 (2003).
12. Li X, Liu B, Xiao J, Yuan Y, Ma J, Z. Y. Roles of VEGF-C and Smad4 in the lymphangiogenesis, lymphatic metastasis, and prognosis in colon cancer. *J Gastrointest Surg* 2001–10 (2011).
13. Zhang, C. *et al.* Elevated IGFIR expression regulating VEGF and VEGF-C predicts lymph node metastasis in human colorectal cancer. *BMC Cancer* **10**, 184 (2010).
14. Onogawa, S. *et al.* Expression of VEGF-C and VEGF-D at the invasive edge correlates with lymph node metastasis and prognosis of patients with colorectal carcinoma. *Cancer Sci.* **95**, 32–39 (2004).
15. Soker, S., Miao, H. Q., Nomi, M., Takashima, S. & Klagsbrun, M. VEGF165 mediates formation of complexes containing VEGFR-2 and neuropilin-1 that enhance VEGF165-receptor binding. *J. Cell. Biochem.* **85**, 357–368 (2002).
16. Favier, B. *et al.* Neuropilin-2 interacts with VEGFR-2 and VEGFR-3 and promotes human endothelial cell survival and migration. *Blood* **108**, 1243–1250 (2006).
17. Yuan, L. *et al.* Abnormal lymphatic vessel development in neuropilin 2 mutant mice. *Development* **129**, 4797–4806 (2002).

18. Caunt, M. *et al.* Blocking Neuropilin-2 Function Inhibits Tumor Cell Metastasis. *Cancer Cell* **13**, 331–342 (2008).
19. Snoeren, N. *et al.* Exploring Gene Expression Signatures for Predicting Disease Free Survival after Resection of Colorectal Cancer Liver Metastases. *PLoS One* **7**, (2012).
20. Khambata-Ford, S. *et al.* Expression of Epiregulin and Amphiregulin and K-ras Mutation Status Predict Disease Control in Metastatic Colorectal Cancer Patients Treated With Cetuximab. *J. Clin. Oncol.* **25**, 3230–3237 (2007).
21. Nelson, G. M., Padera, T. P., Garkavtsev, I., Shioda, T. & Jain, R. K. Differential Gene Expression of Primary Cultured Lymphatic and Blood Vascular Endothelial Cells. *Neoplasia* **9**, 1038–1045 (2007).
22. Govaert, K. M. *et al.* Recurrence Location After Resection of Colorectal Liver Metastases Influences Prognosis. *J. Gastrointest. Surg.* **18**, 952–960 (2014).
23. Smith, J. J. *et al.* Experimentally Derived Metastasis Gene Expression Profile Predicts Recurrence and Death in Patients With Colon Cancer. *Gastroenterology* **138**, 958–968 (2010).
24. De Sousa E Melo, F. *et al.* Poor-prognosis colon cancer is defined by a molecularly distinct subtype and develops from serrated precursor lesions. *Nat. Med.* **19**, 614–8 (2013).
25. Li, H. W. & Shan, J. X. Effects of hepatocyte growth factor/scatter factor on the invasion of colorectal cancer cells in vitro. *World J. Gastroenterol.* **11**, 3877–3881 (2005).
26. Cao, Y. *et al.* Neuropilin-2 promotes extravasation and metastasis by interacting with endothelial α5 integrin. *Cancer Res.* **73**, 4579–4590 (2013).
27. Yasuoka, H. *et al.* Neuropilin-2 expression in breast cancer: correlation with lymph node metastasis, poor prognosis, and regulation of CXCR4 expression. *BMC Cancer* **9**, 220 (2009).
28. Yasuoka, H. *et al.* VEGF-D expression and lymph vessels play an important role for lymph node metastasis in papillary thyroid carcinoma. *Mod. Pathol.* **18**, 1127–1133 (2005).
29. de Jong, M. C. *et al.* Rates and patterns of recurrence following curative intent surgery for colorectal liver metastasis: an international multi-institutional analysis of 1669 patients. *Ann. Surg.* **250**, 440–8 (2009).
30. Hoshida, T. *et al.* Imaging steps of lymphatic metastasis reveals that vascular endothelial growth factor-C increases metastasis by increasing delivery of cancer cells to lymph nodes: Therapeutic implications. *Cancer Res.* **66**, 8065–8075 (2006).
31. Ogura, A. *et al.* The significance of extended lymphadenectomy for colorectal cancer with isolated synchronous extraregional lymph node metastasis. *Asian Journal of Surgery* (2015). doi:10.1016/j.asjsur.2015.10.003

Supplemental figures

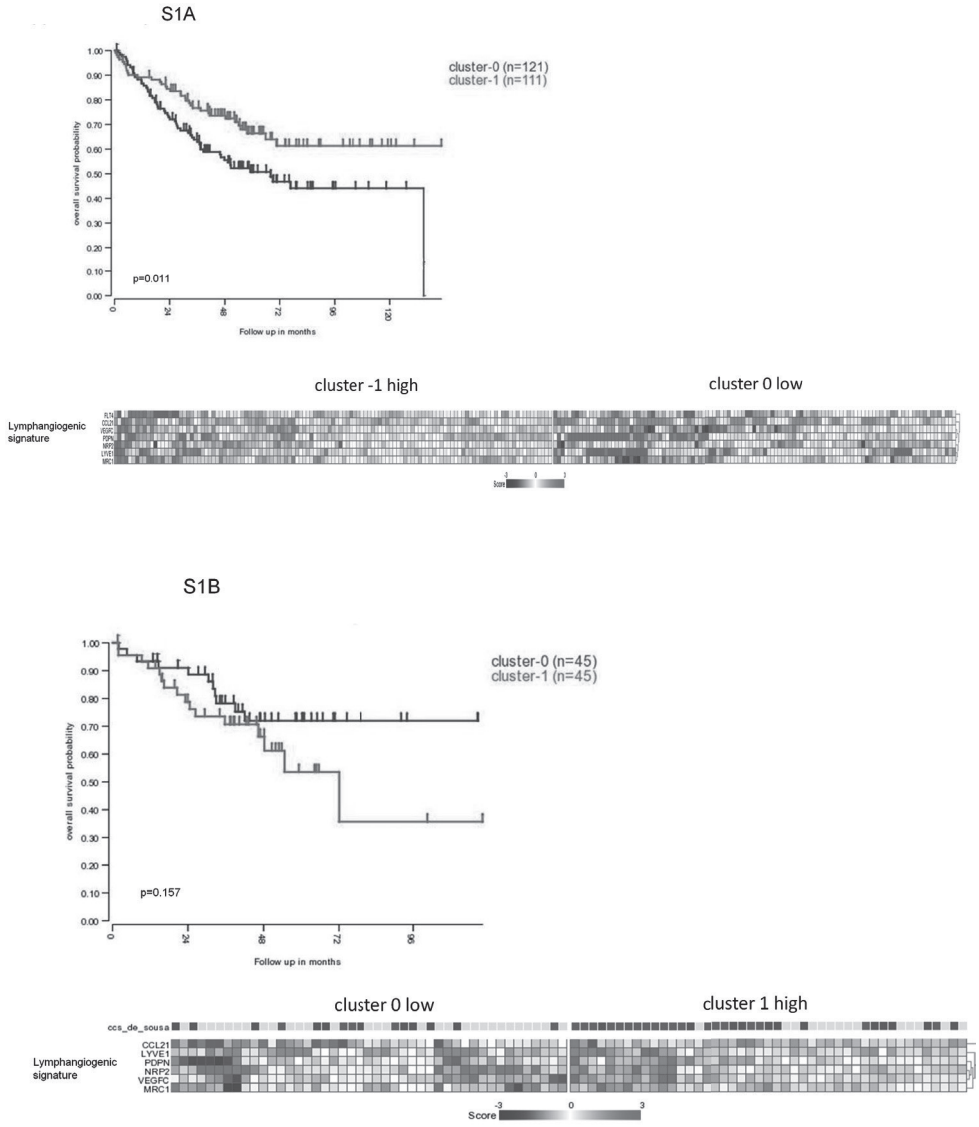

Supplemental figure S1

(A) Kaplan Meier analysis of overall survival (OS) of the Smith cohort according to expression of lymphangiogenic (LA) signature (high versus low cluster). High expression of the LA signature is associated with significantly worse OS (p=0.011). (B) Kaplan Meier analysis of OS of the AMC 90 cohort according to expression of lymphangiogenic (LA) signature (high versus low cluster). High expression of the LA signature shows a trend towards worse OS (p=0.157).

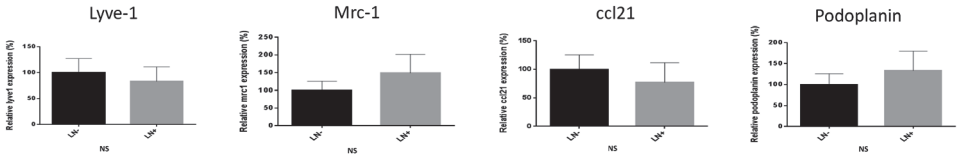

Supplemental figure S2

RT-qPCR analysis of lymphatic vessel endothelial hyaluronan receptor 1 (LYVE-1), mannose receptor-C type 1 (MRC1), Chemokine (C-C motif) ligand 21 (CCL-21) and podoplanin (PDPN) expression in CRLM.

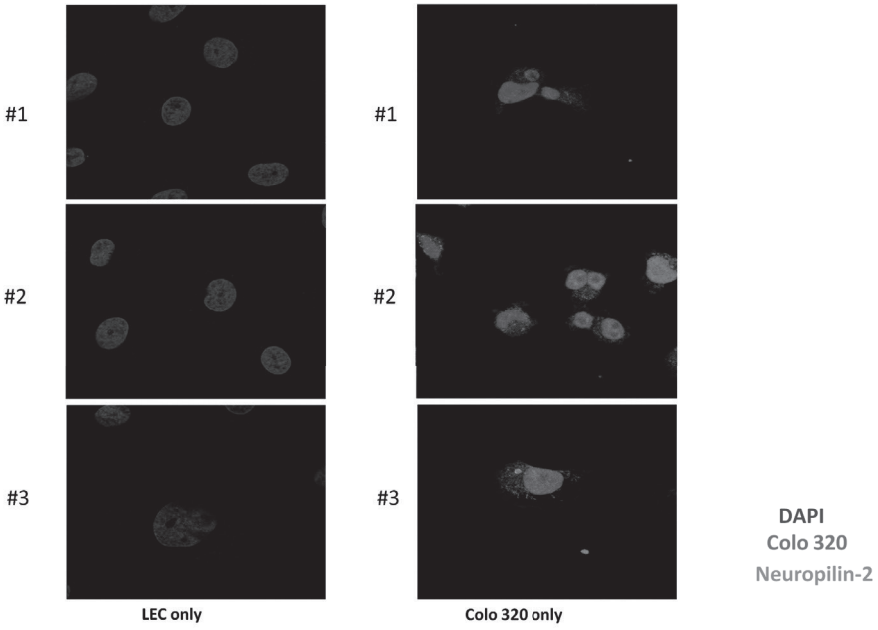

Supplemental figure S3

Western blot analysis of Nrp-2 and PDPN protein levels in Colo320 and LECs. LECs express both PDPN and Nrp-2 protein, Colo320 cells only express Nrp-2 protein.

CHAPTER 6

6

Inhibition of RAF1 kinase activity restores apico-basal polarity and impairs tumor growth in human colorectal cancer

Tijana Borovski, Thomas T. Vellinga, Jamila Laoukili, Evan E. Santo, Szabolcs Fatrai, Susanne van Schelven, André Verheem, Dieuwke Marvin, Inge Ubink, Inne H.M. Borel Rinkes, Onno Kranenburg.

Gut. 2017 Jun;66(6):1106-1115

Abstract

Background and Aim

Colorectal cancer (CRC) remains one of the leading causes of cancer-related death. Novel therapeutics are urgently needed, especially for tumors with activating mutations in *KRAS* (~40%). Here we investigated the role of RAF1 in CRC, as a potential, novel target.

Methods

Colonosphere cultures were established from human tumor specimens obtained from patients who underwent colon or liver resection for primary or metastatic adenocarcinoma. The role of RAF1 was tested by generating knock-downs (KDs) using three independent shRNA constructs or by using RAF1-kinase inhibitor GW5074. Clone- and tumor-initiating capacities were assessed by single-cell cloning and injecting CRC cells into immune-deficient mice. Expression of TJs proteins, localization of polarity proteins and activation of MEK-ERK pathway was analyzed by western blot, immunohistochemistry and immunofluorescence.

Results

Knock-down or pharmacological inhibition of RAF1 significantly decreased clone- and tumor-forming capacity of all CRC cultures tested, including *KRAS*-mutants. This was not due to cytotoxicity but, at least in part, to differentiation of tumor cells into goblet-like cells. Inhibition of RAF1-kinase activity restored apico-basal polarity and the formation of tight junctions (TJ) *in vitro* and *in vivo,* without reducing MEK-ERK phosphorylation. MEK-inhibition failed to restore polarity and TJs. Moreover, RAF1-impaired tumors were characterized by normalized tissue architecture.

Conclusion

RAF1 plays a critical role in maintaining the transformed phenotype of CRC cells, including those with mutated *KRAS*. The effects of RAF1 are kinase-dependent, but MEK-independent. Despite the lack of activating mutations in RAF1, its kinase domain is an attractive therapeutic target for CRC.

Introduction

Colorectal cancer (CRC) is the third most common cancer worldwide. Unless resectable, CRC has a dismal prognosis and continues to be a major cause of mortality. Systemic therapy has prolonged the life-expectancy of patients with metastatic CRC (mCRC) to approximately two years, but therapy resistance is virtually unavoidable. Standard chemotherapy regimens consist of fluoropyrimidines, combined with either oxaliplatin or irinotecan. More recently, monoclonal antibodies targeting VEGF and EGFR have also been approved for the treatment of mCRC. Anti-VEGF therapy has become part of the standard treatment, but predictors of response are currently missing. Resistance to anti-EGFR therapy can be caused by RAS pathway activation, most commonly through activating mutations in the *KRAS* oncogene[1]. Activating mutations in *KRAS* result in a constitutively active protein which no longer relies on upstream signals from the EGFR, providing a rationale for the observed resistance. Currently, assessing the mutational status of *KRAS* is being used to exclude patients for EGFR-targeted therapy. Therefore, the treatment of CRC, and mutant *KRAS* tumors in particular, remains a huge challenge and novel therapeutic strategies need to be identified.

The RAF-kinases (ARAF, BRAF, CRAF/RAF1) are well known activators of the classical MEK-ERK pathway. CRCs frequently carry activating mutations in *KRAS* (~40%) or *BRAF* (~10%) leading to constitutive activation of this pathway. Surprisingly, activating mutations in *ARAF* or *RAF1* are infrequent in human CRC (<1%, COSMIC), despite the fact that both kinases can replace BRAF in activating the MEK-ERK cascade, although with less potency. Even though RAF1 has been extensively studied as a link between RAS activation and downstream MEK-ERK signaling, genetic ablation studies in mice have revealed that it is not essential for activating this pathway, but rather for suppressing apoptosis during embryonic development and in adult, healthy tissue [2;3]. Intriguingly, RAF1 suppresses apoptosis by inhibiting pro-apoptotic kinases independently of its kinase activity[4;5]. RAF1 also regulates RHO signaling in a kinase-independent manner, which has at least two context-dependent effects. First, RAF1-mediated ROK inhibition results in a decreased sensitivity to death receptor-mediated apoptosis and hence increases tumor cell survival[6;7]. Second, in epidermal cells RAF1/ROK interaction prevents keratinocyte differentiation and this is essential for the formation of squamous cell carcinomas (SCC) driven by mutant *RAS*[8]. Likewise, RAF1 is critical for development of *KRAS*-mutated lung cancer [9].

RAF1 has received relatively little attention in the context of CRC biology, at least in part due to the lack of activating mutations[10]. However, microarray data of multiple colon cancer cohorts show that RAF1 is highly expressed in virtually all human CRCs (Cartes d'Identité des Tumeurs (CIT)=GSE39582; MVRM =GSE14333, GSE17536, GSE17537)[11-13]. Therefore, we set out to elucidate its role in CRC. We show that RAF1 knockdown (KD) or inhibition of

its kinase activity strongly decreased clone- and tumor-forming capacity in CRC cells with different genetic backgrounds, including *KRAS*-mutants. Suppression or pharmacological inhibition of RAF1 restored apico-basal polarity and functional tight junctions (TJs). This was observed both *in vitro* and *in vivo*. In RAF1-impaired tumors, cancer cells grew in ordered monolayers while control tumors grew as disorganized masses. Furthermore, RAF1-KD or treatment with kinase inhibitor promoted differentiation of tumor cells into goblet-like lineage. By contrast, MEK kinase inhibition did not restore polarity or TJ formation, pointing to a RAF1 kinase-dependent, but MEK-independent pathway. We conclude, thus, that RAF1-kinase domain is a compelling therapeutic target for CRC.

Material and methods

Cell culture

Human colonosphere cultures were isolated from patients undergoing colon or liver resection of primary or metastatic CRC and were cultured as described previously[14]. For polarity experiments, cells were plated on collagen-coated plates.

Colony forming assay

Colonospheres were dissociated with Accumax (Innovative Cell Technologies) into singe cell suspension, filtered through 40μM filter and 1000 cells/well were plated in matrigel (BD) in 6-well plates. Fresh medium was added and refreshed every two days. Colonies were counted after two weeks and colonosphere-forming efficiency was calculated as the percentage of seeded cells that formed colonospheres.

Inhibitors and antibodies

Antibodies: RAF1 (BD), beta-actin (Novus Biologicals), Occludin (Invitrogen), JAM-A (Sigma), E-cadherin (BD), Alexa Fluor 488 phalloidin (Invitrogen), Ezrin (BD), Villin (Leica), Par3 (Millipore), aPKC (Santa Cruz), p-Erk (Cell Signaling), ERK (Cell Signaling), Muc2 (Santa Cruz), Ki67 (Novocastra), Cleaved caspase 3 (Cell Signaling), Alexa Fluor 488 (Invitrogen), p-MEK (Cell Signaling), MEK (Cell Signaling). Inhibitors: GW5074 (Enzo), U0126 (Cell Signaling), Selumetinib (Selleckchem).

Treatment of cells with the inhibitors was done as follows: Cells were treated either with 1μM GW5074, 1μM selumetinib or 10μM U0126. For all the inhibitors experimental setup (timing) was the same, depending on what was measured. For measuring phosphorylation of MEK and ERK, cells were treated 3 and/or 24 hours with the inhibitor. Restoration of polarity and expression of tight junction proteins was measured three days after incubation with the inhibitor, and in colony forming assay inhibitor was refreshed two times per week for two weeks.

Tumor formation

Control and RAF1-KD spheroids were dissociated into single cell suspension using Accumax, resuspended in aliquots containing ~10.000 cells and mixed with Matrigel (BD) at 1:1 ratio (total volume 100 µl) prior to subcutaneous injection into the flanks of 10 weeks old BALB/c $^{nu/nu}$ mice.

GW5074 treatment experiment: mice were injected with ~50.000 cells and randomly divided in two groups. Immediately upon the injection, treatment group received 10mg/kg of GW5074 and control group PBS intraperitoneally, and mice were injected 3x/week until they were sacrificed.

Mice were sacrificed when tumors reached a maximum of 1cm^3. All experiments involving the use of animals were performed in accordance with University of Utrecht institutional animal welfare guidelines.

Lentiviral transduction

The shRNA-RAF1 plasmids were obtained from the MISSION® shRNA TRC library (Sigma) #4[TRCN0000196264], #5[TRCN0000195646] and #7[TRCN0000197115]. shSCR plasmid (SHC002) was used as a control. RAF1-WT was a kind gift from prof. W.Kolch and BRAF-WT from prof. D.J.Maly. Lentiviral particles were generated by transfecting 293T cells with pLKO and packaging vectors using Fugine (Roche). Selection of transduced cells was done with Puromycin (Sigma).

Immunofluorescence and immunohistochemistry

Immunofluorescence: Cells were fixed with 4% paraformaldehyde, permeabilized with 0,1% Triton X-100 in PBS, blocked with 1% BSA in PBS. After incubation with primary antibodies for 2h at RT, cells were washed 3xPBS and incubated with the secondary antibody for 30' at RT. Following the final washing step, cells were incubated with 5ug/ml DAPI.

Immunohistochemistry: Tumor tissue samples were deparaffinised, antigens were retrieved with 10mM sodium citrate buffer pH6, followed by peroxide blocking (1%H_2O_2 in methanol) and serum blocking, after which primary antibody was incubated at RT for 2h. For detection Powervision (Immunologic) and DAB solution (DAKO) were used, and counterstaining with haematoxylin.

Statistics

All values are presented as mean (SEM). Student *t* test (unpaired 2-tailed) was used to compare statistical differences between groups. Differences with a *P*-value<0.05 were considered statistically significant.

Microarray data analysis

Gene-expression analysis was performed using the genomics analysis and visualization platform R2 (http://r2.amc.nl). To find differentially expressed genes between the groups, we used FDR-corrected p-values of <0.1 (ANOVA). This yielded a list of 223 upregulated and 186 downregulated genes following RAF1-KD (supplementary table 1), that were further submitted to "Gene Ontology Analysis" to get significant GO classifications. Lincscloud analysis (http://www.lincscloud.org) was performed by submitting these genesets (up & downregulated as a single signature) to the 'Query' tool. To assess the relationship between these genesets in normal *versus* tumor cells we used a dataset containing expression profiles of tumor and normal colonic organoids from the same patients[15]. All organoids were assigned two z-scores each; one for 223 upragulated and another for 186 downregulated genes upon RAF1-KD by using the 'View Geneset' option in R2 and saving the resulting z-values as a new track. The compiled z-scores were then plotted in an XY-graph, assigning different colors to normal and tumor organoids.

Results

RAF1-KD reduces clonogenic and tumorigenic capacity of CRC cells

In order to investigate the role of RAF1 in CRC cells, we used 'colonosphere' cultures with high RAF1 expression and different genetic backgrounds, established from resected primary CRC or liver metastases (supplementary fig 1A and supplementary table 2). RAF1 expression was suppressed in three independent cultures (CR16, CRC29, L145) by stable expression of RAF1-targeting shRNA (fig 1A). We used three different constructs to establish efficient RAF1-KD in all three cell cultures (#4, #5, #7). All the experiments were done with at least two different KDs. shRNA construct targeting GFP was used as a control. First, we determined whether RAF1-KD had an effect on clone-forming capacity. RAF1-KD cells formed significantly less colonies when compared to control cells in all three colonosphere cultures and with both KD constructs (fig 1B). Next, we investigated whether tumor-forming capacity was affected by RAF1-KD. When injected into nude mice, control L145 cells readily generated fast growing tumors, but the tumor-forming capacity of RAF1-KD cells (2 independent shRNAs) was significantly impaired (fig 1C). Due to the changes we observed on clonogenicity and tumorigenicity upon RAF1-KD, we measured if any of the cancer stem cell markers are altered (supplementary fig 1B).

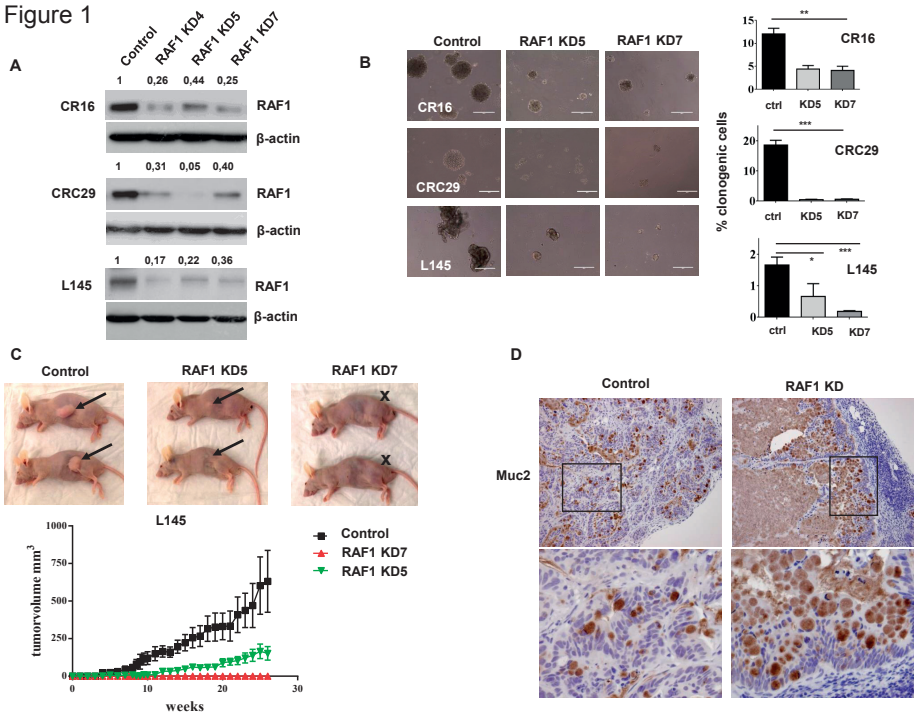

Figure 1

RAF1-KD impairs clonogenicity and tumorigenicity of CRC cells

(A) Generating RAF1-KDs in CRC cultures CR16, CRC29 and L145, using three independent shRNAs #4, #5 and #7 resulted in significant down-regulation of RAF1, measured by WB. Numbers represent quantification of the bands on the WBs. (B) Clonogenic assay demonstrated that RAF1-KD colonospheres (CR16, CRC29 and L145) have decreased sphere-forming ability. Statistical significances: *P<0.05, **P<0.01 and ***P<0.001. (C) Tumor-forming capacity of L145 RAF1-KD5 and KD7 is significantly impaired. (D) Muc2 staining showing differentiation of L145 RAF1-KD5 tumors into goblet cells.

We measured Aldefluor activity (ALDH), CD133 expression and CD44v6 levels and did not detect any significant change in the expression of these markers upon RAF1-KD. This could be explained by already published reports showing that CSC markers are not reliable criteria (proper read-out) for selecting tumorigenic cells as tumor cells negative for those markers can exhibit similar tumorigenic and proliferative capacities[16-18]. RAF1 plays an important role in suppressing apoptosis[4;5]. Thus we investigated whether increased apoptosis in the RAF1-KD cultures could explain their diminished clonogenic and tumorigenic capacity. However, the percentage of apoptotic cells was comparable between control and RAF1-KD cells *in vitro* and *in vivo* (supplementary fig 1C and D). Rather, we found that RAF1-KD tumors displayed a strongly reduced number of proliferating (Ki67+) cells (supplementary fig 1D). When analyzing the morphology of the tumors we noticed that, unlike control

tumors, the majority of RAF1-KD tumor cells had large vacuoles and a goblet-like morphology, suggesting a more pronounced differentiation in this group. Muc2 and PAS staining confirmed a goblet-like phenotype of cancer cells in RAF1-KD tumors (fig 1D and supplementary fig 1E). Unlike Muc2, staining for FABP1 and Chromogranin A showed no significant difference between control and RAF1-KD group, suggesting that other differentiation lineages were unaltered upon RAF1-KD (supplementary fig 1F).

RAF1-KD restores functional tight junctions in CRC cells

During the culturing of control and RAF1-KD colonospheres, we noticed a striking morphological difference: RAF1-KD cultures formed larger, more tightly packed spheroids than control cultures (supplementary fig 2A). Phalloidin staining showed increased and more ordered cortical actin organization between neighboring cells in RAF1-KD spheroids, suggesting increased formation of junctional complexes and cell-cell interactions (fig 2A and supplementary fig 2B). Western blot and immunofluorescence analysis revealed that expression of the TJ proteins JAM-A and Occludin was significantly increased in RAF1-KD cultures (fig 2B, 2C; supplementary fig 2C). By contrast, adherens junction protein E-cadherin was unaffected by RAF1-KD (supplementary fig 2D). Moreover, comparing gene expression profiles of RAF1-KD and control tumors revealed that genes involved in actin cytoskeleton organization, intercellular junctions and establishment of cell polarity are significantly upregulated in RAF1-KD (fig 2D). Consistent with the previous experiments, these results also confirm major phenotypic change in RAF1-KD. In the normal intestinal epithelium, TJs form a physical barrier for peri-cellular transport of macromolecules and bacteria, and this is (partially) lost during oncogenic transformation. The re-establishment of TJs in RAF1-KD cultures prompted us to analyze epithelial barrier function by using fluorescently labeled dextran. In control cultures Dextran-Red readily diffused between the cells and accumulated throughout the spheroids. However, in RAF1-KDs Dextran-Red was retained on the surface of the monolayer, demonstrating the re-establishment of epithelial barrier function (fig 2E).

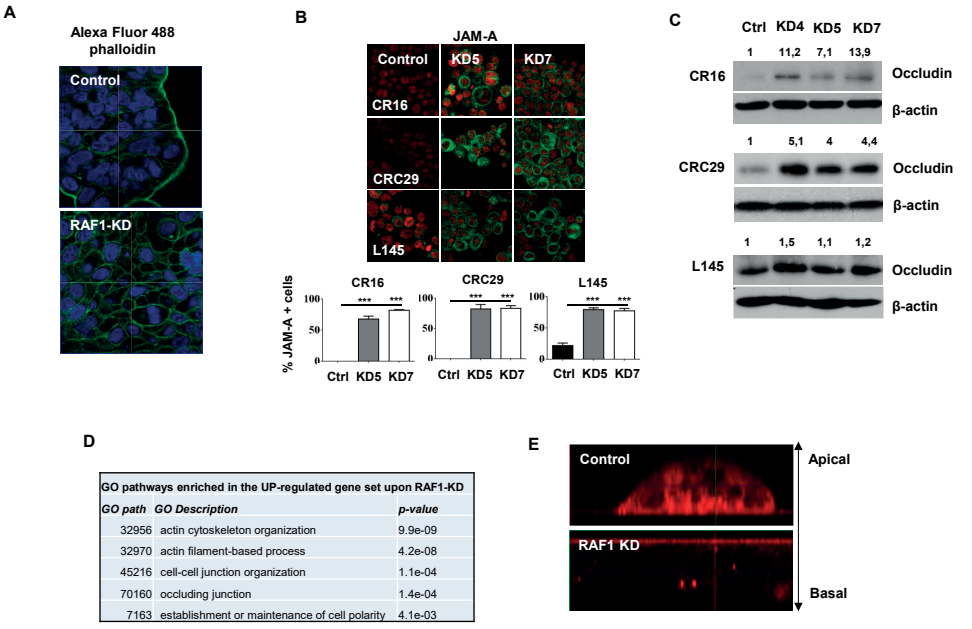

D

GO pathways enriched in the UP-regulated gene set upon RAF1-KD		
GO path	*GO Description*	*p-value*
32956	actin cytoskeleton organization	9.9e-09
32970	actin filament-based process	4.2e-08
45216	cell-cell junction organization	1.1e-04
70160	occluding junction	1.4e-04
7163	establishment or maintenance of cell polarity	4.1e-03

Figure 2

RAF1-KD restores TJs in CRC cells

(A) Phalloidin staining demonstrated more organized cortical actin between neighboring cells in L145 RAF1-KD7 compared to control. (B) Staining for TJ protein JAM-A showed significant upregulation in RAF1-KD5 and KD7, in all three colonosphere cultures, quantification depicted on the graphs. Statistical significance: ***P<0.001. (C) TJ protein Occludin was significantly upregulated in all the RAF1-KDs (#4, #5, #7) of CR16, CRC29 and L145, measured by WB. Numbers represent quantification of the bands on the WBs. (D) Gene ontology analysis demonstrated significant enrichment in genes involved in actin organization, cell-cell junctions and cell polarity in L145 RAF1-KD5 xenografts compared to Control samples. (E) Incubation with Dextran-Red demonstrated that newly formed TJs retain Dextran-Red on the surface of the L145 RAF1-KD5 cells whereas in control samples it infiltrates in-between the cells due to the lack of functional TJs.

RAF1-KD restores cell polarity in CRC cells *in vitro* and *in vivo*

TJs help the establishment and maintenance of cell polarity in untransformed tissues. They are essential for maintenance of epithelial barrier function, preventing the lateral diffusion of membrane-associated proteins between the apical and baso-lateral domains, thus preserving the specialized function of each region[19]. Loss of polarity and downregulation of TJs are commonly associated with cancer. Therefore, we analyzed whether cell polarity was normalized upon RAF1-KD. When seeded on adherent plates, control cells retained their spherical architecture. By contrast, RAF1-KD cells spread out to form a monolayer (supplementary fig 3A). To study cell polarity, we analyzed the localization of apical markers. In RAF1-KD tumor cells, Ezrin and Villin distribution was specifically localized at the actin-rich apical side of the tumor cells and excluded from the basal side (fig 3A).

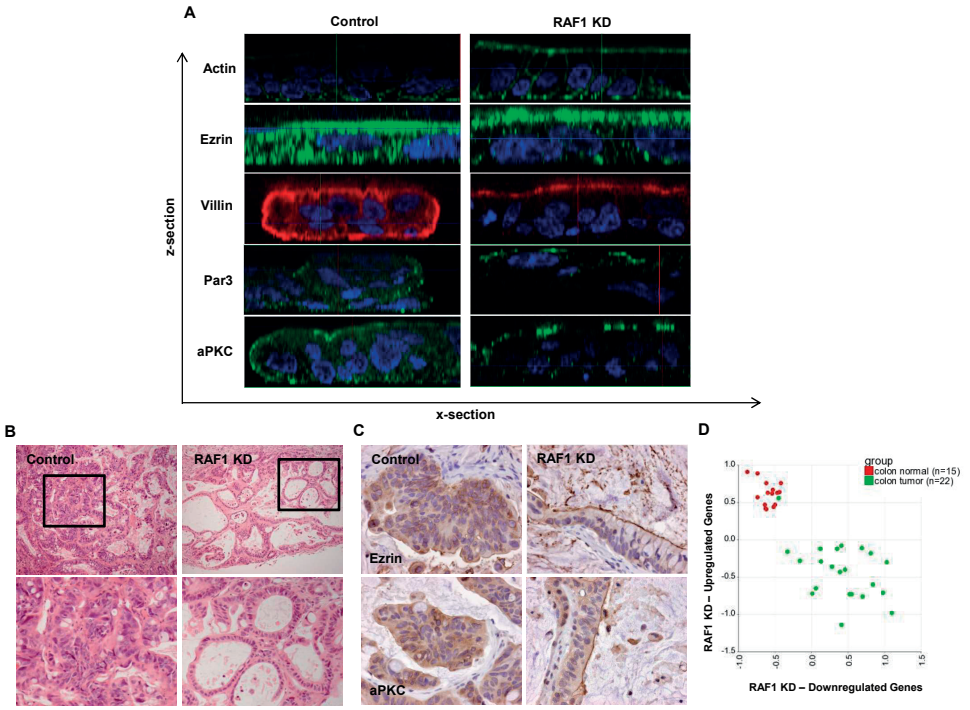

Figure 3

RAF1-KD restores polarity in tumor cells *in vitro* and *in vivo*

(A) IF staining for apical markers (Actin, Ezrin, Villin, Par3, aPKC) on L145 revealed uniform distribution of these proteins in control samples and apical localization in RAF1-KD5 and KD7. (B) H&E staining of L145 xenografts demonstrated that RAF1-KD5 cells form monolayers in tumors as opposed to control samples where tumors grew as disorganized mass. (C) Staining for Ezrin and aPKC confirmed polarization of cells in L145 RAF1-KD5 tumors; these proteins are exclusively localized on the apical side of the KD cells and uniformly distributed throughout control tumors. (D) Normal and tumor tissue can be separated based on genes altered upon RAF1-KD. Upregulated genes upon KD show a strong correlation with normal tissue, whereas downregulated genes show a strong correlation with tumor tissue.

By contrast, in control cells these proteins were uniformly distributed. Furthermore, in control cells both Par3 and aPKC polarity proteins were distributed in a non-polarized fashion. However, they were restricted to the apical part of RAF1-KD cells, further confirming the restoration of polarity (fig 3A). Next, we analyzed histological sections of control and RAF1-KD tumors from figure 1C to determine if the effect on polarity also occurs in tumors. There was a striking difference in tissue organization. Whereas L145 control tumors grew as disorganized masses, RAF1-KD5 tumors mainly consisted of highly organized monolayer structures (fig 3B). Immunohistochemistry for apical markers (Ezrin, aPKC), revealed a uniform distribution of these proteins throughout the tumor tissue in the control group. However, both markers were exclusively localized on the apical side

of RAF1-KD tumor cells, confirming restoration of polarity (fig 3C). Accordingly, staining for tight junction protein Occludin demonstrated apical localization in RAF1-KD tumors compared to control group (supplementary fig 3B). Interaction between epithelial cells and extracellular matrix is critical aspect of cell polarization. Body of literature demonstrated vinculin to be the key regulator of focal adhesions, enabling cells to adhere to variety of ECM proteins [20;21]. Thus we performed Vinculin staining on L145 Control and RAF1-KD xenografts. Vinculin expression was increased in the RAF1-KD tumors compared to the control samples (supplementary fig 3C). This correlates with microarray data also demonstrating increased RNA levels of Vinculin in RAF1-KD xenografts compared to Control group (supplementary fig 3C). These results are in line with the higher degree of clustering and attachment of RAF1-KD cells that we observe in the rest of our experiments, as well as with their restored polarity. Microarray data further support normalization of tumor tissue upon RAF1-KD. Strikingly, genes altered upon RAF1-KD can completely separate healthy colon tissue from tumor tissue (fig 3D). Genes upregulated upon RAF1-KD show a strong correlation with normal colon tissue, and downregulated genes are strongly associated with tumor tissue. These data further confirm that KD of RAF1 can fully reestablish cell polarity and normalize the structure of the tissue.

Effects of RAF1-KD on clonogenicity and polarity are kinase-dependent

RAF1 can act in a kinase-dependent and -independent manner. In order to assess whether the control of cell polarity and clone/tumor-forming capacity by RAF1 depends on its kinase activity, we used the RAF1-kinase inhibitor GW5074. This inhibitor potently suppressed the kinase activity of ectopically expressed RAF1, as measured by p-MEK levels, and had hardly any effect on BRAF-induced MEK phosphorylation (supplementary fig 4A and 4B). Also, it strongly decreased clonogenic capacity of colonospheres (fig 4A). In addition to L145, we included two additional *KRAS*-mutant CRC cultures: L169 (spheroid) and p9t (organoid) (supplementary table 3). The colony-forming capacity of both cultures was significantly affected by GW5074 treatment (supplementary fig 4C). However, the effect was dependent on the presence of the inhibitor. Once the inhibitor was removed, cells regained their growth potential (supplementary figure 4D). Furthermore, treatment with the GW5074 inhibitor also induced expression of TJ proteins *in vitro* and *in vivo* (fig 4C, 4D, supplementary fig 4E). Importantly, GW5074 treatment also restored the polarity in colonospheres and this was accompanied by the formation of large spheroid aggregates, an effect also observed in RAF1-KD (fig 4B and supplementary fig 4F, 4G). Localization of adherens junction protein, E-cadherin, was also normalized upon GW5074 treatment (supplementary figure 4H). These results demonstrate that RAF1-kinase activity is required for regulation of cell polarity and clone-forming capacity in human CRC cells.

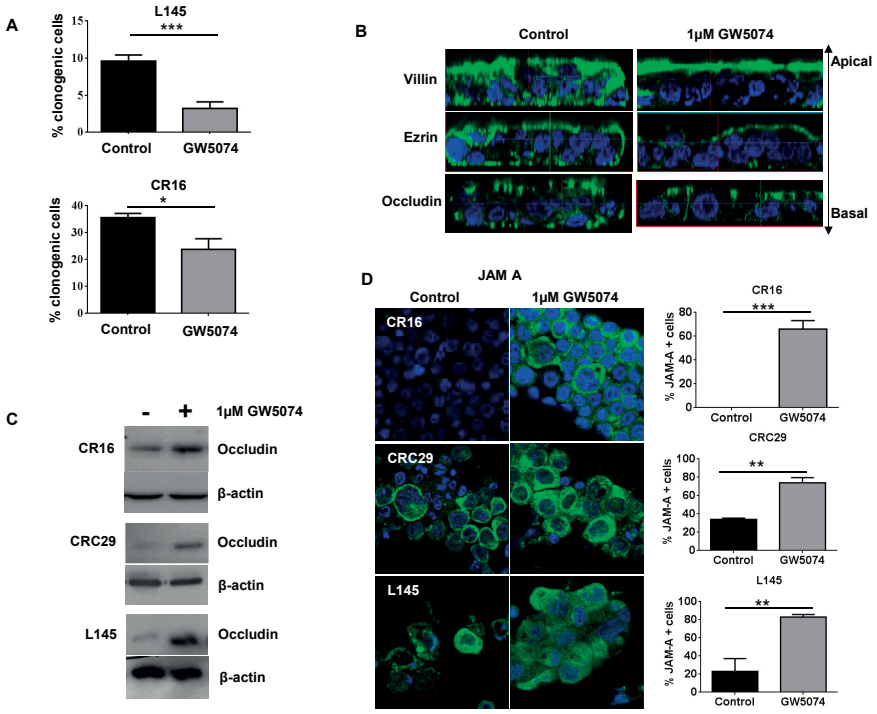

Figure 4

Effects of RAF1 on TJs and polarity are kinase-dependent

(A) Clonogenic capacity of CRC cells CR16 and L145 is significantly decreased when treated with RAF1-kinase inhibitor GW5074 (1μM). Statistical significances: *P<0.05 and ***P<0.001. (B) Treatment with GW5074 restores cell polarity in L145 colonospheres, demonstrated by apical localization of Ezrin, Villin and tight junction protein Occludin. (C) GW5074 treatment increased Occludin expression in CR16, CRC29 and L145 compared to control, measured by WB. (D) JAM-A is elevated upon treatment with GW5074 inhibitor compared to control samples in CR16, CRC29 and L145, quantification depicted on the graphs. Statistical significances: **P<0.01 and ***P<0.001.

Effects of RAF1-KD on clonogenicity and polarity are MEK-ERK independent

We next investigated whether RAF1 regulates TJs and cell polarity through MEK-ERK signaling. Analysis of p-ERK and p-MEK in colonospheres and tumors showed that this pathway was not inhibited upon RAF1-KD. The levels of p-ERK and p-MEK were either comparable between the samples or increased upon RAF1-KD, consistent with previous studies (fig 5A, 5B)[22]. Moreover, we used Lincscloud database to compare the profiles of differentially regulated genes in RAF1-KD with the profiles generated after the treatment with various MEK-inhibitors (fig 5C). The closer the score is to 100 the more significant the match to the signature created by the compound is. 4 out of 5 MEK-inhibitors tested on 55 cell lines induced the changes in gene expression that had no correlation (or even an inverse association) with the changes in gene expression following RAF1-KD. This is in line

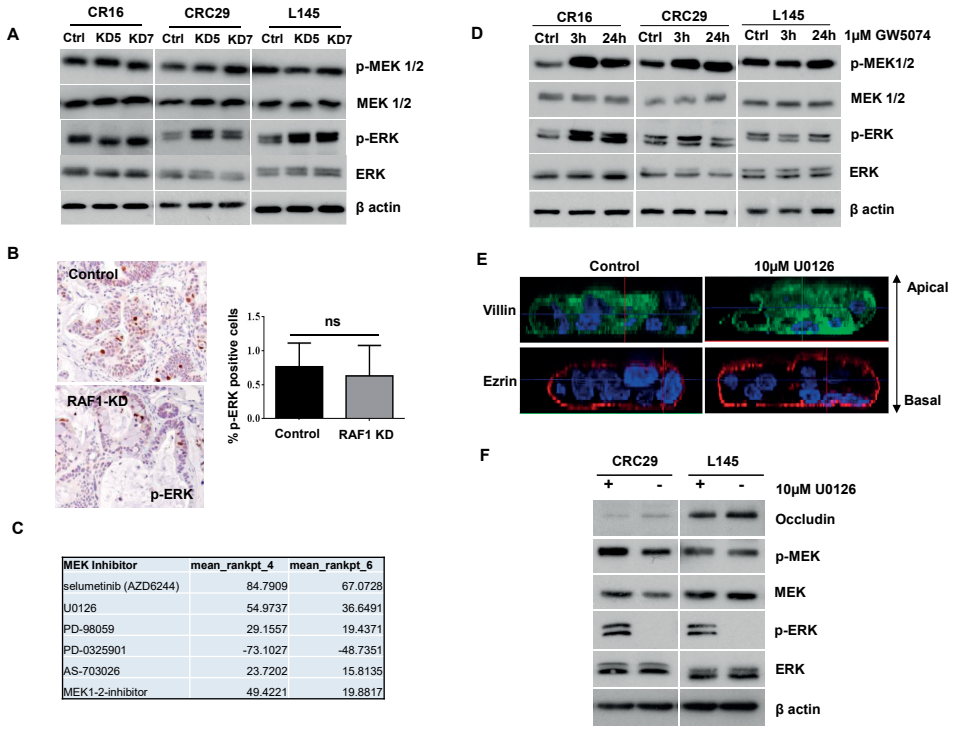

MEK Inhibitor	mean_rankpt_4	mean_rankpt_6
selumetinib (AZD6244)	84.7909	67.0728
U0126	54.9737	36.6491
PD-98059	29.1557	19.4371
PD-0325901	-73.1027	-48.7351
AS-703026	23.7202	15.8135
MEK1-2-inhibitor	49.4221	19.8817

Figure 5

(A) p-ERK and p-MEK levels are not decreased upon RAF1-KD, as shown in CR16, CRC29 and L145 when comparing Control samples to RAF1-KD5 and KD7, measured by WB. (B) p-ERK staining in L145 RAF1-KD5 and control xenografts demonstrated comparable levels between the groups, quantification depicted in the graph. (C) Lincscloud analysis comparing RAF-KD profiles with the signatures generated by the listed MEK-inhibitors using two different thresholds. (D) WB demonstrated that p-ERK and p-MEK levels are not inhibited by GW5047 treatment in any of the CRC cultures (CR16, CRC29 and L145). (E) Cell polarity is not restored in L145 upon U0126 treatment, judging by the uniform distribution of Ezrin and Villin. (F) Phosphorylation of ERK is significantly decreased, while Occludin levels are unaltered upon treatment with MEK-inhibitor U0126 in CRC29 and L145, measured by WB.

with the notion that the effects of RAF1-KD are largely independent of MEK-ERK signaling. In addition, p-ERK and p-MEK levels were not decreased by GW5074 treatment, but were unaltered or even upregulated (fig 5D and supplementary fig 5A). This points to a MEK-ERK-independent effect of GW5074, which is in line with a recent study in hepatocellular carcinoma cells[23]. Treatment with the MEK-inhibitors U0126 or selumetinib successfully inhibited MEK-ERK signaling, but did not restore polarity, nor did it induce an increase in Occludin expression (fig 5E, 5F, supplementary fig 5B, 5C). These data demonstrate that the kinase-dependent effects of RAF1 do not occur via canonical MEK-ERK signaling.

Inhibition of RAF1-kinase activity reduces tumor growth and restores polarity of CRC cells

The above data show that RAF1-kinase activity plays a role in maintenance of the transformed phenotype of human CRC cells. We next investigated whether this feature can be exploited therapeutically. Mice carrying subcutaneous L145 (KRAS-mutant) tumors were treated with either RAF1-kinase inhibitor GW5074 or with saline as a control. As shown in figure 6A, tumor growth was significantly reduced in GW5074 treated mice.

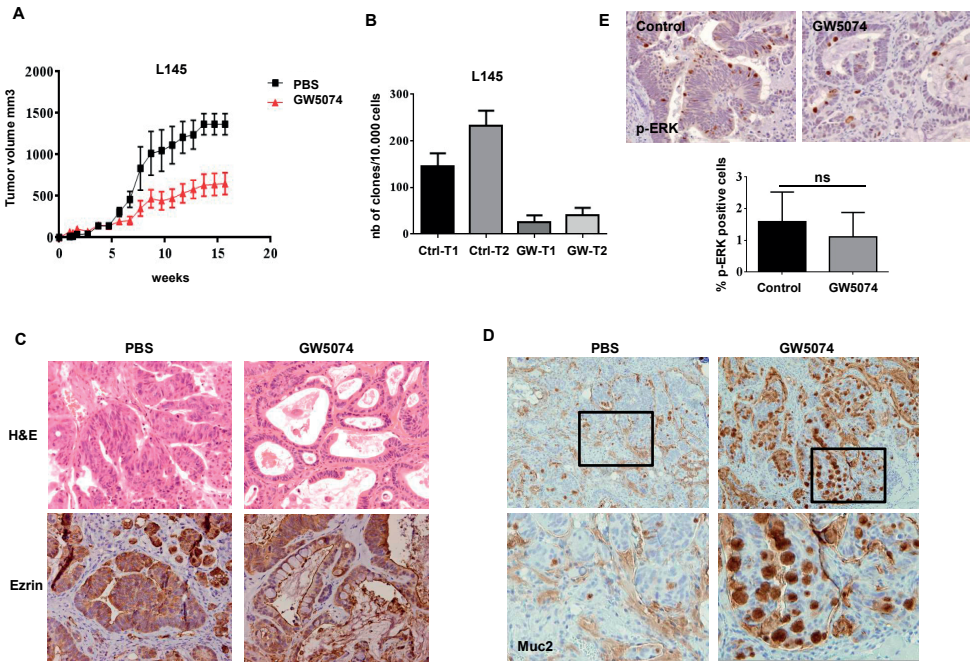

Figure 6

Inhibition of RAF1-kinase activity impairs tumorigenic capacity and restores tissue polarity

(A) Treatment with RAF1-kinase inhibitor GW5074 impairs tumorigenic capacity of L145 CRC cells. (B) Clonogenic capacity of L145 cells isolated from GW5074-treated tumors is significantly decreased compared to control samples. (C) H&E staining shows monolayers of cells in L145 GW5074-treated tumors in contrast to control tumors that grew as disorganized mass. IHC for Ezrin showed apical localization of this protein in treated mice, and uniform expression in control samples. (D) Unlike control tumors, majority of cells in L145 GW5074-treated tumors differentiated into goblet cells, demonstrated by Muc2 staining. (E) p-ERK staining in L145 GW5074 treated and control tumors and quantification, demonstrating comparable expression between the groups.

This was not due to increased apoptosis, but rather to decreased proliferation (supplementary fig 6A). Moreover, cells isolated from GW5074 treated tumors had

significantly reduced colony-forming capacity when compared to cells isolated from control tumors (fig 6B). Comparable to RAF1-KD tumors, but unlike control, GW5074 treated tumors were characterized by low cell density and highly organized monolayers (fig 6C). Furthermore, immunohistochemistry for Ezrin showed that cell polarity was restored in tumors treated with the inhibitor (fig 6C). In addition, the majority of cells in GW5074 treated tumors expressed high levels of mucin-2, indicating goblet-like differentiation (fig 6D and supplementary fig 6B). Thus, inhibition of RAF1-kinase activity severely affected tumor growth and pushed cells into a goblet-like differentiation pathway, acting in a MEK-ERK independent manner (fig 6E). In order to see if the effect of inhibitor is permanent, we serially transplanted L145 xenografts from Fig 6A. As shown in the supplementary figure 6C, tumors that were treated with GW5074 started growing with a significant delay. However, eventually they equalized their growth with the control tumors. Thus, reduced tumor growth is dependent on the presence of the inhibitor.

Discussion

In the present study we provide evidence that RAF1 is required for maintenance of the clonogenic and tumorigenic capacity of human CRC cells, including those carrying *KRAS* mutations. This is in line with previous studies showing that deletion of RAF1 is detrimental for tumor initiation and maintenance of *RAS*-driven SCC and lung cancer[8;24]. Strikingly, we found that RAF1-KD or pharmacological inhibition of its kinase activity caused a profound re-establishment of apico-basal polarity and restoration of functional TJs. To our knowledge, this is only the second report in which modulation of the activity of a single protein has such a dramatic effect on (tumor) cell polarity. A previous study showed that, similar to RAF1-KD/inhibition, LKB1 activation by STRAD causes complete polarization of intestinal epithelial cells[25]. Restored polarity could have major implications for the tumorigenesis. Reduced cell-cell contacts and loss of polarity are commonly associated with oncogenic transformation, especially with advanced malignant tumors. In fact, in human cancers crucial cell polarity proteins are directly targeted by oncogenes or tumor-suppressor genes such as ErbB2, TGBFβ or PTEN and data from *Drosophila* show clearly that loss of polarity and changes in adhesion can be initiating events in tumor formation[26]. The disruption of apico-basal polarity helps tumor cells to extrude from epithelial sheets at the basal side, rather than being shed apically into the lumen[27]. This not only helps establishing a multi-layered tumor mass, but also promotes invasion of the surrounding tissue. In line with these studies, our data show that RAF1 suppression or inhibition yields tumors with restored polarity, and is accompanied by the formation of monolayer structures with apoptotic tumor cells being predominantly found in the lumen that is encased by them. Thus, RAF1 suppression is sufficient to cause normalization of tissue architecture and epithelial growth.

Re-expression of TJ proteins in cancer cells induced apoptosis and suppressed metastasis in several cancer models, supporting the notion that a reduction in TJs is critical for maintenance of the transformed phenotype[28-30]. Moreover, leaky TJs may help the diffusion of growth factors and nutrients through multi-layered tumor cell masses and can thereby promote tumor growth[31]. TJ formation following RAF1 suppression or inhibition was accompanied by increased expression of the core TJ proteins Occludin and JAM-A. This result extends previously published data showing that overexpression of a constitutively active RAF1 suppresses Occludin expression in salivary gland epithelial cells[32]. The effect of RAF1 suppression/inhibition on diminished clonogenicity and tumorigenicity could thus be, at least in part, the consequence of newly restored TJs and polarity. Furthermore, in the SCC model RAF1 ablation induced terminal differentiation of tumor cells[8]. Likewise, our results show that RAF1 impaired tumors were significantly enriched in differentiated goblet-like cells which could, in addition to restored polarity, also effect tumor growth.

The effects of RAF1 were kinase-dependent, but were not accompanied by inhibition of the MEK-ERK pathway and could not be phenocopied by MEK inhibition. This is in line with previous studies showing that RAF1 supports tumorigenesis primarily in a MEK-ERK-independent fashion [8;9;24]. What are the clinical implications of our findings? Large clinical trials with agents targeting RAF or MEK have shown that such drugs do not dramatically improve survival. Activation of feedback pathways and the fact that these studies were done in unselected patient populations may underlie this failure. Indeed, BRAF inhibitors fail to be effective in *BRAF* mutant CRCs due to activation of an EGFR-PI3K feedback pathway[33]. Upregulation of PI3K/ERBB3 appears to mediate resistance to MEK inhibitors in *KRAS*-mutant CRC [34;35]. Thus, re-activation of feedback signaling pathways is greatly undermining the efficacy of these treatments. Selective RAF1 inhibition, without concomitant BRAF inhibition, is not expected to affect MEK-ERK activity and, in all likelihood, would not cause activation of these rescue pathways. Recent reports demonstrated indeed that suppression of RAF1 dramatically increased the efficiency of MEK inhibitors in *KRAS* mutant tumors, leading to permanent MEK-ERK inhibition and apoptosis [36;37]. We propose that, in addition to preventing MEK-ERK re-activation following BRAF or MEK inhibition, RAF1 inhibition simultaneously causes tumor cell polarization and differentiation in a MEK-ERK-independent manner and impairs tumor growth. The development of potent and specific RAF1-kinase inhibitors could have an impact on (colon) cancer treatment and should be tested as a novel RAF-targeting strategy for improving the treatment of CRC.

References

1 Prenen H, Tejpar S, Van CE. New strategies for treatment of KRAS mutant metastatic colorectal cancer. *Clin Cancer Res* 2010;**16**(11):2921-6.

2 Huser M, Luckett J, Chiloeches A *et al*. MEK kinase activity is not necessary for Raf-1 function. *EMBO J* 2001;**20**(8):1940-51.

3 Mikula M, Schreiber M, Husak Z *et al*. Embryonic lethality and fetal liver apoptosis in mice lacking the c-raf-1 gene. *EMBO J* 2001;**20**(8):1952-62.

4 O'Neill E, Rushworth L, Baccarini M *et al*. Role of the kinase MST2 in suppression of apoptosis by the proto-oncogene product Raf-1. *Science* 2004;**306**(5705):2267-70.

5 Chen J, Fujii K, Zhang L *et al*. Raf-1 promotes cell survival by antagonizing apoptosis signal-regulating kinase 1 through a MEK-ERK independent mechanism. *Proc Natl Acad Sci U S A* 2001;**98**(14):7783-8.

6 Piazzolla D, Meissl K, Kucerova L *et al*. Raf-1 sets the threshold of Fas sensitivity by modulating Rok-alpha signaling. *J Cell Biol* 2005;**171**(6):1013-22.

7 Hoogwater FJ, Nijkamp MW, Smakman N *et al*. Oncogenic K-Ras turns death receptors into metastasis-promoting receptors in human and mouse colorectal cancer cells. *Gastroenterology* 2010;**138**(7):2357-67.

8 Ehrenreiter K, Kern F, Velamoor V *et al*. Raf-1 addiction in Ras-induced skin carcinogenesis. *Cancer Cell* 2009;**16**(2):149-60.

9 Blasco RB, Francoz S, Santamaria D *et al*. c-Raf, but not B-Raf, is essential for development of K-Ras oncogene-driven non-small cell lung carcinoma. *Cancer Cell* 2011;**19**(5):652-63.

10 Emuss V, Garnett M, Mason C *et al*. Mutations of C-RAF are rare in human cancer because C-RAF has a low basal kinase activity compared with B-RAF. *Cancer Res* 2005;**65**(21):9719-26.

11 Marisa L, de RA, Duval A *et al*. Gene expression classification of colon cancer into molecular subtypes: characterization, validation, and prognostic value. *PLoS Med* 2013;**10**(5):e1001453.

12 Jorissen RN, Gibbs P, Christie M *et al*. Metastasis-Associated Gene Expression Changes Predict Poor Outcomes in Patients with Dukes Stage B and C Colorectal Cancer. *Clin Cancer Res* 2009;**15**(24):7642-51.

13 Smith JJ, Deane NG, Wu F *et al*. Experimentally derived metastasis gene expression profile predicts recurrence and death in patients with colon cancer. *Gastroenterology* 2010;**138**(3):958-68.

14 Emmink BL, VAN Houdt WJ, Vries RG *et al*. Differentiated human colorectal cancer cells protect tumor-initiating cells from irinotecan. *Gastroenterology* 2011;**141**(1):269-78.

15 van de Wetering M, Francies HE, Francis JM *et al*. Prospective derivation of a living organoid biobank of colorectal cancer patients. *Cell* 2015;**161**(4):933-45.

16 Muraro MG, Mele V, Daster S *et al*. CD133+, CD166+CD44+, and CD24+CD44+ phenotypes fail to reliably identify cell populations with cancer stem cell functional features in established human colorectal cancer cell lines. *Stem Cells Transl Med* 2012;**1**(8):592-603.

17 Lehmann C, Jobs G, Thomas M *et al*. Established breast cancer stem cell markers do not correlate with in vivo tumorigenicity of tumor-initiating cells. *Int J Oncol* 2012;**41**(6):1932-42.
18 Rocco A, Liguori E, Pirozzi G *et al*. CD133 and CD44 cell surface markers do not identify cancer stem cells in primary human gastric tumors. *J Cell Physiol* 2012;**227**(6):2686-93.
19 Shin K, Fogg VC, Margolis B. Tight junctions and cell polarity. *Annu Rev Cell Dev Biol* 2006;**22**:207-35.
20 Jockusch BM, Rudiger M. Crosstalk between cell adhesion molecules: vinculin as a paradigm for regulation by conformation. *Trends Cell Biol* 1996;**6**(8):311-5.
21 Ziegler WH, Liddington RC, Critchley DR. The structure and regulation of vinculin. *Trends Cell Biol* 2006;**16**(9):453-60.
22 Desideri E, Cavallo AL, Baccarini M. Alike but Different: RAF Paralogs and Their Signaling Outputs. *Cell* 2015;**161**(5):967-70.
23 Breunig C, Mueller BJ, Umansky L *et al*. BRaf and MEK inhibitors differentially regulate cell fate and microenvironment in human hepatocellular carcinoma. *Clin Cancer Res* 2014;**20**(9):2410-23.
24 Karreth FA, Frese KK, DeNicola GM *et al*. C-Raf is required for the initiation of lung cancer by K-Ras(G12D). *Cancer Discov* 2011;**1**(2):128-36.
25 Baas AF, Kuipers J, van der Wel NN *et al*. Complete polarization of single intestinal epithelial cells upon activation of LKB1 by STRAD. *Cell* 2004;**116**(3):457-66.
26 Lee M, Vasioukhin V. Cell polarity and cancer--cell and tissue polarity as a non-canonical tumor suppressor. *J Cell Sci* 2008;**121**(Pt 8):1141-50.
27 Slattum GM, Rosenblatt J. Tumour cell invasion: an emerging role for basal epithelial cell extrusion. *Nat Rev Cancer* 2014;**14**(7):495-501.
28 Osanai M, Murata M, Nishikiori N *et al*. Epigenetic silencing of occludin promotes tumorigenic and metastatic properties of cancer cells via modulations of unique sets of apoptosis-associated genes. *Cancer Res* 2006;**66**(18):9125-33.
29 Hoevel T, Macek R, Swisshelm K *et al*. Reexpression of the TJ protein CLDN1 induces apoptosis in breast tumor spheroids. *Int J Cancer* 2004;**108**(3):374-83.
30 Michl P, Barth C, Buchholz M *et al*. Claudin-4 expression decreases invasiveness and metastatic potential of pancreatic cancer. *Cancer Res* 2003;**63**(19):6265-71.
31 Mullin JM, Laughlin KV, Ginanni N *et al*. Increased tight junction permeability can result from protein kinase C activation/translocation and act as a tumor promotional event in epithelial cancers. *Ann N Y Acad Sci* 2000;**915**:231-6.
32 Li D, Mrsny RJ. Oncogenic Raf-1 disrupts epithelial tight junctions via downregulation of occludin. *J Cell Biol* 2000;**148**(4):791-800.
33 Prahallad A, Sun C, Huang S *et al*. Unresponsiveness of colon cancer to BRAF(V600E) inhibition through feedback activation of EGFR. *Nature* 2012;**483**(7387):100-3.
34 Wee S, Jagani Z, Xiang KX *et al*. PI3K pathway activation mediates resistance to MEK inhibitors in KRAS mutant cancers. *Cancer Res* 2009;**69**(10):4286-93.

35 Sun C, Hobor S, Bertotti A *et al*. Intrinsic resistance to MEK inhibition in KRAS mutant lung and colon cancer through transcriptional induction of ERBB3. *Cell Rep* 2014;**7**(1):86-93.

36 Lito P, Saborowski A, Yue J *et al*. Disruption of CRAF-mediated MEK activation is required for effective MEK inhibition in KRAS mutant tumors. *Cancer Cell* 2014;**25**(5):697-710.

37 Lamba S, Russo M, Sun C *et al*. RAF suppression synergizes with MEK inhibition in KRAS mutant cancer cells. *Cell Rep* 2014;**8**(5):1475-83.

Supplementary information

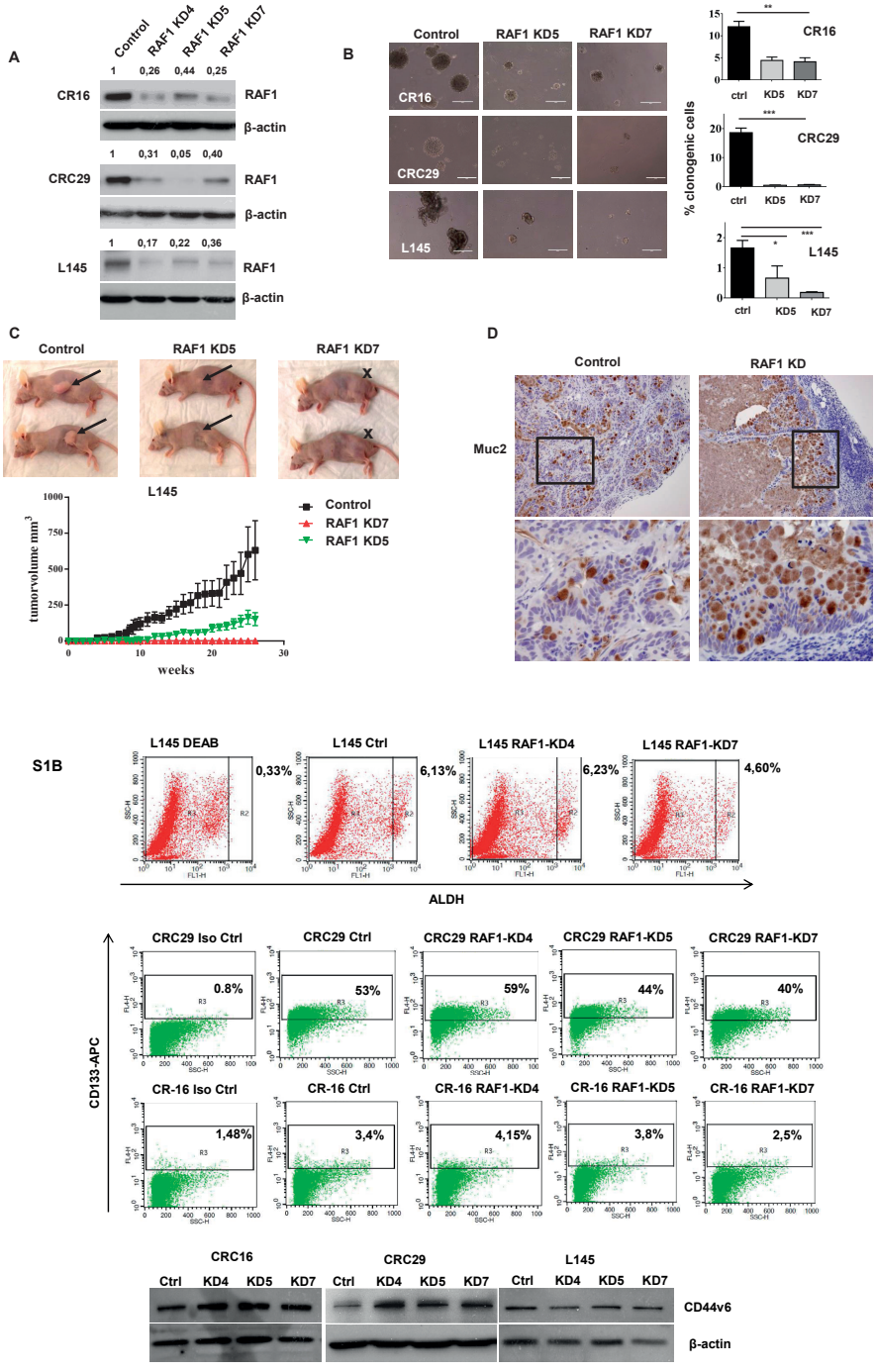

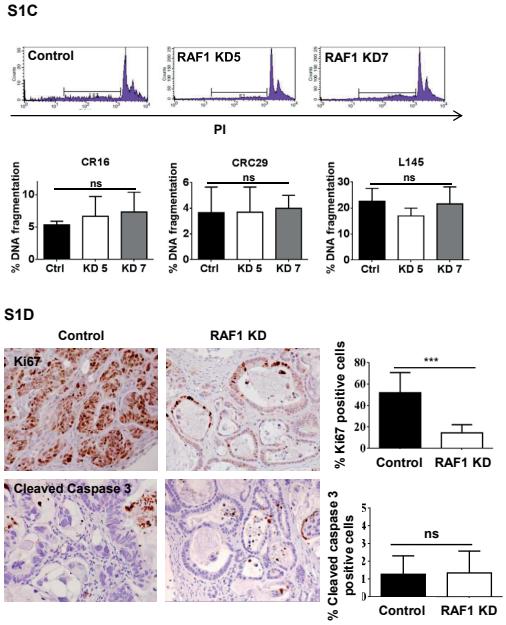

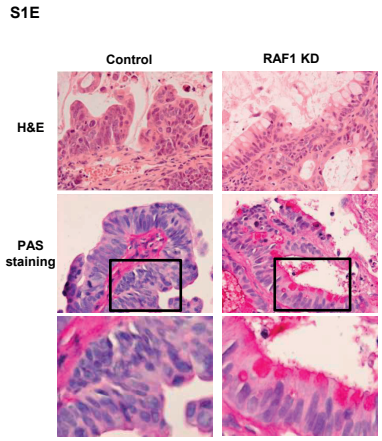

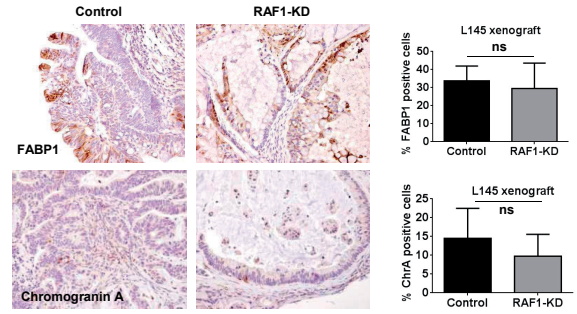

Supplementary Figure 1

(A) RAF1 expression in three different CRC cultures used in the study, CR16, CRC29 and L145, measured by WB. (B) FACS profiles of ALDH activity in L145, CD133 expression in CRC29 and CR16 and WB of CD44v6 in all three CRC cultures. (C) Measuring DNA fragmentation by Nicoletti assay demonstrated apoptotic rates to be comparable between control and RAF1-KD samples. (D) IHC for Ki67 and cleaved caspase 3 revealed significantly lower proliferation rates in L145 RAF1-KD5 tumors compared to control tumors, whereas apoptotic rates were comparable between the groups. Quantification of Ki67 and cleaved caspase 3 positive cells is depicted on graphs. (E) H&E and Pas staining revealed that majority of tumor cells differentiated into goblet cells in L145 RAF1-KD5 tumors unlike control cells. (F) FABP1 and Chromogranin A staining on xenografts showed no significant difference in protein expression between L145 control and RAF1-KD5 group, quantification depicted on the graphs.

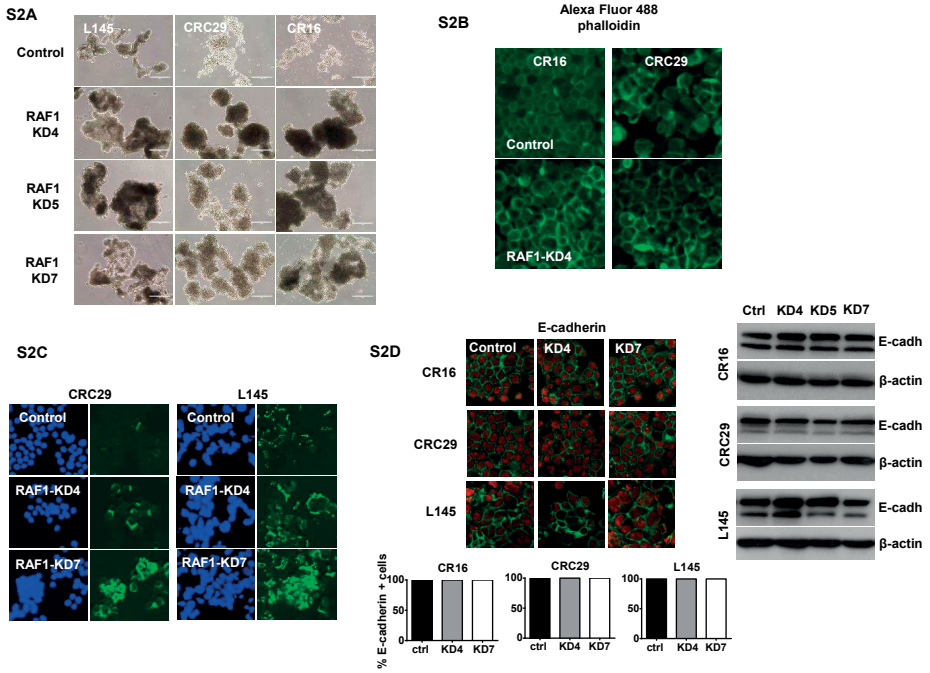

Supplementary Figure 2

(A) RAF1-KD cells (#4, #5 and #7) cluster more and form larger spheroids compared to control samples in all three CRC cultures (CR16, CRC29 and L145). (B) Phalloidin staining demonstrated more organized cortical actin between neighboring cells in CR16 and CRC29 RAF1-KD4 compared to the control. (C) TJ protein Occludin was significantly upregulated in RAF1-KD4 and KD7 samples, measured by IF. (D) E-cadherin, AJ protein, is equally expressed in RAF1-KDs and control samples in all three CRC cultures, measured by WB and IF.

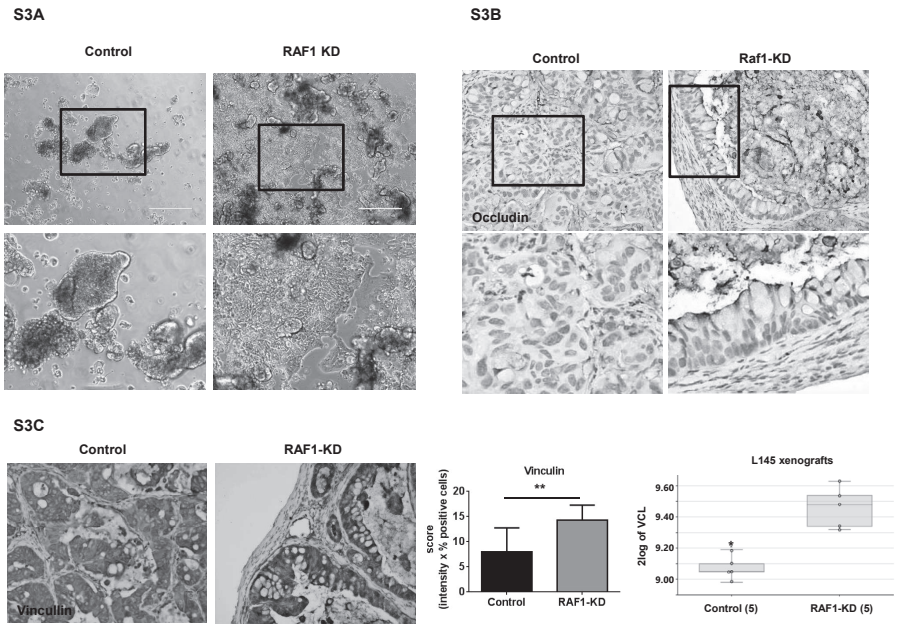

Supplementary Figure 3

(A) Upon plating, L145 RAF1-KD5 cells form a monolayer while control samples continue to grow in clumpy, multilayered fashion. (B) IHC staining for Occludin demonstrated apical localization of this tight junction protein in L145 RAF1-KD5 tumors. (C) Vinculin staining on L145 Control and RAF1-KD5 xenografts, quantification depicted on the graph. Right graph: microarray data showing an increase of VCL expression in RAF1-KD xenografts compared to Control.

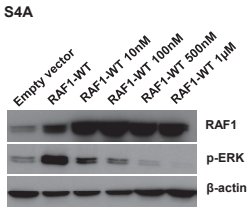
S4A
Empty vector
RAF1-WT
RAF1-WT 10nM
RAF1-WT 100nM
RAF1-WT 500nM
RAF1-WT 1μM
RAF1
p-ERK
β-actin

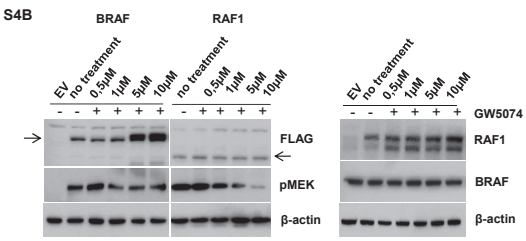
S4B
BRAF
RAF1
EV
no treatment
0.5μM
1μM
5μM
10μM
FLAG
pMEK
β-actin
GW5074
RAF1
BRAF
β-actin

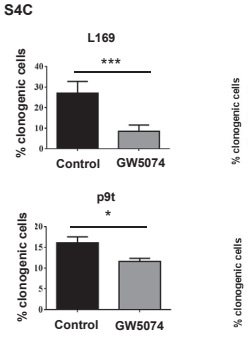
S4C
L169
% clonogenic cells
Control
GW5074
p9t

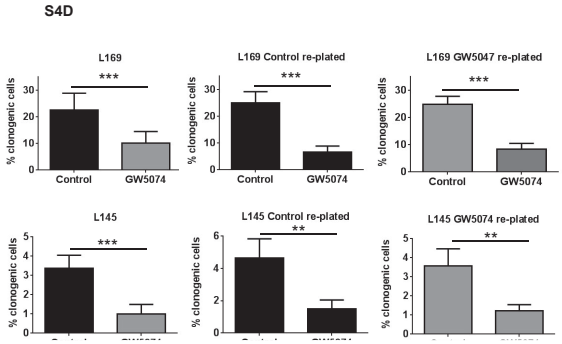
S4D
L169
L169 Control re-plated
L169 GW5047 re-plated
L145
L145 Control re-plated
L145 GW5074 re-plated
% clonogenic cells
Control
GW5074

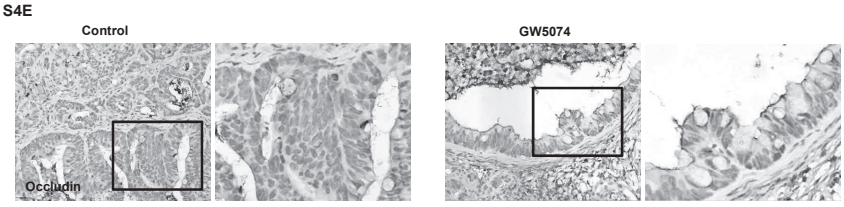
S4E
Control
GW5074
Occludin

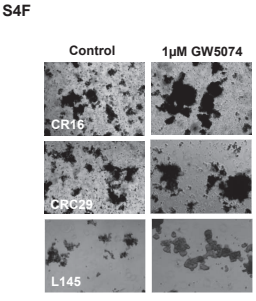
S4F
Control
1μM GW5074
CR16
CRC29
L145

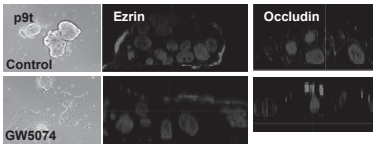
S4G
p9t
Ezrin
Occludin
Control
GW5074

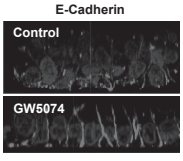
S4H
E-Cadherin
Control
GW5074

Supplementary Figure 4

(A) p-ERK inhibition upon titration of RAF1-kinase inhibitor GW5074 in 293T cells with overexpressed RAF1-WT protein. (B) p-MEK inhibition upon titration of GW5074 in 293T cells overexpressing RAF1-WT protein compared to BRAF-WT overexpression, both constructs FLAG-tagged. The setup of the experiment was as follows: Day 0- cells were transfected using Fugine; Day 1- the transfection reagent was washed off; Day 2- 1μM GW5074 was added for 24 hours; Day 3-samples were harvested and lysed for WB. The left panel shows overexpression of the constructs by increased FLAG expression in transfected samples for both RAF1 and BRAF (labeled on top), and MEK-ERK changes upon GW5074 treatment upon their overexpression. The very right panel shows RAF1 and BRAF expression in those same samples. (C) Treatment of L169 and p9t with 1μM GW5074 significantly decreased clonogenic capacity of CRC cells. (D) L145 and L169 CRC cultures were seeded for colony forming assay as a control and GW5074 treated group, and after two weeks both groups were re-seeded under the same conditions (+/- 1μM GW5074). (E) IHC staining for Occludin demonstrated apical localization of this tight junction protein in L145 GW5074 treated xenografts (F) Treatment of CR16, CRC29 and L145 cultures with GW5074 inhibitor induced cell clustering, comparable to RAF1-KDs. (G) p9t CRC organoids restore polarity upon treatment with 1μM GW5074, unlike control sample, measure by localization of apical marker ezrin and tight junction protein occludin. (H) Localization od adheres junction protein E-cadherin is normalized upon treatment with RAF1-kinase inhibitor GW5074.

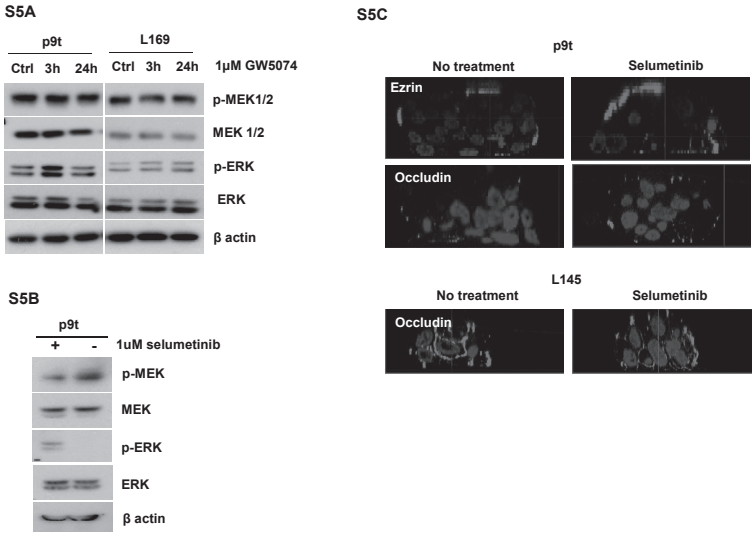

Supplementary Figure 5

(A) WB demonstrated p-ERK and p-MEK levels not to be inhibited by GW5047 treatment in L169 and p9t. (B) MEK-ERK phosphorylation is inhibited upon treatment with 1μM Selumetinib in organoid p9t, measured by WB (C) Polarity is not restored in p9t and L145 upon 1μM Selumetinib treatment, judging by Ezrin and Occludin distribution.

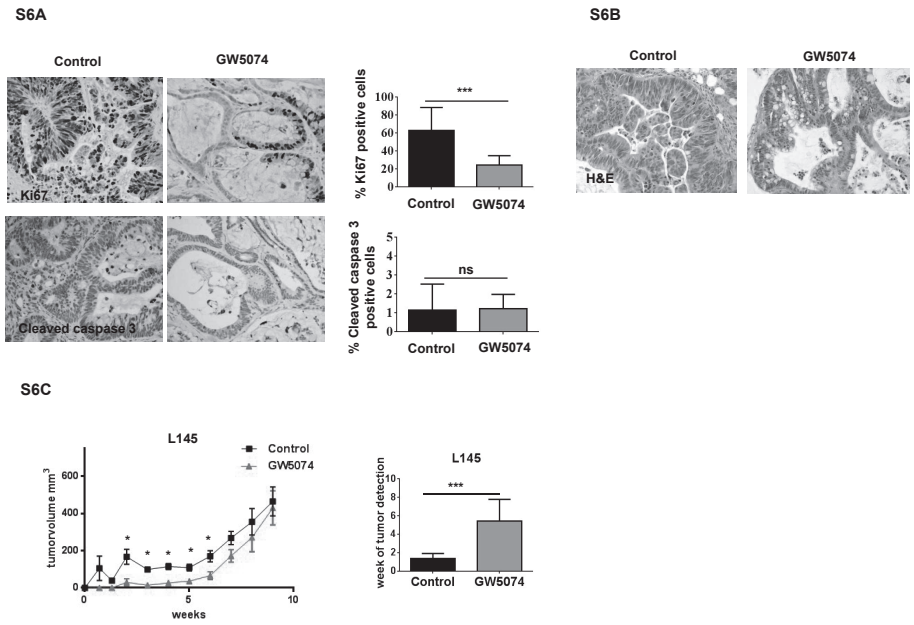

Supplementary Figure 6

(A) Ki67 and cleaved caspase 3 staining revealed decreased rates of cycling cells in L145 GW5074 treated tumors as compared to control group, whereas amount of apoptotic cells was comparable. Quantification of positive cells is depicted on graphs. (B) H&E staining demonstrated mucin vacuoles in majority of cells in L145 GW5047 tumors, showing their differentiation into goblet-like cells. (C) L145 CRC cells were isolated from the xenografts (Figure 6A) and re-injected into new mice. Growth curve shows that tumors previously treated with RAF1-kinase inhibitor GW5074 regain their growth capacity upon the removal of the inhibitor and equalize in size with control group.

Supplementary Table 1
List of 223 upregulated and 186 downregulated genes following RAF1-KD, when comparing RAF1-KD and Control xenografts

Supplementary Table 2
Mutational status of CRC cultures CR16, CRC29 and L145

Supplementary Table 3
Mutational status of L169; for the details on mutational status of p9t see: van de Wetering et al[15], Cell, 2015

Supplementary Table 1,2 and 3 can be downloaded at: https://gut.bmj.com/content/66/6/1106

CHAPTER 7

General discussion

CRC is a leading cause of cancer-related deaths worldwide. Initial patient management is determined by the TNM stage at diagnosis, based on depth of colon wall invasion, lymph node involvement and distant metastasis.[1] The TNM classification is widely used and clinically useful in terms of its good correlation with 5-year overall survival. Current guidelines for the treatment of CRC limit the use of adjuvant chemotherapy to patients with high-risk stage II and stage III disease, leading to possible undertreatment of certain CRC patients, and overtreatment of others. In case of stage IIb CRC, the risk of undertreatment is even more pronounced. Patients with T1-2N1M0 tumors (stage IIIA) treated with adjuvant chemotherapy have significantly better survival rates than patients with less advanced stage IIB tumors, who did not receive adjuvant chemotherapy.[2] Taken together, these observations indicate that the TNM classification fails to accurately select patients who might benefit from adjuvant therapy. In search of factors that influence therapy outcome, multiple molecular factors have meanwhile been identified.[3–5] This prompted the development of several classifications of CRC based on gene expression profiling.[6–12] Six of these molecular classifications were coalesced by the CRC Subtyping Consortium (CRCSC) into 1 Consensus Molecular Subtype (CMS) classification.[13] This CMS classification defined 4 different consensus molecular subtypes of CRC (i.e. CMS1-4), each reflected by specific molecular features. The different molecular subtypes all have their distinct prevalence. In the analyzed datasets 14% of tumors were clustered to CMS1, 37% to CMS2, 13% to CMS3 and 23% to CMS4. In terms of prognosis, CMS1-3 have similar survival rates, unlike CMS4, which has a dismal prognosis. Therefore, CMS4 is referred to as the poor prognosis subtype in CRC.

The molecular subtypes identified in CRC are based on RNA isolated from bulk tumor material. Consequently, the RNA analyzed in these arrays originated from cells of both the neoplastic and stromal compartment of tumors. High stromal content is characteristic of CMS4 and two studies challenged the 'true' mesenchymal nature of CMS4 tumors. These reports show that the mesenchymal genes defining the poor prognosis subtype are expressed by the stromal cells rather than the cancer cells.[14,15] In another study 55 patient-derived CRC organoids were generated and classified according to the CMS classification.[16] However, none of these classified as CMS4, despite the fact that CMS1-3 were represented and statistically 23% of 55 = +/- 13 organoids should have been assigned to CMS4. This lack of identification of CMS4 CRC organoids again questions the existence of a mesenchymal subtype in CRC. In **chapter 2**, we set out to answer this question and designed a stromal gene filter (SGF) to separately study the neoplastic and stromal compartment of CRC. Our study showed the neoplastic compartment of stroma-high tumors is actually characterized by a distinct mesenchymal gene expression program. Although gene ontology and gene set enrichment analyses failed to identify EMT as a defining feature of this distinct gene expression program, there was a good correlation with the gene set of core EMT inducing transcription factors ZEB2, TWIST1 and TWIST2. Possibly these analyses failed to

identify EMT since the 'classical' EMT genes CDH2, ZEB1 and FN1 were excluded as being part of the SGF. RT-qPCR analysis of EMT markers CDH2, VIM and FN1 in tumor cells, that underwent EMT versus the expression in cancer associated fibroblasts (CAFs), revealed the expression of these genes in tumor cells was 50-500 fold lower compared to the CAFs. So even a small amount of CAFs could easily overshadow the differential expression of classical mesenchymal markers in the neoplastic compartment when analyzing EMT in whole-tumor material. A recent study by Linnekamp et al. confirmed that CMS4 can be classified without stromal contribution and support the idea that the tumor cells of CMS4 are responsible for the stromal influx.[17] Furthermore, Eide et al. developed an algorithm for CMS classification in the absence of human tumor stroma. The genes in this algorithm are all tumor-intrinsic and takes stroma out of the equation to identify CMS subtype.[18] This algorithm is known as the CMScaller and recently Sveen et al. showed it can robustly classify patient tumors, cell lines and patient derived xenografts.[19]

The organoid system is an effective way to generate patient derived CRC tumors in vitro. CRC organoids maintain a high degree of similarity to the original tumor.[16,20] The organoid system was originally developed to culture human intestinal stem cells. The human intestinal system was mimicked by providing a support system of Matrigel, and specific factors (EGF, Noggin, R-Spondin, Wnt-3A, TGF-β inhibitor and p38 inhibitor). Subsequently, this 3D organoid culture system was adapted for human CRC cells. The only adjustment required was omitting Wnt-3A and R-Spondin-1, two substances essential for human healthy intestinal organoids. Without Wnt-3A and R-Spondin-1 it resulted in selective expansion of CRC cells.[21] In the human intestine the basement membrane (BM) is mainly composed of laminins and collagen type IV, like Matrigel. So Matrigel is the optimal choice in a system designed to stimulate intestinal crypt formation. We identified collagen type I as one of the most significantly enriched genes in the extracellular matrix (ECM) of mesenchymal type CRC. Collagen type I is mostly part of the underlying stromal matrix of the intestine and localized loss of BM integrity is associated with EMT and correlates with disease progression.[22] To resemble the ECM of mesenchymal type CRC, we replaced Matrigel with collagen type I in the organoid culture system. Embedded in collagen type I, the organoids displayed an invasive phenotype with tumor cells invading the surrounding collagen matrix. And indeed, collagen I induced the expression of genes part of the previously identified tumor specific mesenchymal gene expression program and core EMT transcription factors ZEB1, TWIST1 and 2. In concert with upregulation of mesenchymal genes, there was downregulation of epithelial transcription factor Hepatocyte Nuclear Factor 4-alpha (HNF4α) and its target genes. Collagen type I is mainly produced by fibroblasts and CAFs are one the most abundant cell types in the stroma of CMS4 tumors.[14,15] One of the characteristics of CMS4 is activated Transforming Growth Factor Beta (TGF-β) signaling and high levels of circulating TGF-β1 in CRC patients are a predictive factor for liver metastasis.[13,23] TGF-β increases collagen deposition by fibroblasts[24] and

TGF-β pre-treated CAFs boost tumor initiating capacity.[15] Our data provide a connection between collagen I, mesenchymal gene expression and TGF-β signaling. Another line of evidence for the relation between stroma and poor prognosis is presented by the amount of stroma, irrespective of its exact composition. This is known as the tumor-stroma ratio and has recently been reviewed by van Pelt et al.[25] High stromal content in CRC is a strong predictor of prognosis and the authors propose that scoring the tumor stroma ratio should be added to the routine diagnostic practice. This underscores the importance of designing novel therapeutic interventions (co-)targeting the tumor-stroma interface.

In **chapter 3**, we searched for drugs to interfere with the tumor-ECM-stroma interaction. We generated gene expression profiles of CRC organoids cultured in collagen I and identified proto-oncogene tyrosine-protein kinase Src as possible central regulator, and the c-Src inhibitor dasatinib as a potentially effective CMS4-targeting drug. Dasatinib is approved by the Food and Drug Administration (FDA) and is currently used in the treatment of chronic myeloid leukemia and acute lymphatic leukemia. In our study dasatinib significantly inhibited the invasive behavior of CRC organoids in collagen type I, restored the epithelial integrity at the tumor-matrix interface and caused apoptosis of collagen-invading tumor cells. These results are in line with previous studies demonstrating anti-invasive and anti-metastatic effects of dasatinib in pre-clinical models of pancreatic adenocarcinoma, CRC cell lines, thyroid and prostate cancer.[26–30] To study the effects of intercellular interaction and therapeutic intervention we developed a co-culture system for CRC organoids and fibroblasts. Fibroblasts promoted the development of invasive strands by CRC organoids. Dasatinib reduced the number of fibroblasts, the number of invasive strands and caused apoptosis of tumor cells located at the tips of invasive strands. Unfortunately, monotherapy with dasatinib failed to show any survival benefit in our in vivo experiments. This was in concordance with an in vivo model of metastatic pancreatic adenocarcinoma. Dasatinib reduced metastasis, but had no effect on survival due to continued growth of the primary tumor. The concentration of dasatinib required to inhibit proliferation is higher than the concentration required to inhibit c-Src. This first concentration was not reached during the in vivo experiments.[30] Likewise, dasatinib monotherapy had little effect on growth of colorectal cancer xenografts.[31] Combination therapy could provide a promising alternative strategy. Standard chemotherapy to target the proliferation of the tumor bulk and dasatinib to target both the stromal fibroblasts and the invasive (non-proliferating) tumor cells. One phase I and one phase IB/II study showed that addition of dasatinib to current standard chemotherapeutic regimens is safe.[32,33] Currently, metastatic CRC is treated irrespective of molecular subtype and KRAS mutational status and MSI status are the only criteria used in treatment selection. The discovery of different molecular subtypes should be considered a breakthrough in CRC research. It opens the door to improve patient selection, staging and therapeutic outcome. For example, if a CMS4 targeting drug is developed that has a response rate of 50% in this

particular subgroup, this would greatly improve survival in this subset of patients. Without knowledge of the different CMSs, the drug would be tested in the entire CRC population resulting in a response rate of 23%/50% = 11,5%. Probably, the drug would be wrongfully discarded.[34] Subtype analysis can also work the other way around and reveal that current therapies are ineffective in certain subtypes. Song et al. reported that patients with the stemlike subtype of CRC did not benefit from adjuvant oxaliplatin treatment.[35] Conversely, some therapies are highly effective in certain subtypes, as is demonstrated in a study by Del Rio. They identified one molecular subtype that was highly sensitive to irinotecan.[36] In this study multiple classification systems were used and the irinotecan sensitive subtype identified, was classified as subtype C5 in the classification of Marisa et al.[10] Important to note is that the majority of the tumors classified as subtype C5 were also classified as CMS4. However, there was no significant relation between irinotecan responders and CMS4. Recently, two studies have shown that the CMS classification can successfully be deployed to evaluate chemotherapy efficacy.[35,37] Sveen et al. demonstrated the feasibility of using the CMS classification to design subtype targeted therapy.[19]

Chemotherapy resistance is the innate and/or acquired ability of cancer cells to evade the effects of chemotherapeutics and is one of the major challenges in cancer therapy. In **chapter 4**, we generated gene expression profiles from resected livermetastases from chemonaïve versus chemo-treated (oxaliplatin and 5-FU) patients to study mechanisms of chemotherapy resistance. Gene expression analysis revealed a difference in cellular energy metabolism between the two groups. The energy metabolism of cancer cells is characterized by the well-known Warburg effect: a high rate of aerobic glycolysis.[38] This is in contrast to healthy cells, which use oxidative phosphorylation (OXPHOS) as their main energy metabolism. There are multiple explanations why the Warburg effect is beneficial for cancer cells. Aerobic glycolysis is the fastest way to generate ATP and generates biomass, which is fuel for proliferation.[39] Lactic acid, the excreted byproduct of aerobic glycolysis lowers extracellular pH and this favors tumor invasion.[40] Interestingly, our data demonstrate that first line chemotherapy of CRC (oxaliplatin and 5-FU) changes the energy metabolism in CRC colonospheres and that this confers a tumor survival advantage. Oxaliplatin and 5-FU induce upregulation of OXPHOS in CRC colonospheres. Enhanced oxidative phosphorylation is also linked to drug resistance in other cancer types. Chemotherapy resistant glioma and prostate cancer cells also exhibit enhanced OXPHOS. [41,42] A 2018 report by Lee et al. demonstrated irinotecan resistant non small lung cancer cells (NSCLC) also showed increased OXPHOS.[43] We identified the SIRT1/PGC1α axis as responsible for the upregulation of OXPHOS. In melanoma cells high expression of PGC1α causes an increase in OXPHOS, ROS-detoxifying enzymes and resistance to ROS-inducing drugs.[44] PGC1α is responsible for mitochondrial biogenesis and drives metastasis in invasive breast cancer cells.[45] Knock-down of SIRT1/PGC1α improved chemosensitivity of CRC colonospheres in vitro and in vivo. Increased OXPHOS in response to acute and

chronic DNA damage seems to be a general survival strategy in cells.[46] Our data indicate that exploiting the (post) chemotherapy metabolic changes in CRC cells may be an effective strategy to improve chemotherapy efficacy. This idea is supported by a recent report by Lee et al., showing synergistic effects of the combination of irinotecan with two OXPHOS targeting agents (gossypol and penformin) in NSCLC in vitro and in vivo.[43]

CMS4 CRC has the highest propensity to form distant metastasis.[13] Metastasis or cancer cell dissemination occurs both via the hematogenous and lymphatic route. The lymphatic system is considered a significant route of cancer spread. Unlike vascular vessels, lymphatic vessels are highly permeable. The flow rate of lymph is approximately 100–500x slower and coupled with less shearing stress due to vasodilation. As a tumor continues to grow, intratumoral interstitial fluid pressure rises and interstitial fluid is released as the body attempts to maintain extracellular homeostasis, facilitating entry of tumor cells into the lymphatic system.[47,48] In **chapter 5**, we identified CMS4 as the CRC subtype with highest enrichment of lymphangiogenic genes. In primary CRC lymphadenectomy of locoregional lymph nodes is a fundamental part of CRC surgery. Cancer spread to lymph nodes is part of the TNM classification and the number of lymph nodes removed is a direct parameter of surgical performance. In partial hepatectomy for liver metastases the role of lymphadenectomy has yet to be determined. Partial hepatectomy for liver metastases has an overall 5-year survival of >50%.[49] Lymph node metastases in the hepatoduodenal ligament is the worst prognostic factor with 5-year survival dropping to around 17%.[6,50,51] Multiple studies found lymph node metastases in up to 28% of patients undergoing partial hepatectomy.[6,52–55] Lymphadenectomy combined with partial liver resection significantly improved survival in patients with liver metastases and suspected hepatic lymph node involvement.[55,56] However, 3 studies showed no survival benefit of performing routine lymphadenectomy during partial hepatectomy.[55,57,58] Which makes sense, because 72% of patients do not have lymph node metastases and performing a lymphadenectomy will not remove more cancer cells and therefore not improve survival. In these cases lymphadenectomy only increases operation time and has potential complications, including postoperative bleeding, lymphatic leakage and ischemic bile duct stricture. This suggest performing lymphadenectomy during partial hepatectomy is only justified in case of suspected lymphatic disease. Identifying these patients has proven to be difficult, as both CT and MRI have a positive predictive value of around 50%. In staging for primary colorectal cancer two reports show FDG-PET imaging can help improve diagnostic accuracy.[59,60] More studies are needed to confirm its value in the detection of hepatic lymph node metastases. We demonstrated higher VEGF-C and Nrp-2 expression in liver metastases of patients subsequently developing lymph node metastases. Therefore, VEGF-C and Nrp-2 could be used to identify patients at risk for lymph node dissemination and serve as a selection tool for patients that might benefit from lymphadenectomy and/or targeted therapy. Two recent reports highlight the potential danger of lymph node

metastases. Both reports show in mouse models that lymph node metastases are not confined to the lymphatic system. Intralymphatic cancer cells make use of lymph node blood vessels and colonize distant organs.[61,62] This suggest that (potential) lymph node metastases might require a more aggressive approach.

Oncogenic KRAS is one of the most frequently occurring oncogenes in CRC (50%) and causes resistance to anti-EGFR therapy. EGFR activates RAS, which via activation of RAF leads to activation of MEK-ERK. ERK translocates to the nucleus and activates multiple proto-oncogenes (c-myc, c-jun, c-fos), all involved in cell proliferation, survival and metastasis. There are 3 RAF kinases: ARAF, BRAF and CRAF/RAF1 of which BRAF is well known and most frequently mutated (10%). Although activating mutations in RAF1 are rare in CRC (<1% COSMIC, the Catalogue Of Somatic Mutations In Cancer), gene expression data in multiple cohorts show that RAF1 is highly expressed in virtually all human CRC.[10,63,64] In **chapter 6**, we investigated the role of RAF1 in CRC. We show inhibition of RAF1 causes tumor cell polarization and differentiation in a MEK-ERK-independent manner and impairs tumor growth. In order for CRC cells to metastasize they need to break free from the primary tumor and invade surrounding tissues. Tight junctions (TJs) maintain epithelial integrity and thereby prevent movement of individual cells. Downregulation of TJs and subsequent loss of apico-basal polarization is a requisite for EMT. Re-expression of TJs in cancer cells induced apoptosis and suppressed metastasis in several cancer models.[65–67] Furthermore, leaky TJs help the diffusion of growth factors and nutrients through multilayered tumor cell masses and can thereby promote tumor growth.[68] Our data indicate inhibition of RAF1 results in upregulation of core TJ proteins occludin and JAM-A and restored epithelial integrity. Poor prognosis subtype CMS4 has the highest tendency to metastasize and specific inhibition of RAF1 in these patients could provide a strategy to reduce metastasis.

Taken together, the experimental work described in this thesis advocates further delineation and characterization of molecular signatures in cancer in general and CRC in particular. It provides new insights into the molecular background of the poor prognosis subtype CMS4 and its interaction with the ECM and stromal cells. It emphasizes the potential of targeted therapy in conjunction with standard chemotherapy regimens to optimize treatment and confirms the promising results of disrupting the tumor-ECM-stroma interaction. It contributes to further insights into how CRLM react to chemotherapy at the molecular level and presents cellular energy metabolism as a novel strategy to reduce chemotherapy resistance in metastatic CRC patients. It provokes the use of lymphatic gene expression in the context of CRLM and presents RAF1 as a novel target in the treatment of metastatic CRC. The response to systemic therapy remains limited in metastatic CRC and with rapidly expanding treatment options patient selection and therapy prediction will become essential. Molecular signatures of CRC have great potential in optimizing treatment outcome by guiding the design of targeted therapies.

References

1. Edge SB, Fritz AG, Byrd DA, Greene FL, Trotty A, Compton CC. *AJCC Cancer Staging Manuel, 7th Edition*.; 2010. doi:10.1007/978-1-4757-3656-4
2. O'Connell JB, Maggard MA, Ko CY. Colon cancer survival rates with the new American Joint Committee on Cancer sixth edition staging. *J Natl Cancer Inst*. 2004. doi:10.1093/jnci/djh275
3. De Roock W, Claes B, Bernasconi D, et al. Effects of KRAS, BRAF, NRAS, and PIK3CA mutations on the efficacy of cetuximab plus chemotherapy in chemotherapy-refractory metastatic colorectal cancer: A retrospective consortium analysis. *Lancet Oncol*. 2010. doi:10.1016/S1470-2045(10)70130-3
4. Ribic CM, Sargent DJ, Moore MJ, et al. Tumor Microsatellite-Instability Status as a Predictor of Benefit from Fluorouracil-Based Adjuvant Chemotherapy for Colon Cancer. *N Engl J Med*. 2003. doi:10.1056/NEJMoa022289
5. Jo WS, Carethers JM. Chemotherapeutic implications in microsatellite unstable colorectal cancer. *Cancer Biomarkers*. 2006. doi:10.3233/CBM-2006-21-206
6. Jaeck D, Nakano H, Bachellier P, et al. Significance of hepatic pedicle lymph node involvement in patients with colorectal liver metastases: A prospective study. *Ann Surg Oncol*. 2002. doi:10.1245/aso.2002.9.5.430
7. Sadanandam A, Lyssiotis CA, Homicsko K, et al. A colorectal cancer classification system that associates cellular phenotype and responses to therapy. *Nat Med*. 2013. doi:10.1038/nm.3175
8. Perez Villamil B, Romera Lopez A, Hernandez Prieto S, et al. Colon cancer molecular subtypes identified by expression profiling and associated to stroma, mucinous type and different clinical behavior. *BMC Cancer*. 2012. doi:10.1186/1471-2407-12-260
9. Budinska E, Popovici V, Tejpar S, et al. Gene expression patterns unveil a new level of molecular heterogeneity in colorectal cancer. *J Pathol*. 2013. doi:10.1002/path.4212
10. Marisa L, de Reyniès A, Duval A, et al. Gene Expression Classification of Colon Cancer into Molecular Subtypes: Characterization, Validation, and Prognostic Value. *PLoS Med*. 2013. doi:10.1371/journal.pmed.1001453
11. De Sousa E Melo F, Wang X, Jansen M, et al. Poor-prognosis colon cancer is defined by a molecularly distinct subtype and develops from serrated precursor lesions. *Nat Med*. 2013. doi:10.1038/nm.3174
12. Roepman P, Schlicker A, Tabernero J, et al. Colorectal cancer intrinsic subtypes predict chemotherapy benefit, deficient mismatch repair and epithelial-to-mesenchymal transition. *Int J Cancer*. 2014. doi:10.1002/ijc.28387
13. Guinney J, Dienstmann R, Wang X, et al. The consensus molecular subtypes of colorectal cancer. *Nat Med*. 2015;21(11):1350-1356. doi:10.1038/nm.3967
14. Isella C, Terrasi A, Bellomo SE, et al. Stromal contribution to the colorectal cancer transcriptome. *Nat Genet*. 2015. doi:10.1038/ng.3224
15. Calon A, Lonardo E, Berenguer-Llergo A, et al. Stromal gene expression defines poor-prognosis subtypes in colorectal cancer. *Nat Genet*. 2015. doi:10.1038/ng.3225

16. Fujii M, Shimokawa M, Date S, et al. A Colorectal Tumor Organoid Library Demonstrates Progressive Loss of Niche Factor Requirements during Tumorigenesis. *Cell Stem Cell*. 2016. doi:10.1016/j.stem.2016.04.003
17. Linnekamp JF, Van Hooff SR, Prasetyanti PR, et al. Consensus molecular subtypes of colorectal cancer are recapitulated in in vitro and in vivo models. *Cell Death Differ*. 2018. doi:10.1038/s41418-017-0011-5
18. Eide PW, Bruun J, Lothe RA, Sveen A. CMScaller: An R package for consensus molecular subtyping of colorectal cancer pre-clinical models. *Sci Rep*. 2017. doi:10.1038/s41598-017-16747-x
19. Sveen A, Bruun J, Eide PW, et al. Colorectal cancer consensus molecular subtypes translated to preclinical models uncover potentially targetable cancer cell dependencies. *Clin Cancer Res*. 2018. doi:10.1158/1078-0432.CCR-17-1234
20. Van De Wetering M, Francies HE, Francis JM, et al. Prospective derivation of a living organoid biobank of colorectal cancer patients. *Cell*. 2015. doi:10.1016/j.cell.2015.03.053
21. Sasaki N, Clevers H. Studying cellular heterogeneity and drug sensitivity in colorectal cancer using organoid technology. *Curr Opin Genet Dev*. 2018. doi:10.1016/j.gde.2018.09.001
22. Spaderna S, Schmalhofer O, Hlubek F, et al. A Transient, EMT-Linked Loss of Basement Membranes Indicates Metastasis and Poor Survival in Colorectal Cancer. *Gastroenterology*. 2006. doi:10.1053/j.gastro.2006.06.016
23. Tsushima H, Ito N, Tamura S, et al. Circulating transforming growth factor β1 as a predictor of liver metastasis after resection in colorectal cancer. *Clin Cancer Res*. 2001.
24. Narayanan AS, Page RC, Swanson J. Collagen synthesis by human fibroblasts. Regulation by transforming growth factor- β in the presence of other inflammatory mediators. *Biochem J*. 1989. doi:10.1042/bj2600463
25. van Pelt GW, Sandberg TP, Morreau H, et al. The tumour–stroma ratio in colon cancer: the biological role and its prognostic impact. *Histopathology*. 2018. doi:10.1111/his.13489
26. Serk IP, Zhang J, Phillips KA, et al. Targeting Src family kinases inhibits growth and lymph node metastases of prostate cancer in an orthotopic nude mouse model. *Cancer Res*. 2008. doi:10.1158/0008-5472.CAN-07-2997
27. Haeger A, Krause M, Wolf K, Friedl P. Cell jamming: Collective invasion of mesenchymal tumor cells imposed by tissue confinement. *Biochim Biophys Acta - Gen Subj*. 2014. doi:10.1016/j.bbagen.2014.03.020
28. Serrels A, Macpherson IRJ, Evans TRJ, et al. Identification of potential biomarkers for measuring inhibition of Src kinase activity in colon cancer cells following treatment with dasatinib. *Mol Cancer Ther*. 2006. doi:10.1158/1535-7163.MCT-06-0382
29. Erami Z, Herrmann D, Warren SC, et al. Intravital FRAP Imaging using an E-cadherin-GFP Mouse Reveals Disease- and Drug-Dependent Dynamic Regulation of Cell-Cell Junctions in Live Tissue. *Cell Rep*. 2016. doi:10.1016/j.celrep.2015.12.020
30. Morton JP, Karim SA, Graham K, et al. Dasatinib Inhibits the Development of Metastases in a Mouse Model of Pancreatic Ductal Adenocarcinoma. *Gastroenterology*. 2010. doi:10.1053/j.gastro.2010.03.034

31. Scott AJ, Song E-K, Bagby S, et al. Evaluation of the efficacy of dasatinib, a Src/Abl inhibitor, in colorectal cancer cell lines and explant mouse model. *PLoS One*. 2017;12(11):e0187173. https://doi.org/10.1371/journal.pone.0187173.
32. Strickler JH, McCall S, Nixon AB, et al. Phase i study of dasatinib in combination with capecitabine, oxaliplatin and bevacizumab followed by an expanded cohort in previously untreated metastatic colorectal cancer. *Invest New Drugs*. 2014. doi:10.1007/s10637-013-0042-9
33. Parseghian CM, Parikh NU, Wu JY, et al. Dual inhibition of EGFR and c-Src by cetuximab and dasatinib combined with FOLFOX chemotherapy in patients with metastatic colorectal cancer. *Clin Cancer Res*. 2017. doi:10.1158/1078-0432.CCR-16-3138
34. Menter, D.G., Davis, J.S., Broom BM et al. Back to the Colorectal Cancer Consensus Molecular Subtype Future. *Curr Gastroenterol Rep*. 2019;21(5).
35. Song N, Pogue-Geile KL, Gavin PG, et al. Clinical Outcome From Oxaliplatin Treatment in Stage II/III Colon Cancer According to Intrinsic Subtypes. *JAMA Oncol*. 2016. doi:10.1001/jamaoncol.2016.2314
36. Del Rio M, Mollevi C, Bibeau F, et al. Molecular subtypes of metastatic colorectal cancer are associated with patient response to irinotecan-based therapies. *Eur J Cancer*. 2017. doi:10.1016/j.ejca.2017.02.003
37. Okita A, Takahashi S, Ouchi K, et al. Consensus molecular subtypes classification of colorectal cancer as a predictive factor for chemotherapeutic efficacy against metastatic colorectal cancer. *Oncotarget*. 2018. doi:10.18632/oncotarget.24617
38. Warburg O. On the origin of cancer cells. *Science (80-)*. 1956. doi:10.1126/science.123.3191.309
39. Lunt SY, Vander Heiden MG. Aerobic Glycolysis: Meeting the Metabolic Requirements of Cell Proliferation. *Annu Rev Cell Dev Biol*. 2011. doi:10.1146/annurev-cellbio-092910-154237
40. Estrella V, Chen T, Lloyd M, et al. Acidity generated by the tumor microenvironment drives local invasion. *Cancer Res*. 2013. doi:10.1158/0008-5472.CAN-12-2796
41. Ippolito L, Marini A, Cavallini L, et al. Metabolic shift toward oxidative phosphorylation in docetaxel resistant prostate cancer cells. *Oncotarget*. 2016. doi:10.18632/oncotarget.11301
42. Oliva CR, Moellering DR, Gillespie GY, Griguer CE. Acquisition of chemoresistance in gliomas is associated with increased mitochondrial coupling and decreased ROS production. *PLoS One*. 2011. doi:10.1371/journal.pone.0024665
43. Lee S, Lee JS, Seo J, et al. Targeting Mitochondrial Oxidative Phosphorylation Abrogated Irinotecan Resistance in NSCLC. *Sci Rep*. 2018. doi:10.1038/s41598-018-33667-6
44. Lim JH, Luo C, Vazquez F, Puigserver P. Targeting mitochondrial oxidative metabolism in melanoma causes metabolic compensation through glucose and glutamine utilization. *Cancer Res*. 2014. doi:10.1158/0008-5472.CAN-13-2893-T
45. Lebleu VS, O'Connell JT, Gonzalez Herrera KN, et al. PGC-1α mediates mitochondrial biogenesis and oxidative phosphorylation in cancer cells to promote metastasis. *Nat Cell Biol*. 2014. doi:10.1038/ncb3039
46. Brace LE, Vose SC, Stanya K, et al. Increased oxidative phosphorylation in response to acute and chronic dna damage. *npj Aging Mech Dis*. 2016. doi:10.1038/npjamd.2016.22

47. Rahman M, Mohammed S. Breast cancer metastasis and the lymphatic system (Review). *Oncol Lett*. 2015. doi:10.3892/ol.2015.3486
48. Fischer M, Franzeck UK, Herrig I, et al. Flow velocity of single lymphatic capillaries in human skin. *Am J Physiol*. 1996. doi:10.1183/09031936.00027613
49. Abdalla EK, Vauthey JN, Ellis LM, et al. Recurrence and outcomes following hepatic resection, radiofrequency ablation, and combined resection/ablation for colorectal liver metastases. In: *Annals of Surgery*. ; 2004. doi:10.1097/01.sla.0000128305.90650.71
50. Elias D, Sideris L, Pocard M, et al. Results of R0 resection for colorectal liver metastases associated with extrahepatic disease. *Ann Surg Oncol*. 2004. doi:10.1245/ASO.2004.03.085
51. Elias D, Ouellet JF, Bellon N, Pignon JP, Pocard M, Lasser P. Extrahepatic disease does not contraindicate hepatectomy for colorectal liver metastases. *Br J Surg*. 2003. doi:10.1002/bjs.4071
52. Oussoultzoglou E, Romain B, Panaro F, et al. Long-term survival after liver resection for colorectal liver metastases in patients with hepatic pedicle lymph nodes involvement in the era of new chemotherapy regimens. *Ann Surg*. 2009. doi:10.1097/SLA.0b013e3181a334d9
53. Bennett JJ, Schmidt CR, Klimstra DS, et al. Perihepatic lymph node micrometastases impact outcome after partial hepatectomy for colorectal metastases. In: *Annals of Surgical Oncology*. ; 2008. doi:10.1245/s10434-007-9802-0
54. Beckurts KTE, Hölscher AH, Thorban S, Bollschweiler E, Siewert JR. Significance of lymph node involvement at the hepatic hilum in the resection of colorectal liver metastases. *Br J Surg*. 1997. doi:10.1002/bjs.1800840811
55. Hodgson R, Sethi H, Ling AH, Lodge P. Combined hepatectomy and hepatic pedicle lymphadenectomy in colorectal liver metastases is justified. *HPB*. 2017. doi:10.1016/j.hpb.2017.01.025
56. Wakai T, Shirai Y, Sakata J, Nagahashi M, Kaneko K, Hatakeyama K. Hepatic lymph node dissection provides a survival benefit for patients with nodal disease of colorectal carcinoma liver metastases. *Hepatogastroenterology*. 2009.
57. Grobmyer SR, Wang L, Gonen M, et al. Perihepatic lymph node assessment in patients undergoing partial hepatectomy for malignancy. *Ann Surg*. 2006. doi:10.1097/01.sla.0000217606.59625.9d
58. Pindak D, Pavlendova J, Tomas M, Dolnik J, Duchon R, Pechan J. Selective versus routine lymphadenectomy in the treatment of liver metastasis from colorectal cancer: a retrospective cohort study. *BMC Surg*. 2017. doi:10.1186/s12893-017-0233-y
59. Tsunoda Y, Ito M, Fujii H, Kuwano H, Saito N. Preoperative Diagnosis of Lymph Node Metastases of Colorectal Cancer by FDG-PET/CT. *Jpn J Clin Oncol*. 2008;38(5):347-353. http://dx.doi.org/10.1093/jjco/hyn032.
60. Inoue, K., Sato, T., Kitamura H et al. Diagnosis supporting algorithm for lymph node metastases from colorectal carcinoma on 18F-FDG PET/CT. *Ann Nucl Med*. 2008;Volume 22(1):41-48.
61. Brown M, Assen FP, Leithner A, et al. Lymph node blood vessels provide exit routes for metastatic tumor cell dissemination in mice. *Science (80-)*. 2018. doi:10.1126/science.aal3662
62. Pereira ER, Kedrin D, Seano G, et al. Lymph node metastases can invade local blood vessels, exit the node, and colonize distant organs in mice. *Science (80-)*. 2018. doi:10.1126/science.aal3622

63. Jorissen RN, Gibbs P, Christie M, et al. Metastasis-associated gene expression changes predict poor outcomes in patients with Dukes stage B and C colorectal cancer. *Clin Cancer Res*. 2009. doi:10.1158/1078-0432.CCR-09-1431
64. Smith JJ, Deane NG, Wu F, et al. Experimentally Derived Metastasis Gene Expression Profile Predicts Recurrence and Death in Patients With Colon Cancer. *Gastroenterology*. 2010. doi:10.1053/j.gastro.2009.11.005
65. Osanai M, Murata M, Nishikiori N, Chiba H, Kojima T, Sawada N. Epigenetic silencing of occludin promotes tumorigenic and metastatic properties of cancer cells via modulations of unique sets of apoptosis-associated genes. *Cancer Res*. 2006. doi:10.1158/0008-5472.CAN-06-1864
66. Michl P, Barth C, Buchholz M, et al. Claudin-4 expression decreases invasiveness and metastatic potential of pancreatic cancer. *Cancer Res*. 2003. doi:10.1158/0008-5472.can-05-2782
67. Hoevel T, Macek R, Swisshelm K, Kubbies M. Reexpression of the TJ protein CLDN1 induces apoptosis in breast tumor spheroids. *Int J Cancer*. 2004. doi:10.1002/ijc.11571
68. Mullin JM, Laughlin K V, Ginanni N, Marano CW, Clarke HM, Peralta Soler A. Increased tight junction permeability can result from protein kinase C activation/translocation and act as a tumor promotional event in epithelial cancers. *Ann N Y Acad Sci*. 2000. doi:10.1111/j.1749-6632.2000.tb05246.x

CHAPTER 8

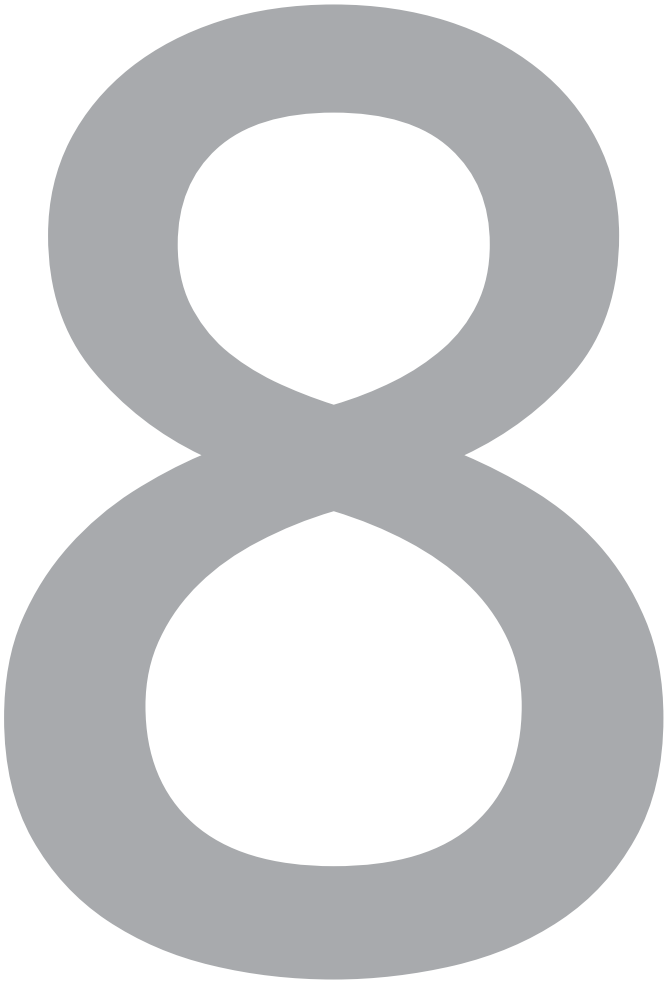

Summary in Dutch – Nederlandse samenvatting

In 2018 kregen wereldwijd naar schatting meer dan 1.8 miljoen mensen darmkanker en stierven er 881.000 mensen aan de gevolgen van deze ziekte. In veruit de meeste gevallen is het overlijden te wijten aan uitzaaiingen elders in het lichaam. De lever is met 50% de meest frequente locatie van deze uitzaaiingen. Ondanks vele verbeteringen in de behandeling van darmkanker, blijft de prognose van uitgezaaide darmkanker zeer somber. 15% van de patiënten leeft na 5 jaar nog. Een operatie is de enige behandeling die kans geeft op genezing, maar deze is slechts bij 1 op de 4 patiënten mogelijk. De overige 75% heeft uitzaaiingen op het moment van diagnose en is dus overgeleverd aan chemo- en/of lokale ablatie/radiotherapie. De huidige chemotherapie bij darmkanker in Nederland bestaat uit 5-fluorouracil (5-FU) en oxaliplatin. In het geval van stadium III darmkanker reduceert chemotherapie het risico op het krijgen van uitzaaiingen van 50 naar 35%. Dit betekent dat slechts 15% van deze patiënten voordeel heeft van de chemotherapie in huidige vorm.

Darmkanker wordt momenteel ingedeeld volgens het TNM-classificatie systeem, waarbij de T staat voor tumor, N voor node (lymfeklier) en M voor metastasen (uitzaaiingen). Het T stadium wordt bepaald door de mate waarin de tumor zich uitbreidt in de verschillende lagen waaruit de darm is opgebouwd. N is het aantal lymfeklieren, waarin tumorcellen worden aangetoond. M de aanwezigheid van uitzaaiingen. Aan de hand van het TNM stadium wordt de behandeling bepaald. Het TNM systeem is alleen gebaseerd op deze anatomische/pathologische factoren en laat onder andere de moleculaire factoren buiten beschouwing. Een tekortkoming van deze classificatie is het onvermogen te voorspellen welke patiënten voordeel zullen ondervinden van aanvullende chemotherapie. Jaren geleden was de KRAS mutatiestatus 1 van de eerste factoren die een relatie liet zien met de werkzaamheid van chemotherapie. Later kwamen BRAF en MSI status hier nog bij. Deze ontwikkelingen droegen bij aan verdere moleculaire karakterisatie van darmkanker. De afgelopen jaren verschenen meerdere moleculaire classificaties van darmkanker, waarbij op basis van moleculaire eigenschappen verschillende subtypen konden worden onderscheiden. Om consensus tussen de verschillende classificaties te bereiken werd een consortium gevormd die zes verschillende gen expressie databases samenvoegde en hieruit 4 verschillende subtypen destilleerde. De zogenaamde Consensus Moleculaire Subtypen (CMS1-4). Deze CMS hebben elk een verschillende moleculaire achtergrond en wat betreft de prognose zijn CMS1-3 vergelijkbaar, maar CMS4 heeft een significant slechtere prognose in vergelijking met de andere subtypen. CMS4 wordt daarom het agressieve of slechte prognose subtype van darmkanker genoemd. CMS4 wordt gekenmerkt door een verhoogde expressie van mesenchymale genen, verhoogde TGF-β activiteit, herstructurering van kankerbindweefsel en vaatnieuwvorming. Mesenchymale genen, in tegenstelling tot epitheliale genen (welke voornamelijk tot uiting komen in darmcellen), zijn genen die bijdragen aan de mobiliteit van cellen. TGF-β is een eiwit dat in darmkanker geassocieerd wordt met het optreden van uitzaaiingen.

Een tumor bestaat uit kankercellen en stroma (bindweefsel). Bij het uitvoeren van de gen expressie analyses (RNA) is tumormateriaal gebruikt, waarbij kankercellen en bindweefsel niet van elkaar zijn gescheiden. Het is daarom achteraf niet vast te stellen of het geanalyseerde RNA afkomstig was uit kanker- of de bindweefselcellen. Twee artikelen laten zien dat de genen die de mesenchymale signatuur van CMS4 bepalen, tot expressie komen in de bindweefsel cellen. Met deze bevinding wordt gesuggereerd dat de kankercellen van het CMS4 subtype mogelijk niet mesenchymaal zijn. In hoofdstuk 2 hebben we een bindweefsel genen filter ontworpen om de bindweefselcomponent en kankercellen component van een tumor apart van elkaar te kunnen bestuderen. We laten zien dat er wel degelijk mesenchymale genen tot expressie komen in de kankercellen van CMS4 tumoren. Echter dit zijn niet de bekende mesenchymale genen. We laten zien dat de bekende mesenchymale genen ook tot expressie komen in de kankercellen, alleen 50-500 keer lager dan in bindweefsel cellen (fibroblasten). Deze mate van de expressie valt dus makkelijk in het niet bij de mate van expressie in bindweefselcellen.

Om darmkanker te bestuderen is het essentieel om een zo waarheidsgetrouw model te gebruiken. De laatste jaren is het organoidsysteem ontwikkeld. Dit systeem bleek zeer succesvol in het kweken van darmcellen. Darmcellen van patiënten konden buiten het lichaam groeien in zogenaamde matrigel. Matrigel bleek een goede vervanger van het basaalmembraan te zijn, waarop in het menselijk lichaam de darmcellen groeien. Ook darmkankercellen konden goed buiten het lichaam worden gekweekt met het tumor organoid systeem. Het aanpassen van het omliggende bindweefsel is 1 van de moleculaire eigenschappen van CMS4. Uit onze analyses blijkt dat het bindweefsel van CMS4 tumoren voornamelijk uit collageen 1 bestaat. Het tumor organoid systeem is net zoals het originele organoid systeem gebaseerd op Matrigel. Matrigel bestaat uit laminine (de belangrijkste component van de basaalmembraan). In hoofdstuk 3 hebben we de genexpressie vergeleken van tumor organoids, die groeiden in collageen I (de natuurlijke habitat van CMS4) ten opzichte van organoids in Matrigel. Deze analyse liet zien dat mesenchymale genen sterker tot expressie kwamen in collageen I ten opzichte van de Matrigel. Verdere analyse liet zien dat het proto oncogene eiwit Src mogelijk een centrale rol in dit effect speelt. Mede op basis hiervan en de genen signatuur van CMS4 hebben we Src-remmer dasatinib onderzocht. Dasatinib remt in vitro het agressieve phenotype van de tumor organoids. Het meest voorkomende celtype in het bindweefsel van CMS4 tumoren zijn de fibroblasten. Om het effect van fibroblasten op de tumor organoids te kunnen bestuderen hebben we een co-culture systeem ontwikkeld. Het toevoegen van fibroblasten aan tumor organoids in collageen I stimuleerde de tumor organoids tot het vormen van uitlopers. Dasatinib reduceerde het aantal uitlopers van de tumor organoids.

Resistentie tegen chemotherapie is een lastig probleem bij de behandeling van darmkanker. Op den duur worden vrijwel alle darmkankercellen resistent tegen de

gangbare chemotherapie. Het is daarom van essentieel belang om deze resistentie mechanismen te bestuderen om zo de effectiviteit van chemotherapie te verbeteren. In hoofdstuk 4 hebben we genexpressie profielen van uitzaaiingen van darmkanker naar de lever bestudeerd. Hierbij vergeleken we de profielen van uitzaaiingen afkomstig van patiënten die niet behandeld waren met chemotherapie met de profielen van uitzaaiingen van patiënten, die wel met chemotherapie waren behandeld. De genen die het sterkst tot expressie waren gekomen, hadden te maken met het energie metabolisme. Gezonde cellen maken voornamelijk gebruik van hun mitochondriën om ATP (energie) te maken. Dit proces heet oxidatieve phosphorylering (OXPHOS). Bij het ontstaan van kanker verandert ook het energie metabolisme. Kankercellen ondergaan het zogenaamde Warburg effect: verhoogde aerobe glycolyse activiteit. We laten zien dat de eerstelijns chemotherapie bij darmkanker, 5-FU en oxaliplatin verhoogde OXPHOS activiteit tot gevolg heeft. Dit wordt in werking gesteld door SIRT1/PGC1α en het uitschakelen van SIRT1/ PGC1α leidt tot een verhoogde gevoeligheid voor chemotherapie.

Het verspreiden van kanker naar de lymfeklieren is geassocieerd met een slechte prognose in nagenoeg alle vormen van kanker. Naast het verwijderen van het stuk darm waar de tumor zich bevindt, is het verwijderen van de locoregionale lymfeklieren een belangrijk onderdeel van de operatie bij primaire darmkanker. Het aantal verwijderde lymfeklieren is onderdeel van de stadiëring van de tumor (TNM-classificatie) en geldt als directe maat voor de kwaliteit van de operatie. Bij de operatie van uitzaaiingen in de lever worden niet standaard de locoregionale lymfeklieren verwijderd. Meerdere studies hebben laten zien, dat dit geen overlevingswinst oplevert. Bij 28% van de patiënten met uitzaaiingen in de lever zijn tegelijkertijd ook uitzaaiingen in nabijgelegen lymfeklieren aanwezig. In hoofdstuk 5 hebben we een signatuur ontworpen, bestaande uit genen betrokken bij het lymfatische systeem. We laten zien dat deze lymfatische genexpressie sterker is vertegenwoordigd in het slechte prognose subtype CMS4. Patiënten met leveruitzaaiingen, die verhoogde expressie van deze lymfatische genen signatuur laten zien, krijgen ook vaker lymfekliermetastasen na de operatie. Deze lymfeklier signatuur zou gebruikt kunnen worden om patiënten met leveruitzaaiingen op te sporen, die een verhoogde kans hebben op uitzaaiingen naar de lymfeklieren. Deze groep patiënten zou dan bijvoorbeeld vaker gecontroleerd kunnen worden op lymfeklieruitzaaiingen of in aanmerking komen voor aanvullend gerichte medicamenteuze therapie of een operatie.

Bij het ontstaan van darmkanker speelt een mutatie in het RAS-gen een belangrijke rol. De helft van alle gevallen van darmkanker heeft een mutatie in KRAS. RAS is een onderdeel van de moleculaire pathway EGFR-RAS-RAF-MEK-ERK. Het activeren van deze pathway leidt onder meer tot proliferatie, het verhinderen van celdood en uitzaaiingen. Mutaties in het KRAS-gen zorgen ervoor dat het RAS eiwit continu actief blijft en niet meer reageert op negatieve feedback, via bijvoorbeeld de EGFR receptor. Dit is de reden

waarom anti-EGFR therapie niet werkt bij patiënten met deze mutatie. De tweede stap in deze pathway betreft de activatie van de RAF kinasen: ARAF, BRAF en CRAF/RAF1. Van deze 3 is BRAF de bekendste en in 10% van de darmkanker patiënten heeft een activerende mutatie in dit gen. Ondanks dat activerende mutaties in ARAF of CRAF (RAF1) zeer zeldzaam zijn in darmkanker (<1%), tonen gen expressie analyses aan dat RAF1 hoog tot expressie komt in darmkanker. Om deze reden hebben we in hoofdstuk 6 de rol van RAF1 in darmkanker bestudeerd. We laten zien dat het uitschakelen van het RAF1 gen de tumorgroei en tumorvormende capaciteit verminderd. Zowel in vivo als in vitro. Het uitschakelen of medicamenteuze onderdrukking van RAF1 leidde tot het herstel van de zogenaamde tight junctions (verbindingen tussen cellen, noodzakelijk om de normale darmarchitectuur te behouden) en er trad normalisatie van de apico-basale gradiënt op (belangrijke eigenschap van epitheliale darmcellen). Dit maakt RAF1 een interessant doelwit in de behandeling van darmkanker.

CHAPTER 9

9

Authors and affiliations
Review committee
Acknowledgements - dankwoord
List of publications
Curriculum vitae auctoris

Authors and affiliations

University Medical Center Utrecht

UMC Utrecht Cancer Center – Surgical oncology

- Inne H.M. Borel Rinkes
- Onno Kranenburg
- Jeroen Hagendoorn
- Klaas M. Govaert
- Benjamin L. Emmink
- Scabolzs Fatrai
- Tijana Borovski
- Jamila Laoukili
- Kari Trumpi
- Inge Ubink
- Nicola Frenkel
- Nikol Snoeren
- Susanne van Schelven
- André Verheem
- Dieuwke Marvin
- Niek Peters
- Kirsten Verheij

Department of Molecular Cancer Research

- Hugo Snippert
- Colinda Scheele
- Bas Ponsioen
- Johan de Rooij
- Adrian Alvarez Varela

UMC Amsterdam, Location AMC

Center of Experimental and Molecular Medicine

- Louis Vermeulen
- Jan-Paul Medema

Department of Clinical Chemistry, Laboratory of Genetic Metabolic Diseases

- Vincent de Boer

Department of oncogenomics
- Jan Koster
- Danny Zwijnenburg

UMC Amsterdam, Location VUMC

Department of pathology
- Sjoerd den Uil
- Remond Fijneman

Radboud University Medical Center, Nijmegen

Institute for molecular life sciences, department of cell biology
- Cornelia Veelken
- Peter Friedl

Spaarne Gasthuis, Haarlem

Department of Surgery
- Hein Stockmann

Weill Cornell Medical College, New York City, New York, USA.

Department of Pathology and Laboratory Medicine
- Evan Santo

Review committee

- Prof. dr. R. Fodde
- Dr. L.M.G. Moons
- Prof. dr. R. van Hillegersberg
- Prof. dr. M.M. Maurice
- Prof. dr. R. Goldschmeding

Acknowledgements – dankwoord

Binnen en buiten de wetenschap ben ik iedereen ongelofelijk dankbaar voor alle hulp en steun bij de totstandkoming van dit proefschrift. In het bijzonder wil ik nog een aantal mensen bedanken:

Prof. dr. I.H.M. Borel Rinkes. Beste Inne, 16 augustus 2011 was de dag dat ik je kamer binnenstapte. Zo begon dit verhaal en dat is nu bijna ten einde. Dat ik nog nooit in een laboratorium was geweest, heeft je niet tegen kunnen houden mij deze kans te geven. Dat vertrouwen en je oneindige energie en humor heb ik altijd enorm gewaardeerd. Het scheelde niet veel in Boekarest, maar soms heb je ook gewoon een beetje geluk nodig. Dank dat ik zoveel van je heb mogen leren!

Prof. dr. O. Kranenburg. Beste Onno, jouw kennis en betrokkenheid zijn van onschatbare waarde geweest bij de totstandkoming van dit proefschrift. Je kritische blik en scherpe geest hebben mij altijd weer gepusht het beste eruit te halen. Je stimuleerde me verder te kijken en me niet te snel uit het veld te laten slaan.

Dr. J. Hagendoorn. Beste Jeroen, veel dank voor je betrokkenheid bij mijn promotieonderzoek. Het lymfe veld is voortdurend in beweging, net zoals jij. Ik heb veel bewondering voor de manier waarop jij de drukke kliniek combineert met basaal onderzoek.

Klaas Govaert. Beste Klaas, zonder jou was ik waarschijnlijk nooit in Utrecht terecht gekomen en was dit proefschrift er helemaal nooit geweest. Veel dank voor al je steun, humor en wijze adviezen.

Tijana Borovski. Dear Tijana, without your help this thesis would have been a fraction of its current form. The quality and relevance of this work is a reflection of your ability to coach and your farsightedness. You always cut straight to the point and have an amazing eye for detail. Thanks so much for all your hard work and endless patience.

Inge Ubink. Beste Inge, wat een talent voor wetenschap! Veel dank voor je interesse en hulp bij dit proefschrift. Ik ben benieuwd naar jouw eindresultaat!

Susanne van Schelven. Beste Susanne, ik vind het geweldig dat jij altijd zo jezelf blijft. Niet gehinderd door enige vorm van gêne. Jij bent de motor van het lab. Veel dank voor al je hulp en harde werk bij mijn experimenten.

André Verheem. Beste André, veel dank voor al je hulp bij de experimenten. Vooral bij alle dierproeven was je onmisbaar! Ook dank voor alle niet zo serieuze minstens zo belangrijke momenten!

Geachte leden van de beoordelingscommissie, veel dank voor uw tijd en inspanning voor het beoordelen van mijn proefschrift. Uw kritische blik wordt zeer gewaardeerd.

Sjoerd den Uil. Beste Sjoerd, uren hebben wij samen stroma gescoord en er toch 2 papers uit weten te halen. Kon slechter!

Vincent de Boer. Beste Vincent, energie metabolisme van cellen blijft een fascinerend, maar uiterst ingewikkeld onderwerp. Dank voor je kennis en hulp bij het in kaart brengen van het tumor metabolisme.

Johan de Rooij. Beste Johan, erg fijn dat je deur altijd voor mij open stond. Dank voor de waardevolle disscussies en suggesties.

Collegas uit het lab. Danielle Raats, Benjamin Emmink, Ernst Steller, Kari Trumpi, Jennifer Jongen, Scabolcz Fatrai, Nicola Frenkel, Lizet van der Waals, Anneta Brousiali, Liza Wijler, Niek Peters, Susanna Poghosyan, Kirsten Verheij, Petra van de Groep.

Studenten: Dieuwke Marvin, Adrian Alvarez Varela, Jan Willem van Wijnbergen, Maura Manzi.

Collega onderzoekers. Amy Gunning, Sjoerd Nel, Wouter Kluijfhout, Lutske Lodewijk, Okan Bastian, Pieter Leliefeld, Steven van Haelst, Hylke Brenkman, Jacob Kist, Maarten Seesing, Els Visser, Tesse Leunissen, Vanessa Pourier, Steffi Rombouts, Morsal Samim, Stefanie Peeters Weem, Lucas Goense, Marieke Walma, Amir Basir, Djurre de Waard, Pieter van de Sluis, Kevin Parry.

Romy Liesdek en Marielle Hoefakker-Saraber. Dank voor jullie niet aflatende inspanningen om alle agendas weer soepel te laten verlopen.

Maten uit Boston. Stephan Tan en Jimme Klaas Wiggers. Dank voor de mooie tijd in Boston.

Emiel Post Uiterweer. Beste Emiel, wat een kilometers hebben wij samen gemaakt en wat gingen we hard.

JC Leon. Adriaan van Zijl, Jurjen Ruts, Benjamin Bourgonje, Bartelt Pekelharing, Marius Tan, Mattijs Franken, Tijs Peskens, Emile Drost, Mark Wijsman, Diederik Goeman Borgesius,

Tim van Hese, Cees Brouwer, David-Jan de Groot, Nigel Kooreman, Alexander Hofstad, Rik van Holthe tot Echten, Laurens Westendorp.

Bree14. Frans van Hoorn, Olaf Vogelaar, Daan Zwitser, Joris Boddaert, Maarten Brood, Steven de Walle, Maarten Koolen, Tamer Fawaz, Mark Lobatto, Floris-Jan Moojen, Gesicht, Marcio Abe Pereira de Carvalho, Eduard Holle, Peter Zeisser, David Weijers, Jeroen Adamse, Gert-jan van Gendt, Bernard Goeman Borgesius, Thomas Wagner, Wout Olieslagers, Jorick Wijnen, Reinier Stijnman, Pepijn Sun, Edmond Rinnooy Kan, Roderick Nielen.

Alp d'Huzessers. Carmen van der Pol, Loek Loozen, Emilie Postma, Margriet Fokkema.

Professor Jon Einarsson and professor Olav Istre. Thank you so much for the opportunity to start my scientific career in the Brigham. Apart from the unique and inspiring learning experience, the two of you made me feel at home and very appreciated.

Radiologie OLVG. Joris Niesten, Erik Buijs, Zeen Aref, Paul Cernohorsky, Joy Vroemen, Iris Kilsdonk, Alexander Schmitz, Max Haloua, Joukje Deinum, Jeroen Markenstein, Loes Huygen, Miou Koopman, Nick Wever, Roderick Holewijn, Stephanie Erdkamp, Esther Wiegerinck, Yves Tutuarima, Jorik Reimerink, Nikki Weil, Sanne Jansen, Meta Tjeenk Willink.

Radiologie AMC. Jeroen Tielbeek, Jan-Jaap Janssen, Eline Claire Grosfeld, Sander Bison, Floortje van Kesteren, Hugo Adams, Kerensa Beekman, Milou Tjong Joe Wai, Laura Kox, Daphne van der Velden, Ploni Witteveen, Lucas Mangnus, Jan Haersma, Willemien van den Bos, Jurgen Runge, Tom Doorschodt, Floor Knuttel, Naomi Haverkamp Begemann, Elsmarieke van de Giessen, Inge Koetser, Ezgi Soykan, Olvert Berkhemer, Marie Louise Bernsen, Femke Alberts, Robert Hemke, Sjoerd Jens, Anneline vd Ende.

Paranimfen Pieter Hebly en Marc de Burlet, jullie zijn helden!

Thomas Slee. Beste Thomas, maatje van het eerste uur! Wat gaaf dat je er nog steeds bij bent.

Lieve pap en mam. Zonder jullie onvoorwaardelijke steun zou ik nooit zijn wie ik nu ben. Veel dank voor alles!

List of publications

Vellinga TT, Veelken C, Ubink I, Verheij K, Peters N, van Schelven S, Verheem A, Friedl P, Borel Rinkes IH, Kranenburg O.
Dasatinib inhibits fibroblast-led invasion and regenerative capacity of colorectal cancer organoids in collagen type I.
Under review

den Uil SH, van den Broek E, Coupé VM, **Vellinga TT**, Delis-van Diemen PM, Bril H, Belt EJ, O. Kranenburg O, Stockmann HB, Belien JA, Meijer GA, Fijneman RJ.
Prognostic value of microvessel density in stage II and III colon cancer patients.
Under review

Vellinga TT, Kranenburg O, Frenkel N, Ubink I, Marvin D, Govaert K, van Schelven S, Hagendoorn J, Borel Rinkes IH.
Lymphangiogenic Gene Expression Is Associated With Lymph Node Recurrence and Poor Prognosis After Partial Hepatectomy for Colorectal Liver Metastasis.
Ann Surg. 2017 Nov;266(5):765-771.

Borovski T, **Vellinga TT**, Laoukili J, Santo EE, Fatrai S, van Schelven S, Verheem A, Marvin DL, Ubink I, Borel Rinkes IHM, Kranenburg O.
Inhibition of RAF1 kinase activity restores apicobasal polarity and impairs tumour growth in human colorectal cancer.
Gut. 2017 Jun;66(6):1106-1115.

Ubink I, Jongen JMJ, Nijkamp MW, Meijer EFJ, **Vellinga TT**, van Hillegersberg R, Molenaar IQ, Borel Rinkes IHM, Hagendoorn J.
Surgical and Oncologic Outcomes After Major Liver Surgery and Extended Hemihepatectomy for Colorectal Liver Metastases.
Clin Colorectal Cancer. 2016 Dec;15(4):e193-e198.

Vellinga TT, den Uil S, Rinkes IH, Marvin D, Ponsioen B, Alvarez-Varela A, Fatrai S, Scheele C, Zwijnenburg DA, Snippert H, Vermeulen L, Medema JP, Stockmann HB, Koster J, Fijneman RJ, de Rooij J, Kranenburg O.
Collagen-rich stroma in aggressive colon tumors induces mesenchymal gene expression and tumor cell invasion.
Oncogene. 2016 Oct 6;35(40):5263-5271.

Vellinga TT, Borovski T, de Boer VC, Fatrai S, van Schelven S, Trumpi K, Verheem A, Snoeren N, Emmink BL, Koster J, Rinkes IH, Kranenburg O.
SIRT1/PGC1α-Dependent Increase in Oxidative Phosphorylation Supports Chemotherapy Resistance of Colon Cancer.
Clin Cancer Res. 2015 Jun 15;21(12):2870-9.

Trumpi K, Egan DA, **Vellinga TT**, Borel Rinkes IH, Kranenburg O.
Paired image- and FACS-based toxicity assays for high content screening of spheroid-type tumor cell cultures.
FEBS Open Bio. 2015 Jan 28;5:85-90.

Gargiulo AR, Srouji SS, Missmer SA, Correia KF, **Vellinga TT**, Einarsson JI.
Robot-assisted laparoscopic myomectomy compared with standard laparoscopic myomectomy.
Obstet Gynecol. 2012 Aug;120(2 Pt 1):284-91.

Einarsson JI, Suzuki Y, **Vellinga TT**, Jonsdottir GM, Magnusson MK, Maurer R, Yoshida H, Walsh B.
Prospective evaluation of quality of life in total versus supracervical laparoscopic hysterectomy.
J Minim Invasive Gynecol. 2011 Sep-Oct;18(5):617-21.

Vellinga TT, Bronkhorst MWGA, Bouwman LH.
De vena cephalica, een analyse en beschrijving van deze alternatieve insertieplaats voor de Port-A-Cath.
Nederlands Tijdschrift voor Heelkunde 2011 Nov(20)8

Einarsson JI, **Vellinga TT**, Twijnstra AR, Chavan NR, Suzuki Y, Greenberg JA.
Bidirectional barbed suture: an evaluation of safety and clinical outcomes.
JSLS. 2010 Jul-Sep;14(3):381-5.

Einarsson JI, Chavan NR, Suzuki Y, Jonsdottir G, **Vellinga TT**, Greenberg JA.
Use of bidirectional barbed suture in laparoscopic myomectomy: evaluation of perioperative outcomes, safety, and efficacy.
Einarsson JI, Chavan NR, Suzuki Y, Jonsdottir G, Vellinga TT, Greenberg JA.
J Minim Invasive Gynecol. 2011 Jan-Feb;18(1):92-5.

Suzuki Y, **Vellinga TT**, Istre O, Einarsson JI.
Small bowel obstruction associated with use of a gelatin-thrombin matrix sealant (FloSeal) after laparoscopic gynecologic surgery.
J Minim Invasive Gynecol. 2010 Sep-Oct;17(5):641-5.

Vellinga TT, De Alwis S, Suzuki Y, Einarsson JI.
Laparoscopic entry: the modified alwis method and more.
Rev Obstet Gynecol. 2009 Summer;2(3):193-8.

Vellinga TT, Suzuki Y, Istre O, Einarsson JI.
Anatomic considerations in gynecologic surgery.
Rev Obstet Gynecol. 2009 Summer;2(3):137-8.

Book chapter

Istre O & **Vellinga TT**
Uterine malformation: Diagnosis and results after hysteroscopic metroplasty.
Minimally Invasive Gynecological Surgery (pp. 35-41). 2015 Springer.

Curriculum vitae auctoris

Thomas Tiede Vellinga was born on February 2nd, 1985 in Delft, the Netherlands. He spent his childhood in Oostvoorne and attended the gymnasium at the Maerlant College in Brielle. In 2003 he started to study Medicine in Leiden. During his studies he performed a one year research elective at the Brigham and Women's Hospital, Harvard Medical School, Boston MA USA in 2009. For his research in Boston under supervision of prof. dr. J.I. Einarsson and prof. dr. O. Istre he later received the Student Research Award from the Leiden University Medical Center. Thomas choose to do his final clinical rotation in general surgery at the Bronovo Hospital in the Hague and continued to work there as a resident not in training for another 6 months. In June 2012, he started his PhD at the University Medical Center in Utrecht under supervision of prof. dr. I.H.M Borel Rinkes and prof. dr. O. Kranenburg. During his PhD he discovered his interest in imaging and decided to pursue a career in Radiology. In January 2017 he started his training to become a radiologist at the Onze Lieve Vrouwe Gasthuis in Amsterdam under supervision of dr. A Driessen and dr. S. Jensch. Currently, Thomas is working at the AMC to perform the academical part of his training under supervision of dr. M.M. de Win and prof. dr. R.J. Bennink.